# e-JSNM

e-JURNAL SAINS NUKLEAR MALAYSIA
e-NUCLEAR SCIENCE JOURNAL OF MALAYSIA

Volume 35 No. 2 (2023)
A scientific journal by Malaysian Nuclear Agency
eISSN 2232-0946

eJURNAL
SAINS NUKLEAR MALAYSIA
VOL 35 NO. 2 (2023)
eISSN: 2232-0946



**Jurnal Sains Nuklear Malaysia** (JSNM, Nuclear Science Journal of Malaysia) is published in the months of June and December annually since 1982 by the Malaysian Nuclear Agency (formerly known as PUSPATI, UTN and MINT). This journal provides a platform for researchers, scientists and engineers (RSEs) to publish their research findings and reviews related to nuclear science and technology so that they can be shared with colleagues throughout the world.

As a means to internationalise JSNM, the Board of Editors welcomes scientific, technical and review articles written by members of the scientific community from home and abroad.

Previously a purely traditional printed journal, JSNM is now adapted and available in electronic form, in keeping with demands and rapid development of ICT. This adaptation also translates to ease of accessibility of JSNM for scientific communities as well as to facilitate knowledge sharing among RSEs.

On behalf of the Editorial Board of JSNM, we would like to acknowledge and thank the authors and referees for their significant contributions to the success of this journal and for embracing this new publication format.

Every effort has been made to trace and acknowledge all copyright holders, but if any have been inadvertently overlooked, the publishers would please to make the necessary arrangements at the first opportunity.

**Publishing Office**
Malaysian Nuclear Agency, Bangi,
43000 Kajang,
Selangor Darul Ehsan,
MALAYSIA
Tel : +6 03 8911 2000
Fax : +6 03 8911 2154

**Website**
http://jsnm.nuclearmalaysia.gov.my

## TABLE OF CONTENTS

e-Jurnal Sains Nuklear Malaysia, 2023, Vol. 35 (No.2): 1 – 8
*eISSN: 2232-0946*

# RADIOACTIVITY IN COMMERCIAL PACKAGED DRINKING AND NATURAL MINERAL WATER IN MALAYSIA

***Nooradilah Abdullah[1*], Norfaizal Mohamed[1], Mohd Zuhair Mohd Sanusi[1], Salahuddin Muhamad[1], Mohamad Noh Sawon[1], Muhammad Izzat Muammar Ramli[1], Nur Rahizatul Atiqah Norhisam[1], Siti Noor Hayani Mohd Noor[1] and Farizz Iskandar Mohd Yazid[2]***

[1]Radiochemistry and Environment Laboratory, Waste and Environmental Technology Division, Malaysian Nuclear Agency, Bangi, 43000 Kajang, Selangor
[2]Universiti Teknologi Mara (UiTM) Cawangan Perlis, 02600 Arau, Perlis.
*Corresponding author: nooradilah@nm.gov.my

***ABSTRACT***

*Radiochemistry and Environment Laboratory (RAS) had received bottled drinking water and natural mineral water samples throughout Malaysia from the Ministry of Health Malaysia (MOH). These samples need to undergo radioactivity analysis of gross alpha and gross beta which is part of the drinking water licensing requirements in Malaysia. A total of 83 samples were received in year 2020 and analysed using low background gross alpha gross beta counting system. The results of the analysis found that all samples complied with the mandatory standard requirements set by the MOH, which is not more than 0.1 Bq/L for gross alpha activity and 1.0 Bq/L for gross beta activity.*

**Keywords**: Drinking water, gross alpha, gross beta, natural mineral water

## INTRODUCTION

Water is one of the basic necessities in human daily life. Due to the risk of exposure to chemical contamination, microorganisms and radioactive materials, water resource management is important to ensure the safety of a country's water supply. Monitoring program of drinking water is one of the necessary actions in order to ensure the safety of the water supply received. Microorganisms, heavy metals and radioactive substances are the most commonly monitored parameters in drinking water. Among these parameters, radioactive substances found in natural mineral water and drinking water pose the least risk to human health as compared to chemical contamination and microorganisms. This lower risk is attributed to the fact that the radiation dose resulting from the consumption of radionuclides in drinking water is significantly lower than doses from other sources of radiation, as highlighted by the World Health Organization (WHO) in 2017.

The presence of radionuclides in drinking water supplies can occur naturally as well as from human activities that may release radionuclides into the environment such as nuclear facilities, nuclear weapons testing and mining activities. Natural alpha-emitting radionuclides that are the main contributors to gross alpha radioactivity come from the natural decay series of U-238 and Th-232 and their progenies U-234, Th-230, Ra-226, Po-210 and Th-228. The concentrations of natural gross beta activity are from the presence of radionuclides K-40, Ra-228 and Pb-210 (Pintilie et. al., 2016).

The Food Safety and Quality Division (BKKM) under the Ministry of Health Malaysia (MOH) is the governing authority who is responsible to ensure the safety of commercially available bottled drinking water (AMB) and natural mineral water (AMS) that are marketed for public consumption. The Twenty-Five Schedule (Sub-regulation 360B(3)) and the Twenty-Six Schedule (Regulation 360A(7)) of the Food Regulations 1985, Food Act 1983 (Act 281), specify that the standard mandatory limit

for gross alpha radioactivity is 0.1 Bq/L and 1.0 Bq/L for gross beta. WHO on the other hand states that the maximum limit for gross alpha is 0.5 Bq/L and 1.0 Bq/L for gross beta to ensure that the dose received by an adult does not exceed 0.1mSv per year, as suggested by the International Commission on Radiological Protection (ICRP, 2008).

The primary objective of this paper is to present the findings of the radioactivity analysis conducted by Radiochemistry and Environment Laboratory (RAS) on bottled drinking water and natural mineral water samples received from across Malaysia. The study aims to assess compliance with the drinking water licensing requirements in Malaysia, specifically focusing on the mandatory standards set by the MOH, which stipulate that gross alpha activity should not exceed 0.1 Bq/L and gross beta activity should not exceed 1.0 Bq/L.

## MATERIALS AND METHODS

### Study Area and Sampling

Malaysia, located in Southeast Asia, is comprised of two distinct regions, 13 states and three federal territories. The two regions, Peninsular Malaysia, which shares a border with Thailand and East Malaysia, situated on the island of Borneo alongside Indonesia and Brunei are separated by the South China Sea.

The sampling of AMB and AMS throughout Malaysia was conducted by BKKM. The number of samples per state in Malaysia is shown in Table 1. The sampling was conducted for the purpose of license application by companies that wish to market AMB and AMS locally. Apart from that, this sampling was also done to monitor licensed AMB and AMS that are currently marketed. The samples were then sent to RAS Laboratory for analysis.

Table 1. Number of samples per state in Malaysia

| State | Number of Samples |
|---|---|
| Johor | 9 |
| Kedah | 2 |
| Kelantan | 4 |
| Melaka | 5 |
| Negeri Sembilan | 5 |
| Pahang | 5 |
| Perak | 5 |
| Perlis | 5 |
| Pulau Pinang | 2 |
| Sabah | 5 |
| Sarawak | 14 |
| Selangor | 18 |
| Terengganu | 1 |
| Federal Territory Labuan | 1 |
| Federal Territory Putrajaya | 2 |

**Sample Pre-treatment and Preparation**

A total of two liter (L) of water was used for analysis. Water was measured using a measuring cylinder and then poured into a 2 L beaker. The samples were evaporated without boiling at temperature less than 85°C (Ho et.al., 2020, Borrego-Alonso et.al., 2023). After the sample volume was reduced to approximately 5-10 ml, the sample was then transferred onto a 2 inch diameter stainless steel planchet with 1/8-inch depth using a dropper. The sample in the planchet was dried under an infrared lamp (Figure 1). The sample was continuously added onto the planchet until all samples were completely transferred and dried.

Figure 1. Sample drying under an infrared lamp

**Sample Counting**

Low Background Gross Alpha Gross Beta Counting System (Canberra Tennelec Series 5 XLB, Mirion Technologies, USA) was used to obtain gross alpha and gross beta activity as shown in Figure 2. The alpha and beta efficiency of the instrument was determined by using Am-241 and Sr-90 standard source, respectively. For samples with residual weight of more than 5mg/cm$^2$, the efficiency was determined using attenuation standards prepared at different weights of $U_3O_8$ for gross alpha and KCl for gross beta. The counting was conducted for 100 minutes of 3 cycles.

Figure 2: Low Background Gross Alpha Gross Beta Counting System

**Calculation of Gross Alpha and Gross Beta Activity**

The raw data in count per minute (cpm) obtained from the counting system was used to calculate gross alpha and gross beta activity in Bq/L. The calculation of gross alpha and gross beta activity is

performed using Equation (1) (Norfaizal et. al., 2016) and uncertainty is estimated using Equation (2) (Zal U'yun et. al.(a), 2016). The minimum detectable activity (MDA) is calculated based on Equation (3) (Zal U'yun et. al. (b), 2016).

$$A_{GAB} = \frac{cpm_s - cpm_b}{E \times V \times 60} \quad (1)$$

Where:
$A_{GAB}$ : specific activity of gross alpha or gross beta (Bq/L)
$cpm_s$ : gross alpha or gross beta counts per minute in sample
$cpm_b$ : gross alpha or gross beta counts per minute in background
E : counting efficiency
V : sample volume (L)

$$U_c(A)/A = [\sqrt{[(U(n)/n)2 + (U(t)/t)2 + (U(\text{Ɛ})/\text{Ɛ})2 + (U(V)/V)2 + \ldots.] \quad (2)$$

Where:
$U_c(A)$ : uncertainty of gross alpha or gross beta (Bq/L)
A : activity of gross alpha or gross beta (Bq/L)
U(n) : uncertainty of net count for gross alpha or gross beta (cpm)
n : net count for gross alpha or gross beta (cpm)
U(t) : uncertainty of counting time (second)
t : counting time (second)
U(Ɛ) : uncertainty of counting efficiency
Ɛ : counting efficiency
U(V) : uncertainty of sample volume (L)
V : sample volume (L)

$$MDA = (1.645)(\sqrt{(C_{bg}/t_c)}) \quad (3)$$

Where:
1.645 : confidence level 95%
$C_{bg}$ : background count (cps)
$t_c$ : counting time (second)

## RESULTS AND DISCUSSION

Table 2 shows the results of gross alpha and gross beta activity in the AMB sample. Gross alpha activity in the AMB sample was found to be between <0.0011 – 0.0551 Bq/L. Only 6 (9.7%) out of 62 samples received indicated an activity reading above MDA which is between 0.0061 - 0.0551 Bq/L. On the other hand, gross beta activity was in the range of <0.0036 – 0.2087 Bq/L. A total of 25 (40.3%) out of 62 samples had a result that was higher than the MDA which specified between 0.0105 to 0.2087 Bq/L. MDA for gross alpha ranged 0.0011 – 0.0135 Bq/L, and 0.0036 – 0.0060 Bq/L for gross beta. MDA for both gross alpha and gross beta revealed no significant variations between samples.

Table 2. Gross alpha and gross beta activity in bottled drinking water (AMB)

| Sample No. | Gross Alpha Activity (Bq/L) | Uncertainty (Bq/L) | MDA (Bq/L) | Gross Beta Activity (Bq/L) | Uncertainty (Bq/L) | MDA (Bq/L) |
|---|---|---|---|---|---|---|
| AMB1 | 0.0266 | 0.0087 | 0.0049 | 0.1969 | 0.0116 | 0.0055 |
| AMB2 | <0.0015 | - | 0.0015 | <0.0055 | - | 0.0055 |

| | | | | | | |
|---|---|---|---|---|---|---|
| AMB3 | <0.0015 | - | 0.0015 | <0.0055 | - | 0.0055 |
| AMB4 | <0.0015 | - | 0.0015 | <0.0055 | - | 0.0055 |
| AMB5 | <0.0017 | - | 0.0017 | <0.0060 | - | 0.0060 |
| AMB6 | <0.0017 | - | 0.0017 | <0.0060 | - | 0.0060 |
| AMB7 | <0.0017 | - | 0.0017 | <0.0060 | - | 0.0060 |
| AMB8 | <0.0014 | - | 0.0014 | <0.0051 | - | 0.0051 |
| AMB9 | <0.0014 | - | 0.0014 | <0.0051 | - | 0.0051 |
| AMB10 | <0.0019 | - | 0.0019 | 0.0135 | 0.0057 | 0.0051 |
| AMB11 | <0.0045 | - | 0.0045 | 0.0406 | 0.0074 | 0.0052 |
| AMB12 | <0.0016 | - | 0.0016 | <0.0056 | - | 0.0056 |
| AMB13 | <0.0016 | - | 0.0016 | 0.0114 | 0.0057 | 0.0052 |
| AMB14 | <0.0016 | - | 0.0016 | <0.0048 | - | 0.0048 |
| AMB15 | <0.0016 | - | 0.0016 | <0.0048 | - | 0.0048 |
| AMB16 | <0.0014 | - | 0.0014 | <0.0047 | - | 0.0047 |
| AMB17 | <0.0011 | - | 0.0011 | <0.0045 | - | 0.0045 |
| AMB18 | <0.0015 | - | 0.0015 | <0.0045 | - | 0.0045 |
| AMB19 | <0.0014 | - | 0.0014 | <0.0046 | - | 0.0046 |
| AMB20 | <0.0023 | - | 0.0023 | 0.0115 | 0.0051 | 0.0046 |
| AMB21 | <0.0014 | - | 0.0014 | <0.0046 | - | 0.0046 |
| AMB22 | <0.0014 | - | 0.0014 | <0.0046 | - | 0.0046 |
| AMB23 | <0.0014 | - | 0.0014 | <0.0046 | - | 0.0046 |
| AMB24 | <0.0014 | - | 0.0014 | <0.0046 | - | 0.0046 |
| AMB25 | <0.0014 | - | 0.0014 | <0.0046 | - | 0.0046 |
| AMB26 | <0.0025 | - | 0.0025 | 0.0705 | 0.0082 | 0.0044 |
| AMB27 | <0.0014 | - | 0.0014 | 0.0146 | 0.0052 | 0.0044 |
| AMB28 | <0.0020 | - | 0.002 | 0.0275 | 0.0063 | 0.0048 |
| AMB29 | <0.0019 | - | 0.0019 | <0.0044 | - | 0.0044 |
| AMB30 | <0.0015 | - | 0.0015 | <0.0047 | - | 0.0047 |
| AMB31 | <0.0015 | - | 0.0015 | <0.0047 | - | 0.0047 |
| AMB32 | <0.0015 | - | 0.0015 | 0.0257 | 0.0062 | 0.0048 |
| AMB33 | <0.0015 | - | 0.0015 | <0.0048 | - | 0.0048 |
| AMB34 | <0.0015 | - | 0.0015 | <0.0048 | - | 0.0048 |
| AMB35 | <0.0018 | - | 0.0018 | 0.0232 | 0.0058 | 0.0046 |
| AMB36 | <0.0015 | - | 0.0016 | 0.0255 | 0.0059 | 0.0046 |
| AMB37 | <0.0015 | - | 0.0015 | 0.0486 | 0.0073 | 0.0046 |
| AMB38 | 0.0484 | 0.0071 | 0.0018 | 0.1431 | 0.0111 | 0.0045 |
| AMB39 | 0.0551 | 0.0088 | 0.0025 | 0.2087 | 0.0132 | 0.0045 |
| AMB40 | <0.0015 | - | 0.0015 | <0.0045 | - | 0.0045 |
| AMB41 | <0.0015 | - | 0.0015 | <0.0048 | - | 0.0048 |
| AMB42 | <0.0013 | - | 0.0013 | <0.0051 | - | 0.0051 |
| AMB43 | <0.0135 | - | 0.0135 | 0.0105 | 0.0053 | 0.0048 |
| AMB44 | <0.0025 | - | 0.0025 | 0.0145 | 0.0044 | 0.0036 |
| AMB45 | <0.0013 | - | 0.0013 | <0.0051 | - | 0.0051 |
| AMB46 | <0.0019 | - | 0.0019 | 0.0131 | 0.0053 | 0.0046 |
| AMB47 | <0.0015 | - | 0.0015 | 0.0479 | 0.0079 | 0.0053 |
| AMB48 | <0.0015 | - | 0.0015 | <0.0053 | - | 0.0053 |

| | | | | | | |
|---|---|---|---|---|---|---|
| AMB49 | 0.0099 | 0.0049 | 0.0035 | 0.1384 | 0.0111 | 0.0048 |
| AMB50 | 0.0063 | 0.0038 | 0.0033 | 0.1205 | 0.0104 | 0.0048 |
| AMB51 | <0.0015 | - | 0.0015 | <0.0046 | - | 0.0046 |
| AMB52 | <0.0012 | - | 0.0012 | <0.005 | - | 0.005 |
| AMB53 | <0.0012 | - | 0.0012 | <0.005 | - | 0.005 |
| AMB54 | <0.0013 | - | 0.0013 | <0.0036 | - | 0.0036 |
| AMB55 | <0.0015 | - | 0.0015 | <0.005 | - | 0.005 |
| AMB56 | <0.0015 | - | 0.0015 | 0.0199 | 0.0063 | 0.005 |
| AMB57 | <0.0018 | - | 0.0018 | <0.0052 | - | 0.0052 |
| AMB58 | 0.0061 | 0.0027 | 0.0019 | 0.0141 | 0.0056 | 0.0042 |
| AMB59 | <0.0017 | - | 0.0017 | 0.0302 | 0.0063 | 0.0044 |
| AMB60 | <0.0017 | - | 0.0017 | <0.0044 | - | 0.0044 |
| AMB61 | <0.0019 | - | 0.0019 | 0.0405 | 0.0064 | 0.0042 |
| AMB62 | <0.0017 | - | 0.0017 | 0.0765 | 0.0085 | 0.0044 |
| **Range** | <0.0011 – 0.0551 | | 0.0011 - 0.0135 | <0.0036 – 0.2087 | | 0.0036 – 0.0060 |
| **Mean** | 0.0254 | | 0.0020 | 0.0555 | | 0.0048 |

The results of the analysis of gross alpha and gross beta in AMS are shown in Table 3. The results revealed that the activity of gross alpha and gross beta ranged between <0.0013 - 0.0469 Bq/L and <0.0048 - 0.2245, respectively. A total of 21 samples were received, with 6 (28.6%) values above the MDA for gross alpha and 15 (71.4%) exceeding the MDA for gross beta.

The percentage of AMS samples that exceed the MDA value for AMS was much higher as compared to AMB. This demonstrated that the activity of gross alpha and gross beta in AMS, is higher in general compared to AMB. The typical processing of AMB involves filtration and purification procedures, which have the potential to eliminate radioactive-contained minerals and heavy metals, resulting in a reduced presence of radioactivity (Khandaker, et.al., 2017).

However, this finding needs further investigation due to the smaller number of AMS samples as compared to AMB, which also causes the percentage of AMS samples with activity more than MDA to be higher.

Table 3. Gross alpha and gross beta activity in bottled natural mineral water (AMS)

| **Sample No.** | **Gross Alpha Activity (Bq/L)** | **Uncertainty (Bq/L)** | **MDA (Bq/L)** | **Gross Beta Activity (Bq/L)** | **Uncertainty (Bq/L)** | **MDA (Bq/L)** |
|---|---|---|---|---|---|---|
| AMS1 | <0.0013 | - | 0.0013 | <0.0053 | - | 0.0053 |
| AMS2 | <0.0036 | - | 0.0036 | 0.0107 | 0.0053 | 0.0049 |
| AMS3 | <0.0021 | - | 0.0021 | <0.0053 | - | 0.0052 |
| AMS4 | <0.0021 | - | 0.0021 | <0.0052 | - | 0.0052 |
| AMS5 | <0.0021 | - | 0.0021 | <0.0052 | - | 0.0052 |
| AMS6 | <0.0123 | - | 0.0094 | 0.0123 | 0.0065 | 0.006 |
| AMS7 | <0.0021 | - | 0.0021 | 0.0732 | 0.007 | 0.0049 |
| AMS8 | <0.0021 | - | 0.0021 | <0.0048 | - | 0.0048 |
| AMS9 | 0.0063 | 0.0036 | 0.0028 | 0.0667 | 0.0082 | 0.0045 |
| AMS10 | 0.0039 | 0.0029 | 0.0024 | 0.0474 | 0.0074 | 0.0047 |

| | | | | | | |
|---|---|---|---|---|---|---|
| AMS11 | <0.0014 | - | 0.0014 | 0.0129 | 0.0061 | 0.0045 |
| AMS12 | <0.0013 | - | 0.0013 | <0.0051 | - | 0.0051 |
| AMS13 | 0.0102 | 0.0048 | 0.0033 | 0.2245 | 0.0105 | 0.0036 |
| AMS14 | <0.0038 | - | 0.0038 | 0.0243 | 0.0061 | 0.0048 |
| AMS15 | <0.0034 | - | 0.0034 | 0.0144 | 0.0053 | 0.0045 |
| AMS16 | <0.0042 | - | 0.0042 | 0.0139 | 0.0053 | 0.0046 |
| AMS17 | 0.0094 | 0.005 | 0.0038 | 0.0424 | 0.0105 | 0.0044 |
| AMS18 | 0.0469 | 0.012 | 0.0058 | 0.0771 | 0.0086 | 0.0046 |
| AMS19 | <0.0038 | - | 0.0038 | 0.0681 | 0.0080 | 0.0043 |
| AMS20 | 0.0141 | 0.0053 | 0.0032 | 0.0439 | 0.0073 | 0.0043 |
| AMS21 | <0.0047 | - | 0.0047 | 0.0224 | 0.0058 | 0.0044 |
| **Range** | <0.0013 – 0.0469 | | 0.0013 – 0.0094 | <0.0048 – 0.2245 | | 0.0036 - 0.0060 |
| **Mean** | 0.0151 | | 0.0020 | 0.05028 | | 0.0048 |

The gross beta activity in all samples was found higher than the gross alpha activity. This finding is in agreement with Yussuf, et. al, (2012) who determined the activity of U-238, Th-232 and K-40 in natural mineral and drinking water samples. The activity concentration of U-238 and Th-232 which contributed to gross alpha activity in a sample, was found to be substancially lower than activity of K-40 which correlated to gross beta activity in a sample. Hence, the activity of gross beta was found to be higher compared to gross alpha. Apart from that, secular equilibrium that has been established between U-238 and its progenies, Th-234 and Pa-234m, making both radionuclides prominent β emitters alongside K-40 (Borrego-Alonso et.al., 2023).

The range of MDA for gross alpha and gross beta in AMB is 0.0011 – 0.0135 Bq/L and 0.0036 – 0.0060 Bq/L, respectively. The MDA range for gross alpha in AMS was 0.0013 – 0.0094, which was greater than the MDA range for gross alpha in AMB. On the other hand, the range of MDA for gross beta was found to be consistent in both AMB and AMS samples. This is in line with the findings by Ho et. al., (2020) that MDA for gross alpha was less consistent compared to gross beta. The inconsistent MDA value of gross alpha in the AMS sample was caused by the presence of more residues in the sample compared to AMB resulting in different MDA values. Higher residues level in a sample will contribute to lower counting efficiency, thus elevating the MDA value.

Although there are samples that have radioactivity more than MDA, but the activity concentration is still lower than the standard mandatory limit set by MOH. Thus, it is safe to say that the radiation dose received from consuming AMS and AMB marketed in Malaysia does not exceed the limit suggested by ICRP.

## CONCLUSION

The results of gross alpha and gross beta analysis on all AMB and AMS samples received from MOH in the year 2020 shown that the values obtained are below the mandatory standard limit, which is 0.1 Bq/L for gross alpha and 1.0 Bq/L for gross beta. This shows that the radiation exposure received from the consumption of marketed AMB and AMS in Malaysia is at a safe level.

**ACKNOWLEDGEMENT**

The authors would like to thank the Food Safety and Quality Division (BKKM) under the Ministry of Health Malaysia (MOH) for the samples provided and all personnels of RAS at the Division of Waste Technology and Environment of the Malaysian Nuclear Agency who were directly or indirectly involved in this work.

**REFERENCES**

Borrego-Alonso, D., Quintana, B. & Lozano, J.C. Revisiting methods for the assessment of naturally-occurring radioactivity in drinking water. Applied Radiation and Isotopes 193, 110667 (2023).

Food Act 1983 (Malaysia) (Akta 281).

Ho, P.L., Hung, L.D., Minh, V.T. et al. Simultaneous Determination of Gross Alpha/Beta Activities in Groundwater for Ingestion Effective Dose and its Associated Public Health Risk Prevention. Sci Rep 10, 4299 (2020).

ICRP. Nuclear decay data for dosimetric calculations. ICRP Publication 107. Annals of the ICRP, Volume 38(3), (2008).

Khandaker, M.U., Mohd Nasir, N. L., Zakirin, N.S., Abu Kassim, H., Asaduzzaman, K., Bradley, D.A., Zulkifli, M.Y. & Hayyan, A. Radiation dose to the Malaysian populace via the consumption of bottled mineral water. Radiation Physics and Chemistry (140), 173-179 (2017).

Norfaizal Mohamed@Mohamad, Zal U'yun Wan Mahmood & Nita Salina Abu Bakar. Procedure for Radioactivity Determination of Gross Alpha and Gross Beta in Bottled Drinking/Mineral Water and Environmental Sample using Low Background Gross Alpha/Beta Counting System, May 2016, NUKLEARMALAYSIA/L/2016/64(S).

Pintilie, V., Ene, A., Georgescu, L. P., Morar, L. & Iticescu, C. Measurements of gross alpha and beta activity in drinking water from Galati region, Romania. Romanian Reports in Physics 68(3), 1208–1220 (2016).

WHO. Guidelines for drinking-water quality 4ed Ch. 9, 203–218, WHO publications, Geneva (2017).

Yussuf, N. M., Hossain, I. & Wagiran, H.. Natural radioactivity in drinking and mineral water in Johor Bahru (Malaysia). Scientific Research and Essays Vol. 7(9), 1070-1075 (2012).

Zal U'yun Wan Mahmood, Norfaizal Mohamed@Mohamad & Nita Salina Abu Bakar. Uncertainty Measurement for Radioactivity nalysis of Gross Alpha and Gross Beta in Bottled Drinking/Mineral Water and Environmental Sample using Low Background Gross Alpha/Beta Counting System, May 2016, NUKLEARMALAYSIA/L/2016/66(S).

Zal U'yun Wan Mahmood, Norfaizal Mohamed@Mohamad & Nita Salina Abu Bakar. A Method Validation Procedure for Radioactivity Determination of Gross Alpha and Gross Beta in Bottled Drinking/Mineral Water and Environmental Sample using Low Background Gross Alpha/Beta Counting System, May 2016, NUKLEARMALAYSIA/L/2016/65(S).

e-Jurnal Sains Nuklear Malaysia, 2023, Vol. 35 (No.2): 9 – 24
*eISSN: 2232-0946*

# DETERMINATION OF ARSENIC TEMPORAL ENRICHMENT IN JURU RIVER'S CORES SEDIMENT USING NUCLEAR ANALYTICAL TECHNIQUES

***Yii Mei-Wo***

Malaysian Nuclear Agency,
43000 Kajang, MALAYSIA
Correspondence author: yii@nm.gov.my

***ABSTRACT***

*Perai Industrial Area is one of the densest industrial and heavily populated zones in Malaysia. Land pollutants from human activities potentially be released into nearby water resources. Of concern arsenic concentration levels in sediments were investigated in the nearby Juru River. Using KC™ Kajak corer, one sediment core was collected at the river estuary and another one within the river, about 2-3 km away from the estuary. Arsenic concentrations were measured using Neutron Activation Analysis (NAA) technique; whereas the sediment deposition rates were determined through Lead-210 dating, performed using a Gamma-ray Spectrometry System. The enrichment factor for arsenic in the river was calculated using continental crust values and iron concentration as the normalisation metal. The results (9.7 – 25.9 (average 15.7) µg/g, within river; 10.2 – 24.0 (average 14.5) µg/g, estuary) indicated significant enrichment of arsenic in the study area, and the sedimentation rates (0.94±0.11 cm/y, within river; 2.70±0.68 cm/y, estuary) suggested rapid deposition of contaminants.*

**Keywords:** arsenic, Juru river, Neutron Activation Analysis (NAA), enrichment

## INTRODUCTION

Nearly 40% of the world's population lives within 100 km of the coast. The exploitation of coastal natural resources during development and the use of coastal areas as receptacles for societal waste have promoted sediment contamination and endangered marine resources (Burke et al., 2001; Cochran & Masque, 2004; United Nation, 2017). Erosion process at river and coastal bring soils and terrestrial chemical and biological wastes into the aquatic environment and combined together as sediment. While weathering is a major source of sediments, rapid economic growth and settlement development can lead to the release of domestic waste materials into coastal areas, resulting in their accumulation in sediments (Joseph et al., 2018). The Perai Industrial Estate is one of the major industrial parks in Penang and Malaysia. Due to heavy industrial development and population growth in the vicinity of the Perai industrial area, it is suspected that industrial and household discharges are being released into the river. The nearby Juru River has been reported as one of the most polluted rivers in the country (Zainudin, 2010).

Land pollutants from human activities transported to rivers and end up in marine ecosystem continuously. Time deposition of such pollutants can be chronologised by using natural radionuclides such as $^{210}$Pb. Pb-210 ($T_{1/2}$ = 22.20±0.22 years), a member of the $^{238}$U decay series, is present in the sediments through two main routes. Firstly, there is a continuous *in-situ* production of $^{210}$Pb from

$^{226}$Ra ($T_{1/2}$ = 1600±7 years), and this fraction, known as background or supported $^{210}$Pb, is assumed to be in radioactive secular equilibrium with $^{226}$Ra. On the other hand, $^{222}$Rn ($T_{1/2}$ = 3.8235±0.0003 days) which is a noble gas, emanates from the Earth's surface and goes into the atmosphere where it decays into $^{210}$Pb, which is removed from the atmosphere back to the Earth's surface (by wet precipitation and/or dry fallout) contributing to the unsupported or excess fraction of $^{210}$Pb (Krishnaswami & Lal, 1978). This atmospheric addition of $^{210}$Pb is over of the amount permanently supplied by the *in-situ* decay of $^{226}$Ra. As time goes by, the activity of excess $^{210}$Pb will decay until reaching equilibrium with the supported $^{210}$Pb fraction ($^{226}$Ra). The activity differences between the initial excess $^{210}$Pb (at the surface of the sediment core) and the subjacent core sections can be used to estimate the time when the sediment at this section was deposited (Chakrabarty et al., 2006; Likuku, 2006; Aliev et al., 2007; Sanchez-Cabeza & Ruiz-Fernández, 2012; Wan-Mahmood et al., 2016). Historical deposition of anthropogenic radionuclide such as $^{137}$Cs ($T_{1/2}$ = 30.05±0.08 years) can be used to complement the deposition profile.

Inorganic pollutants such as arsenic, that are released into river water can be accumulated in the aquatic food chain and sediments (Islam et al., 2017; Li et al., 2017; Yunus et al., 2020), and promote adverse effects on aquatic life (Yi et al., 2011; Elias et al., 2012), and also to humans through fish consumption. The major sources of inorganic anthropogenic pollution are from agriculture activities, animal waste, domestic, industrial, mining and petroleum activities, as well as industrial emissions (Shazili et al., 2006; Zhu et al., 2011; Pandey & Singh, 2017). Arsenic is an odourless, tasteless but toxic element that can cause numerous human health effects. Inorganic arsenic is a known carcinogen that can cause various cancers in the skin, lungs, liver and bladder (Yunus et al., 2020). Exposure to high amounts of arsenic can also bring fatality.

This study is aimed to assess the sediment deposition rates by radionuclides measurement, as well as the concentration and enrichment of arsenic in two sediment cores collected from Juru River, Penang, that might have been promoted by the economic development and population growth in the Perai Industrial area.

## MATERIALS AND METHODS

### Sample collection and preparation

Sediment cores were collected at Juru River during the dry season in 2017, one within the estuary zone and another 2 - 3 km upriver, in river (Fig. 1) to avoid massive mud transportation into the river sediment by the heavy downpour during the rainy season and the water turbulence that disturbs the sediment surface. The cores were collected using a KC™ Kajak Core Sampler (Fig. 2) with an 8 cm diameter PVC tube. Pre-preparation, handling and treatment of samples were according to the same procedure as reported earlier by Yii et al. (2020a).

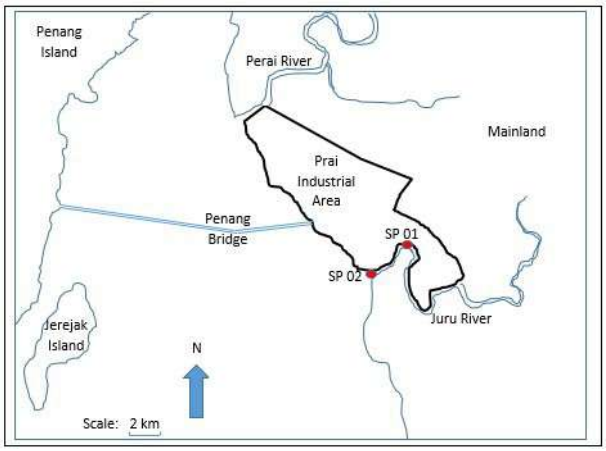


Figure 1. Sampling location

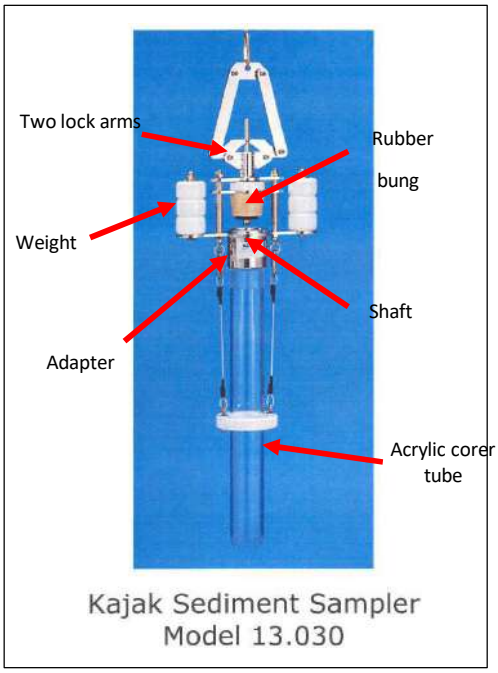


Figure 2. Sampling corer

Table 1. Sampling location details

| Date | Station | Coordinate | Core length (cm) |
|---|---|---|---|
| Feb 2017 | SP 01, Juru River | 5.3464 °N 100.4189 °E | 74 |
| Feb 2017 | SP 02, Juru River | 5.3395 °N 100.4048 °E | 78 |

**Radionuclides analysis**

Pb-210, $^{226}$Ra and $^{137}$Cs activities were determined by gamma-ray spectrometry (Fig. 3) consisting of a high-purity germanium (HPGe) setup and a multichannel analyser (16,384 channels). This 25% relative efficiency p-type closed end coaxial well-detector from CANBERRA™ operates at 2,000 HV bias supply (detector: 62 mm diameter, 49 mm, and 5 mm distance from a window; well: 35.5 mm depth, 23.5 mm diameter, active volume 8.8 cc), is designed to provide FWHM resolution of 1.85 keV at 1332 keV gamma-ray line of $^{60}$Co and 820 eV at 122 keV gamma-ray line of $^{57}$Co. The detector is shielded in an 11 cm thick chamber made of lead, cadmium and copper to reduce cosmic radiation. It was calibrated with the same procedures as reported earlier by Yii et al. (2009) using a customised gamma multi-nuclide standard source (source no. 1290-84 and 1755-30 from Isotope Products Laboratories, USA) comprised of $^{210}$Pb, $^{241}$Am, $^{109}$Cd, $^{57}$Co, $^{123m}$Te, $^{51}$Cr, $^{113}$Sn, $^{85}$Sr, $^{137}$Cs, $^{88}$Y and $^{60}$Co in the same counting geometry. Fine ground dry sediments from each section of the core were sealed in a 6 mL cylindrical HDPE container with thick PVC tape to inhibit radon from escaping

(Yii et al., 2016). The net weight of each sample was recorded and divided by the sample volume to obtain sample density. All samples were stored for at least 30 days to establish secular equilibrium between $^{226}$Ra and their respective progenies before gamma counting (Dowdall & O'dea, 2002; Yang et al., 2005).

Samples were counted for 15 hours and corrected for density and sampling date. Background counts were determined by counting similar geometry containers filled with inert material over the weekend. The counting times were long enough to ensure a 2π counting error of less than 10% (Ahmed & El-Arabi, 2005; Arogunjo et al., 2005; El-Reefy et al., 2006). The $^{226}$Ra were measured through the gamma transitions of its progenies; $^{214}$Pb (295.21 and 351.92 keV) and $^{214}$Bi (609.31 keV, 1120.29 keV and 1764.49 keV). Meanwhile, $^{210}$Pb was measured directly *via* energy 46.5 keV peak and $^{137}$Cs was measured directly *via* energy 661.62 keV peak (Mishra & Sadasivan, 1971; Yang et al., 2005; El-Reefy et al., 2006). The sample activities were calculated using the equation reported by Yang et al. (2005) and Chen et al. (2005). The minimum detectable activity (MDA) for the radionuclides of interest was quantified as follows: $^{226}$Ra (1 Bq/kg), $^{210}$Pb (5 Bq/kg) and $^{137}$Cs (1 Bq/kg). Reference materials IAEA-Soil-6 ($^{226}$Ra, 69.56 – 93.43 Bq/kg; $^{137}$Cs, 51.43 – 57.91 Bq/kg at 30$^{th}$ January 1983) and IAEA-412 ($^{210}$Pb, 85.0 – 91.4 Bq/kg at 1$^{st}$ January 2019) were used for quality control evaluation. The results of samples were accepted if values obtained for the reference material fell within these 95% confidence interval as mentioned in the certificate.


Figure 3. Radioactivity measurement (from left to right): samples, well detector, gamma spectrometry system.

**Trace elements analysis**

Trace elements present in sediment samples were analysed using the NAA method (Fig. 4). Neutron Activation Analysis (NAA) is a non-destructive analytical technique where digestion or extractions, are not required, and therefore the integrity of the sample is not changed by the addition of any foreign materials for irradiation. Thus, the problem of reagent introduced contamination is completely avoided (Elias et al., 2014). The physical phenomenon upon which NAA is based in the properties of the nucleus, radioactivity and the interaction of radiation with matter. The neutron source from the reactor interacts with the target nucleus (samples – soil, sediment, or plant) by non-elastic collision; a compound nucleus is formed in a highly excited state, and a target nucleus (new nucleus) becomes radioactive and will further get de-excited by emitting decay gamma rays (IAEA 1990). The intensities of the gamma rays which can be quantified using the Gamma Spectrometry system are proportional to their concentrations.

For the NAA analysis, approximately 0.1 g powdered duplicate sediment aliquots were stored separately in heat-sealed polyethylene vials. Reference material IAEA-Soil-7 (Arsenic ranged between 12.5 – 14.2 µg/g at 95% confidence interval) was used as quality control material. All

samples were irradiated (up to 6 hours at a rotating rack) with a thermal neutron flux of $4.0\times10^{12}$ n $cm^{-2}$ $s^{-1}$ obtained from the TRIGA Mark II research reactor located at the Malaysian Nuclear Agency which operated at 750 kW using pneumatic transport facility. Irradiated samples were left aside to allow the decay process before gamma-ray spectrometry counting, the cooling duration varied from 2 to 4 days before performing the first counting, and 3 to 4 weeks for the second counting. The radioisotope of the elements counted and their characteristics are shown in Table 2 (Ashraf et al., 2018; Elias et al., 2018).

Table 2. The elements and radionuclides measured using Neutron Activation Analysis (NAA)

| Elements | Radionuclides | Half-life | γ-ray Energy (keV) |
|---|---|---|---|
| As | $^{76}$As | 26.4 hours | 559 |
| Fe | $^{59}$Fe | 45.1days | 1099,1292 |

The gamma-ray detector used for the NAA analysis was a closed end coaxial 3" x 3" HPGe detector connected to a multichannel analyser that was previously calibrated from low to high energies by using a mixed standard solution including $^{241}$Am (59.5 keV), $^{109}$Cd (88.1 keV), $^{57}$Co (122.1, 136.5 keV), $^{133}$Ba (81.0, 303.0, 356.0, 384.0 keV), $^{137}$Cs (661.7 keV), $^{60}$Co (1173.2, 1332.5 keV) and $^{88}$Y (898.0, 1836.1 keV) (Saion et al. 2007; Alnour et al. 2014). The gamma-ray spectrometry counting process of the irradiated samples, mixed standard solution and reference material was performed for one hour each. The results of the samples were accepted when the values obtained for the reference material fell within the 95% confidence interval as mentioned in the certificate.

Figure 4. NAA metal analysis (from left to right): Samples, neutron irradiation, gamma counting

**Enrichment factor (EF)**

The enrichment factor (EF) was calculated based on Equation (1) to evaluate the potential contamination caused by trace elements (Elias et al., 2018):

$$EF = \frac{(M/R)_{measure}}{(M/R)_{CC}} \qquad (1)$$

where $(M/R)_{measure}$ is the concentration ratio of the element of interest (M) to the reference element (R) measured in the sample, and $(M/R)_{CC}$ is the concentration ratio in the continental crust (Wedepohl, 1995).

Iron (Fe) was used as a reference element to normalise the trace element concentrations to compensate for variations in particle size and mineralogy (Loring & Rantala, 1992). Iron was selected as a reference element for normalisation in the EF calculation as no significant correlations were observed between Fe and the trace element concentrations found. Deely & Fergusson (1994) reported that this is due to iron distribution not being related to other elements. The natural concentration of iron is

usually relatively high, and therefore the estuarine sediment not expected to be substantially enriched by the anthropogenic source (Niencheski et al., 1994; Abrahim & Parker, 2008). The EF value will be less than 2.0 if the element found in the sediment originated predominantly from the lithogenous materials, whereas EFs are much greater than 2.0 indicating that the element is of anthropogenic origin (Szefer et al., 1996). EF values were classified according to Abdullah et al. (2020) as shown in Table 3.

Table 3. The indication status of enrichment factor (Abdullah et al., 2020)

| **Enrichment factor (EF) value** | **Enrichment status** |
|---|---|
| < 2 | Depletion to minimal enrichment |
| between 2 to 5 | Moderate enrichment |
| between 5 to 20 | Significant enrichment |
| between 20 to 40 | Very high enrichment |
| more than 40 | Extremely high enrichment |

## RESULTS AND DISCUSSION

### Radionuclide activities

The activity concentrations for $^{137}$Cs, $^{210}$Pb and $^{226}$Ra in each core are illustrated in Fig. 5 and summarised in Table 4. The $^{137}$Cs activities are below the detection limit of 1 Bq/kg for all sediment cores. Meanwhile, $^{226}$Ra activity ranges (Bq/kg) are highly variable among cores, with the highest values observed in the core collected upriver (Table 4). These values are higher than those found in sediment cores from previous studies in Asia (e.g. east coastal area of Peninsular Malaysia, 46.2 – 121.5 Bq/kg (Wan-Mahmood et al., 2005) and Vietnam coast, 23.1 – 40.2 Bq/kg (Nguyen et al., 2009); the Economic Exclusive Zone of the east coast of Peninsular Malaysia, 16 – 46 Bq/kg (Wan-Mahmood & Yii, 2012), or elsewhere, e.g. Gulf of Mexico, 11.8 – 97.3 Bq/kg (James et al., 1998); Santos - Cubatão drainage basin, 28.2 – 80.0 Bq/kg (Sanders et al., 2010); Estuary of Coatzacoalcos River, 15.57±1.4 Bq/kg (Ruiz-Fernandez et al., 2012)), but much lower than values reported for Krka River estuary, 45 – 662 Bq/kg (Cuculic et al., 2006)). A single factor ANOVA analysis revealed that $^{226}$Ra activities are significantly different among cores: where SP 01 (97.0±32.8 Bq/kg) > SP 02 (53.9±9.9 Bq/kg).

Cores SP 01 (the upriver core) shows high variability of $^{226}$Ra activities as shown in Fig. 5. This variability could potentially be attributed to the influx of radioactivity from the mainland, which is likely a result of human activities, such as the use of phosphate fertiliser in agriculture. Transported radionuclides eluted from soil and contained in dry and wet atmospheric precipitation ($^{210}$Pb) are deposited together onto sediment (Li et al., 1977).

Activities of $^{210}$Pb are also found higher than those previously reported in the region such as in Kuala Muda area (north west Peninsular Malaysia), 11.9 – 78.8 Bq/kg (Yii et al., 2010), Linggi River Estuary (south west Peninsular Malaysia), 37.9 – 176.2 Bq/kg (Wan-Mahmood et al., 2016), and Brunei Bay, 2.6 – 32.3 Bq/kg (Joseph et al., 2018). Again, the single factor ANOVA analysis revealed that there are significant differences between cores for the $^{210}$Pb activities where SP01 (154.7±51.5 Bq/kg) > SP02 (100.2±20.0 Bq/kg).

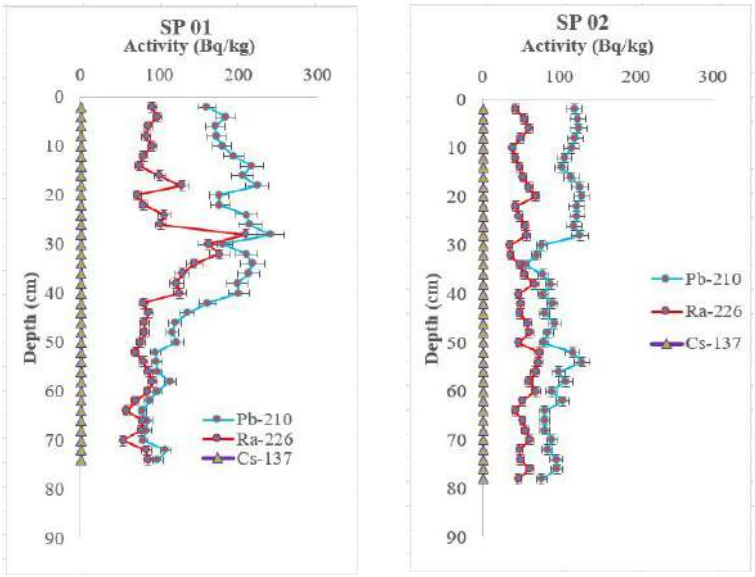


Figure 5. Activity concentrations of $^{137}$Cs, $^{210}$Pb and $^{226}$Ra in the sediment core at Juru River

Figure 5 above clearly shows that the activities of $^{210}$Pb are mostly found higher than $^{226}$Ra along both cores, and the equilibrium between both radionuclides is only achieved at cores SP01(after 50 cm). The excess $^{210}$Pb ($^{210}Pb_{ex}$) activities were estimated from the difference between $^{210}$Pb and $^{226}$Ra activities (Table 4). It has been shown that $^{210}$Pb may be associated with biogenic particles and high $^{210}$Pb activities may be derived from the lithogenic inclusion (Bralower & Thierstein, 1987). Lead-210 is highly particle reactive and is readily scavenged by organic matter and clay size particles (Ontiveros-Cuadras et al., 2012), although under anoxic conditions, $^{210}$Pb can be released back to the water column (Benoit, 1988).

Table 4. Radioactivity concentrations of $^{226}$Ra, $^{210}$Pb, their ratios and sedimentation rate at Juru River

| **Sampling Station** | **Activity concentration (Bq/kg dw.)** | | | **$^{210}$Pb excess (Bq/kg dw.)** | **Sedimentation accumulation rate (cm/y)** |
|---|---|---|---|---|---|
| | **$^{137}$Cs** | **$^{226}$Ra** | **$^{210}$Pb** | | |
| SP 01 | < MDA | 54.0 – 209.9 | 78.8 – 241.0 | 5.9 – 142.0 | 0.94±0.11 |
| SP 02 | < MDA | 36.0 – 74.3 | 56.5 – 129.9 | 8.4 – 79.3 | 2.70±0.68 |

The logarithmic values of $^{210}Pb_{ex}$ activity depth profiles in both cores show significant departures from linearity (Fig. 6), characteristic of a profile resulting only from radioactive decay, in aquatic environments where a steady state sedimentation process occurs. In most cases, such divergences could be the result of strong variations in the sediment accumulation process, sediment sources and mixing (UNESCO, 1978). As described in Yii et al. (in press), $^{210}Pb_{ex}$ activities in the cores of this study are strongly influenced by the variations in grain size, and organic matter content.

Despite all the complex features observed in the $^{210}Pb_{ex}$ activity depth profiles, both of them showed significant ($p<0.05$) decreasing trends with depth, with high slope values, which would account for high accumulation rates (Alongi et al., 2005); although, owing to the non-monotic $^{210}Pb_{ex}$ depth profiles, it is very difficult to derive an age model from them. However, attempts are made to approximate a preliminary mean sedimentation rate for each core, by using the constant flux-constant

sedimentation (CF:CS) model (Krishnaswamy et al., 1971), which assumes a constant $^{210}Pb_{ex}$ flux to the sediment surface and a sediment accumulation rate (Sanchez-Cabeza & Ruiz-Fernandez, 2012). Thus, the logarithm of excess $^{210}Pb$ (ln $^{210}Pb_{ex}$) data obtained in this study was plotted against the depth of the sediment core; and the slope of the regression between both variables was used to estimate the mean sediment accumulation rate (SAR, in cm/y). The mean SAR values obtained (Table 4) ranged from 0.94±0.11 cm/y in SP01 to 2.70±0.68 cm/y in SP02. The highest value recorded at station SP 02 corresponds to the estuarine area of Juru River, where reportedly affected by heavy loads of waste water discharges (Zainudin, 2010).

The mean sedimentation rate interval found in this study of 0.94 – 2.70 cm/y is comparable to those reported by Joseph et al. (2018) for Brunei Bay where the sedimentation rates reported range between 0.47 – 2.13 cm/y and higher sedimentation was attributed to rapid urban and industrial development. The study results are also comparable to the sedimentation rates found at the Linggi River estuary between 0.70 – 1.97 cm/y (Wan-Mahmood & Yii, 2013). However, the sedimentation rate found in this study is much higher than in some other areas as reported by Cheevaporn et al. (1994) at Bang Pakong River, Thailand (0.47 – 0.72 cm/y), and by Xu et al. (2008) at Nile River Delta, Egypt (0.42 – 0.56 cm/y).

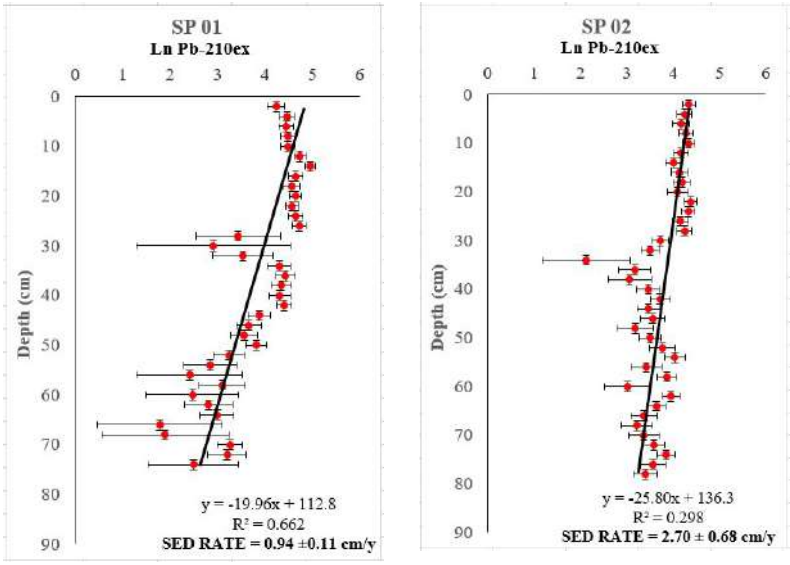


Figure 6. Sedimentation rates in core SP01 and SP02

**Trace elemental concentrations**

Table 5 below summarises the concentration of arsenic and iron found in the study area. Arsenic (As) concentrations in both cores are less than 30 µg/g with a mean of around 15 µg/g. Overall, the concentration ranges for arsenic in this study are comparable to most of the studies reported by other researchers in the same area/region. For instance, studies at Juru River conducted earlier by Wood et al. (1993) reported a range from 0.90 – 12.3 µg/g (As), while Abdullah et al. (2020) reported a range between 1.07 – 12.16 µg/g (As) for surface sediment of Bukit Merah Reservoir, which are half of the current study. A review made by Yunus et al. (2020) reported that most researchers found arsenic concentration level in the sediments at several locations in Peninsular Malaysia ranged between 6.13 – 42.30 µg/g, with an exceptional case where a study in Port Klang's sediment found the arsenic concentration reaching 475.26 µg/g. The study by Yii et al. (2020b) regarding the metal concentration in surface sediment collected along the Juru River indicated that contaminants were released from a

diffuse source upstream at the sampling site.

Table 5. Concentrations and enrichment factor (EF) ranges of arsenic and iron (µg/g) in sediment cores from Juru river

| Element | CC[1] | Location | Concentration Range[2] | EF range |
|---|---|---|---|---|
| **As** | **1.7** | **SP 01** | 9.7 – 25.9 (15.7) | 5.7 – 14.7 (11.3) |
| | | **SP 02** | 10.2 – 24.0 (14.5) | 6.8 – 17.5 (10.0) |
| **Fe** | **43200** | **SP 01** | 25250 – 52560 (36366) | - |
| | | **SP 02** | 33900 – 42100 (37062) | - |

[1]CC = Continental crust values as published by Wedepohl in 1995.
[2]Determined by Neutron Activation Analysis (NAA)
Note: Values given in the parenthesis are the average values

**Enrichment factors**

The enrichment factors obtained in this study (Table 5 and Fig. 7) indicated that sediments are enriched by arsenic in the entire cores collected from SP01 and SP02 with significant enrichment. For core SP 01, the EFs of arsenic showed enrichment throughout the sediment core, especially at the bottom part of the core. Meanwhile, for core SP 02, arsenic also showing significant enrichment especially when reaching the peak at the middle part of the core, while the top and bottom portions of the core are less enriched. Both cores having enrichment with an average EF value of about 10.0.

In summary, the EFs obtained for the arsenic in the sediments from the Juru River are quite significant. The Perai Industrial area is densely populated and is comprised of many heavy industries, and the most probable sources of pollution might be from the manufacturing industries, agriculture and sewage emissions. Other human activities such as the use of arsenical herbicides mining, metallurgy and wood preservation can also introduce arsenic into the water bodies eventually deposited into sediment (Sarmani, 1989; Shazili et al., 2006; Yunus et al., 2020).

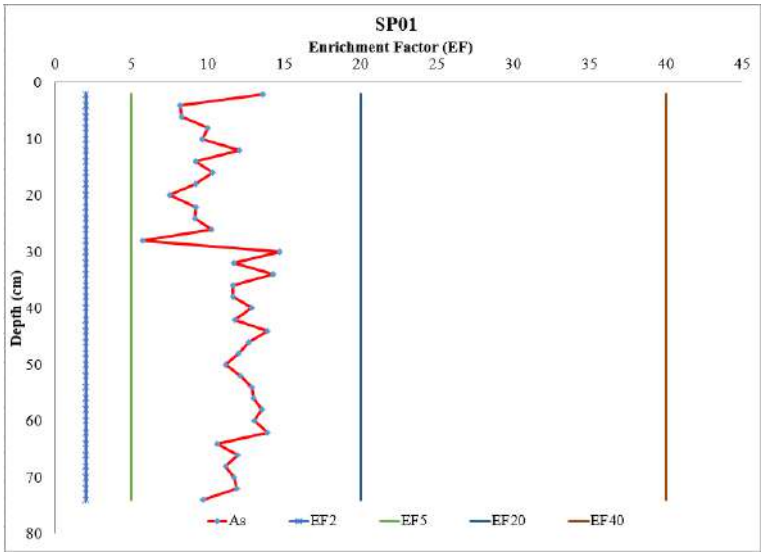

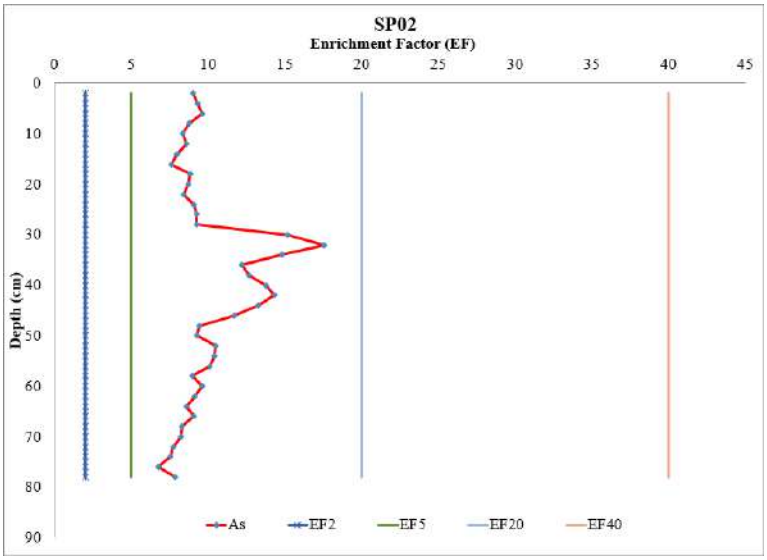


Figure 7. Elemental Enrichment Factor versus depth for core SP01 and SP02

## CONCLUSION

Two sediment cores were collected at the Juru River located in Penang's Perai Industrial Area in February 2017 and analysed using nuclear techniques, with the purpose to evaluate the sediment accumulation rates and to assess the enrichments by arsenic at the study area. Concentrations of arsenic were quantified using Neutron Activation Analysis (NAA) technique. Using gamma spectrometry, $^{210}$Pb and $^{226}$Ra activity profiles were established for each core; however, owing to the complexity of the excess $^{210}$Pb activity profiles obtained, it was not possible to obtain an accurate age model from them. Nonetheless, preliminary apparent sediment accumulation rates were estimated, and were found to range between 0.94 – 2.70 cm/y, with the highest sedimentation rate recorded in the core collected at the estuary of Juru River (SP02). Arsenic was found significantly enriched in the study area but the results are still comparable to other studies, therefore further monitoring and mitigation strategies for the pollutant are strongly recommended to improve environmental sustainability.

## FUTURE WORKS

To have a better understanding of the elemental deposition history at the study area, for future analysis, thin slide of sediment (0.5 cm – 1.0 cm instead of 2 cm that is being practiced now) can be performed to get a better estimation of sediment accumulation rate. Various analytical techniques can be applied as a comparison as well.

## ACKNOWLEDGEMENTS

The author would like to express his special appreciations to the International Atomic Energy Agency for providing research funding under research grant (K41016 – RC 20884), to the project Technical Officer, Ms. Martina Rozmaric Macefat and Member States participating the K41016 project for their

guidance. He would also like to thank the personnel of Radiochemistry and Environment Group (RAS), and Analytical Chemistry Group (ACA) from Malaysian Nuclear Agency for their constant support and cooperation throughout this study.

## REFERENCES

Abrahim, G.M.S. & Parker, R.J. (2008). Assessment of heavy metal enrichment factors and the degree of contamination in marine sediments from Tamaki Estuary, Auckland, New Zealand, *Environ. Monit. Assess.* 136:227–238.

Ahmed, N.K. & El-Arabi, A.G.M. (2005). Natural radioactivity in farm soil and phosphate fertilizer and its environmental implications in Qena governorate, upper Egypt, *J. Environ. Radioact.* 84(1):51–64.

Aliev, R.A., Bobrov, V.A., Kalmykov, St.N., Melgunov, M.S., Vlasova, I.E., Shevchenko, V.P., Novigatsky, A.N. & Lisitzin, A.P. (2007). Natural and artificial radionuclides as a tool for sedimentation studies in the Arctic region, *J. Radioanal. Nucl. Chem.* 274: 315–321.

Alnour, I.A., Wagiran, H., Ibrahim, N., Hamzah, S., Wee, B.S. & Elias, M.S. (2014). New approach for calibration the efficiency of HPGe detectors. In: AIP Conf. Proc. 1584:38–44.

Alongi, D.M., Pfitzner, J., Trott, L.A., Tirendi, F., Dixon, P. & Klumpp, D.W. (2005). Rapid sediment accumulation and microbial mineralization in forests of the mangrove Kandelia candel in the Jiulongjiang Estuary, China, *Estuar. Coast. Shelf Sci.* 63(4):605–618.

Arogunjo, A.M., Ofuga, E.E. & Afolabi, M.A. (2005). Levels of natural radionuclides in some Nigerian cereals and tubers, *J. Environ. Radioact.* 82(1):1–6.

Ashraf, A.R., Saion, E., Gharibshahi, E., Yap, C.K., Kamari, H.M., Elias, M.S. & Rahman S.A. (2018). Distribution of heavy metals in core marine sediments of coastal East Malaysia by instrumental neutron activation analysis and inductively coupled plasma spectroscopy, *Appl. Radiat. Isot.* 132:222–231.

Abdullah, M.I.C., Sah, A.S.R.M. & Haris, H. (2020). Geoaccumulation Index and Enrichment Factor of Arsenic in Surface Sediment of Bukit Merah Reservoir, Malaysia, *Trop. Life Sci. Res.* 31(3): 109–125.

Benoit, G. (1988). The biogeochemistry of $^{210}$Po and $^{210}$Pb in fresh waters and sediments, PhD Dissertation, Massachusetts Institute of Technology, Cambridge, Massachusetts, PB--89-198097/XAB.

Bralower, T.J. & Thierstein, H.R. (1987). Organic carbon and metal accumulation in Holocene and mid-Cretaceous marine sediments: Paleoceanographic significance, *Geol. Soc. Spec. Publ.* 26(1):345–369.

Burke et al. (2001). World Resources Institute (WRI). Washington DC, Paul Harrison and Fred Pearce, AAAS Atlas of Population and Environment 2001, AAAS. University of California Press, Berkeley, 216.

Chakrabarty, A., Jha, S.K., Gothankar, S.S., Tripathi, R.M., Khan, A.H. & Puranik, V.D. (2006). Sedimentation rate of Nagarjuna Sagar Dam using a natural radiotracer. In: Application of Radiotracers in Chemical, Environmental and Biological Sciences, S., Lahiri, D., Nayak, & A. Mukhopadhyay, (eds.). Vol. 2, Saha Institute of Nuclear Physics, Kolkata, 148–150.

Cheevaporn, V., Jacinto, G.S. & Sandiego-Mcglonne, M.L. (1994). History of heavy metal contamination in Bang Pakong river estuary, Thailand, *J. Sci. Soc. Thailand.* 20:9–22.

Chen, S.B., Zhu, Y.G. & Hu, Q.H. (2005). Soil to plant transfer of $^{238}$U, $^{226}$Ra and $^{232}$Th on a uranium mining-impacted soil from south eastern China, *J. Environ. Radioact.* 82(2):223–236.

Cochran, J.K. & Masque, P. (2004). Natural radionuclides applied to coastal zone process. In: Marine Radioactivity, H.D. Livingston, (ed.). Elsevier, Amsterdam, 1–21.

Cuculic, V., Cukrov, N., Barisic, D. & Mlakar, M. (2006). Uranium in sediments, mussels (Mytilus sp.) and seawater of the Krka river estuary, *J. Environ. Radioact.* 85(1):59–70.

Deely, J.M. & Fergusson, J.E. (1994). Heavy metal and organic matter concentration and distributions in dated sediments of a small estuary adjacent to a small urban area, *Sci. Total Environ*. 153(1–2):97–111.

Dowdall, M. & O'dea, J. (2002). Ra-226/$^{238}$U disequilibrium in an upland organic soil exhibiting elevated natural radioactivity, *J. Environ. Radioact.* 59(1):91–104.

Elias, M.S., Hamzah, M.S., Rahman, S.A., Wee, B.S. & Salim, N.A.A. (2012). Assessment of sediment quality collected from Tunku Abdul Rahman Park, Sabah, *Nucl. Sci. J. Malays.* 24(1):59–70.

Elias, M.S., Hamzah, M.S., Rahman, S.A., Wee, B.S., Salim, N.A.A., Sanuri, E., Talib, A., Yatim, J.M., Devi, P., Baharuddin, A.H., Put, E.E., Harun, M.K.A. & Awang, M.K. (2014). Development of Fingerprint Characteristic for forensic Investigation of Elemental Pollution in Sediment From Linggi Area, Tech. Rep. ScienceFund Project (04-03-01-SF0142), NUKLEARMALAYSIA/L/2014/102. Malaysian Nuclear Agency, Kajang, 11.

Elias, M.S., Ibrahim, S., Samuding, K., Rahman, S.A. & Yii, M.W. (2018). Assessment of toxic elements in sediments of Linggi river using NAA and ICP-MS techniques, *MethodsX* 5:454–465.

El-Reefy, H.I., Sharshar, T., Zaghloul, R. & Badran, H.M. (2006). Distribution of gamma-ray emitting radionuclides in the environment of Burullus Lake: I. Soils and vegetation, *J. Environ. Radioact.* 87(2):148–169.

International Atomic Energy Agency (1990). Practical aspects of operating a neutron activation analysis laboratory, TECDOC-564. IAEA, Vienna, 252.

Islam, M.A., Al-Mamun, A., Hossain, F., Quraishi, S.B., Naher, K., Khan, R., Das, R., Tamim, U., Hossain, S.M. & Nahid, F. (2017). Contamination and ecological risk assessment of trace elements in sediments of the rivers of Sundarban mangrove forest, Bangladesh, *Mar. Pollut. Bull.* 124(1):356–366.

James, W.D., Boothe, P.N. & Presley, B.J. (1998). Compton suppression gamma-spectroscopy in the analysis of radium and lead isotopes in ocean sediments, *J. Radioanal. Nucl. Chem.* 236:261–266.

Joseph, B., Adiana, G., Shazili, N.A.M., Ong, M.C., Juahir, H., Shaari, H., Yii, M.W., Kamarudin, M.K.A., Gasim, M.B., Maulud, K.N.A. & Islam, M.S. (2018). The Evaluation of Brunei Bay Sediment Cores Sedimentation Rate Using $^{210}$Pb Radiometric Dating Technique, *Int. J. Res. Eng. Technol.* 7(3.14):107–114.

Krishnaswami, S. & Lal, D. (1978). Radionuclide alimnochronology. In: Lakes, Chemistry, Geology, Physics, A. Lerman, (ed.). Springer Verlag, New York, 153–177.

Krishnaswamy, S., Lal, D., Martin, J. & Meybeck, M. (1971). Geochronology of lake sediments, *Earth Planet. Sci. Lett.* 11(1):407–414.

Li, H., Ye, S., Ye, J., Fan, J., Gao, M. & Guo, H. (2017). Baseline survey of sediments and marine organisms in Liaohe Estuary: heavy metals, polychlorinated biphenyls and organochlorine pesticides, *Mar. Pollut. Bull.* 114(1):555–563.

Li, Y. H., Mathieu, G.G., Biscaye, P. & Simpson, H.J. (1977). The flux of $^{226}$Ra from estuarine and continental shelf sediments, *Earth Planet. Sci. Let.* 37(2):237–241.

Likuku, A.S. (2006). Factors influencing concentrations of $^{210}$Pb and $^{7}$Be over the city of Edinburgh (55.9$^{o}$N, 03.2$^{o}$W), *J. Environ. Radioact.* 87(3): 289–304.

Loring, D.H. & Rantala, R.T.T. (1992). Manual for the geochemical analyses of marine sediments and suspended particulate matter, *Earth-Sci. Rev.* 32(4):235–283.

Mishra, U.C. & Sadasivan, S. (1971). Gamma spectroscopic measurements of soil radioactivity, *Int. J. Appl. Radiat. Isot.* 22:256–257.

Nguyen, T.N., Nguyen, T.B., Nguyen, V.P., Le, N.S., Truong, Y., Mai, T.H., Nguyen, T.L., Nguyen, M.S., Phan, S.H., Le, N.C., Dang, D.N., Nguyen, Q.L., Nguyen, H.Q. & Tran, T.M. (2009). Radionuclides concentration in marine environmental samples along the coast of Vietnam, *Nucl. Sci. J. Malays.* 21(2):12–20.

Niencheski, L.F., Windom, H.L. & Smith, R. (1994). Distribution of particulate trace metal in Patos Lagoon estuary (Brazil), *Mar. Pollut. Bull.* 28(2):96–102.

Ontiveros-Cuadras, J.F., Ruiz-Fernández, A.C., Sanchez-Cabeza, J.A., Wee-Kwong, L.L. & Pérez-Bernal, L.H. (2012). Geochemical fractionation of $^{210}$Pb in oxic estuarine sediments of Coatzacoalcos River, Gulf of Mexico, *J. Radioanal. Nucl. Chem.* 292**:**947–956.

Pandey, J. & Singh, R. (2017). Heavy metals in sediments of Ganga River: Up and down stream urban influences, *Appl. Water Sci.* 7:1669–1678.

Ruiz-Fernandez, A.C., Sanchez-Cabeza, J.A., Alonso-Hernandez, C., Martinez-Herrera, V., Perez-Bernal, L.H., Preda, M., Hillaire-Marcel, C., Gastaud, J. & Quejido-Cabezas, A.J. (2012). Effect of land use change and sediment mobilization on coastal contamination (Coatzacoalcos River, Mexico), *Continental Shelf Res.* 37:57–65.

Saion, E., Wood, A.K.H., Sulaiman, Z.A., Alzahrany, A.A., Elias, M.S. & Wee, B.S. (2007). Determination of heavy metal pollution in depth profile of marine sediment samples from the Strait of Malacca, *Fresenius Environ. Bull*. 16(10):1279–1287.

Sanchez-Cabeza, J.A. & Ruiz-Fernandez, A.C. (2012). Pb-210 sediment radiochronology: An integrated formulation and classification of dating models, *Geochim. Cosmochim. Acta.* 82:183–200.

Sanders, C.J., Sanders, L.M., Smoak, J. M., Patchineelam, S., Machado, W. & Luiz-Silva, W. (2010). Radium-226 and lead-210 ratios along a sediment core profile implying fertilizer industry source. In: Conference AGU meeting of the Americas, August 2010, Foz do Iguacu.

Sarmani, S.B. (1989). The determination of heavy metals in water, suspended materials and sediments from Langat River, Malaysia, *Hydrobiologia.* 176:233–238.

Shazili, N.A.M., Yunus, K., Ahmad, A.S. & Abdullah, N. (2006). Heavy metal pollution status in the Malaysian aquatic environment, *Aquat. Ecosys. Health.* 9(2):137–145.

Skwarzec, B. & Jahnz, A. (2007). The inflow of polonium $^{210}$Po from Vistula river catchments area, *J. Environ. Sci. Health Part A.* 42(14):2117–2122.

Szefer, P., Szefer, K., Glasby, G.P., Pempkowiak, J. & Kaliszan, R. (1996). Heavy–metal pollution in surficial sediments from the Southern Baltic sea off Poland, *J. Environ. Sci. Health.* 31(10):2723–2754.

UNESCO, (1978). UNESCO/SCOR Workshop on The Biogeochemistry of Estuarine Sediments, UNESCO, New York.

United Nation, (2017). Factsheet: People and Oceans. In: The Ocean Conference, United Nations, 05–09 June 2017, New York.

Wan-Mahmood, Z. & Yii, M.W. (2012). Marine radioactivity concentration in the Exclusive Economic Zone of Peninsular Malaysia: $^{226}$Ra, $^{228}$Ra and $^{228}$Ra/$^{226}$Ra, *J. Radioanal. Nucl. Chem.* 292:183–192.

Wan-Mahmood, Z. & Yii, M.W. (2013). Sedimentation rate in the Sungai Linggi estuary using excess $^{210}$Pb and $^{137}$Cs, *J. Radioanal. Nucl. Chem.* 298:1727–1732.

Wan-Mahmood, Z., Ahmad, Z., Ishak, A. K., Yii, M. W., Mohamed, N., Sharib, J., Ishak, K., Razali,

K. N. & Mahmud, M. (2005). Kajian Awal Ke Atas Taburan Radionuklid Tabii Di Perairan Pantai Timur Semenanjung Malaysia, *Malaysian J. Anal. Sci.* 9(2):325–337. (in Malays)

Wan-Mahmood, Z., Yii, M.W. & Ishak, A.K. (2016). Po-210, $^{210}$Pb and $^{210}$Po/$^{210}$Pb in sediment core from surrounding Sungai Linggi estuary, *Nucl. Sci. J. Malays.* 28(1):1–8.

Wedepohl, K.H. (1995). The composition of the continental crust, *Geochim. Cosmochim. Acta* 59(7):1217–1232.

Wood, A.K., Muhammad, N., Mahmood, C.S., Ahmad, Z., Shazili, N.A., Law, A.T. & Yaakob, R. (1993). Corer sampling and the use of neutron activation analysis in evaluating pollution at the Juru waterway, Penang, *Nucl. Sci. J. Malays.* 11(2):105–128.

Xu, Z., Salem, A., Chen, Z.Y., Zhang, W.G., Chen, J., Wang, Z.H., Sun, Q. L. & Yin, D.W. (2008). Pb-210 and Cs-137 distribution in Burullus lagoon sediments of Nile river delta, Egypt: sedimentation rate after Aswan High Dam, *Front Earth Sci-PRC.* 2**:**434–438.

Yang, Y.X., Wu, X.M., Jiang, Z.Y., Wang, W.X., Lu, J.G., Lin, J., Wang, L.M. & Hsia, Y.F. (2005). Radioactivity concentrations in soils of the Xiazhuang granite area, China, *Appl. Radiat. Isot.* 63(2):255–259.

Yi, Y.J., Yang, Z.F. & Zhang, S.H. (2011). Ecological risk assessment of heavy metals in sediment and human health risk assessment of heavy metals in fishes in the middle and lower reaches of the Yangtze River basin, *Environ. Pollut.* 159(10):2575–2585.

Yii, M.W., Ahmad, Z. & Ishak, A.K. (2009). Distribution of naturally occurring radionuclides activity concentration in East Malaysian marine sediment, *Appl. Radiat. Isot.* 67(4):630–635.

Yii, M.W., Ruiz-Fernandez, A.C., Wan-Mahmood, Z. & Paulus, W. (*in press*). Deposition history of Arsenic, Barium, Chromium and Zinc at Perai Industrial Area of Penang, Malaysia–A case study using nuclear techniques, TECDOC. IAEA, Vienna, (*in press*).

Yii, M.W., Paulus, W. & Wan-Mahmood, Z. (2020a). Time deposition of copper, nickel and manganese at Perai river, Penang. In: Seminar R&D 2020, 16–19 November 2020, Nuklear Malaysia, Bangi.

Yii, M.W., Wan-Mahmood, Z., Elias, M.S. & Abdullah, Y. (2020b). The distribution of heavy metals and natural radionuclides within the surface sediments of the Juru river, Penang. In: AIP Conf. Proc. 2295:020006.

Yii, M.W., Wan-Mahmood, Z., Sharib, J. & Ahmad, Z. (2010). Comparison of $^{210}$Pb level in Kuala Muda tsunami affected marine sediment core measured using two different techniques, *Nucl. Sci. J. Malays.* 22(1):29–41.

Yii, M.W. et al. (2016). Ambient radioactivity and radiological studies in the vicinity of Lynas Rare-Earth Processing Plant, Gebeng Industrial Estate, Kuantan, Pahang, Tech. Rep. ScienceFund Project (06-03-01-SF0189), NUKLEARMALAYSIA/L/2016/196. Malaysian Nuclear Agency, Kajang, 145.

Yunus, K., Zuraidah, M.A. & John, A. (2020). A review on the accumulation of heavy metals in coastal sediment of Peninsular Malaysia, *Ecofeminism and Climate Change.* 1(1):21–35.

Zainudin, Z. (2010). Benchmarking River Water Quality in Malaysia, *Jurutera.* 12–15.

Zhu, L.M., Xu, J., Wang, F. & Lee, B. (2011). An assessment of selected heavy metal contamination in the surface sediments from the South China Sea before 1998, *J. Geochem. Explor.* 108(1):1–14.

e-Jurnal Sains Nuklear Malaysia, 2023, Vol. 35 (No.2): 25 – 37
*eISSN: 2232-0946*

# STUDY ON WETTABILITY OF RADIATION-INDUCED GRAFTED INDUSTRIAL POLYETHYLENE (PE) FILTER CARTRIDGE FOR WATER CONTAMINANT ADSORPTION

***Norliza Ishak[1*], Sarala Selambakkannu[1], Nor Azillah Fatimah Othman[1], Ting Teo Ming[1*] and Syaza Farhanah Samsudin[2]***

[1]Radiation Processing Technology Division,
Malaysian Nuclear Agency, Bangi 43000 Malaysia
[2] Faculty of Chemical Engineering, Universiti Teknologi MARA,
Pasir Gudang 81750 Johor, Malaysia
*Corresponding author: norliza@nm.gov.my[1], tmting@nm.gov.my[2]

## *ABSTRACT*

*Synthetic polymeric materials are making their way into water treatment and being utilized due to easy tailoring in promising end applications. Industrial Polyethylene (PE) filter cartridge is a type of water filter cartridge with 100% polyethylene material with superior chemical compatibility and particle retention efficiency for use in a wide range of applications such as industrial water treatment, drinking water treatment, sterilization, gas processing solvent, vent filter, and gas filtration. Radiation-induced grafting technique is one of the most popular methods for polymeric materials surface modification. In this study, an industrial polyethylene filter cartridge was modified via a simultaneous radiation-induced grafting process by employing gamma irradiation at 25 kGy. The Glycidyl Methacrylate (GMA) was grafted onto the material which was followed by subsequent chemical functionalization with an amine functional group. This modification improves the hydrophilic properties of the material as an adsorbent. The amine functionalization was confirmed by FTIR spectroscopy analysis. The unmodified and modified filter cartridges have been subjected to contact angle measurements using the advanced mode contact angle method through an optical contact angle (OCA). This analysis identified changes in material hydrophilicity. According to the results, the modified filter cartridge is more hydrophilic than the unmodified cartridge. A filter cartridge with enhanced hydrophilicity is suitable for the removal of various types of contaminants, including metal ions, dye particles, pathogens, fertilizers and pharmaceutical residues from water.*

**Keywords:** Radiation induced grafting; Industrial PE filter cartridge; Gamma irradiation; Chemical functionalization; Optical contact angle

## INTRODUCTION

Industrialization and economic growth, especially in developing countries, have led to enormous water pollution. This is mainly due to the release of highly toxic and harmful metal ions into water bodies. Addressing the growing emphasis on water pollution and remediation, extensive research has been conducted on the removal of metal ions from water. In particular, this can be accomplished through the modification of polymeric materials. Two prominent factors need to be considered in the modification of polymeric materials, first, the selection of polymeric materials and second is the technique used for modification.

Eco-efficiency is considered a major criterion in the selection of polymers for metal removal from water, whereby the materials should be economical in terms of cost and also promising of an easy and continuous supply (Kumar et al., 2019). Recently, a number of researchers have focused on the usage of cellulosic biofibers or biopolymers due to their abundancy, biodegradability, and hydrophilicity nature (Kolya & Kang, 2023; Kumar et al., 2019; Abinder et al., 2016; Madrid et al., 2013). Abinder et al., (2016) report that these biofibers have several advantages, but also some limitations, including poor mechanical properties and brittleness at room temperature, as well as sensitivity to moisture. Therefore, alternatively, the development of economically viable fabricated polymeric materials for metal ions removal is strongly anticipated.

Synthetic polymeric materials hold advantages over bio-based polymers in terms of mechanical and chemical properties. Moreover, synthetic polymeric materials offer higher flexibility in their physical forms and are also prone to chemical modification for the attachment of various functional groups that cater to the end application (Chalykh et al., 2023; Barsbay et al., 2016; Kavakli et al., 2016). In this study, industrial polyethylene (PE) filter cartridges are subjected to surface modification to improve the properties for the removal of metal ions from water selectively. Practically, industrial polyethylene (PE) filter cartridges is extremely hydrophobic and widely used in water filtration system. But unfortunately, it is incapable of removing some contaminants, especially metal ions. The current industrial PE filter cartridge function based on the size exclusion which is purely physical with involving any chemical interaction (Lombardo & Brigano, 2014). Therefore, this type of filtration system is superficial, compromising and inefficient. The water is contaminated with heavy metals and dyes resulting in major health complications such as the risk of cancer, neuronal damage, diabetes, and cardiovascular disorders (Rehman et al., 2018).

In general, there are several surface modification techniques to enhance polymeric materials' surface properties, including surface coating, surface functionalization, and surface grafting (Mozetič, 2019). The main aim of the modification is to improve and introduce a specific characteristic that acts as a precursor for metal removal from water. Among these modification techniques, graft polymerization is one of the most familiar methods to overcome polymers' shortcomings. Moreover, based on Nor Fadzil et al., (2020) graft polymerization is more stable due to the interaction of covalent bonds by incorporating a monomer onto the porous membrane surface. Despite this, graft copolymerization of a monomer onto surface material by gamma, UV, or electron beam provides an effective approach for incorporating advantageous modification of the surface properties to form active sites for grafting without affecting the basic properties of the polymeric backbone (Artico et al., 2023; Mozetič, 2019; Shin et al., 2017; Barsbay and Güven, 2013; Thakur et al., 2012). According to Shin et al., (2017) radiation-induced grafting polymerization (RIGP) presents unique advantages over other grafting methods due to its simplicity, homogeneous reaction, control over the process, and the absence of initiators and catalysts for polymerization. Hence, this method is an effective approach to improving functional properties by increasing the adsorbent's wetting properties. Basically, the technique involves incorporating a monomer on the surface and functionalization of the grafted polymer chains with known functional groups (Artico et al., 2023; Barsbay and Güven, 2013).

Wettability is the term used for hydrophilicity, while hydrophobicity describes the relative affinity of water molecules to spread on the surface of any substrate (Junchou et al., 2020). In principle, synthetic polymeric materials such as polyethylene, polypropylene, polyvinyl chloride, and nylon possess poor wettability. This is one of the major disadvantages of water-based adsorbents. Thus, synthetic polymeric materials require further improvement for the effective removal of metal ions from water. Generally, radiation-induced grafting and amine functionalization processes could amend the wettability properties of polymeric materials. As a result, evaluating the hydrophilicity behavior of

the adsorbent after surface modification processes is critical. The wettability properties description of the materials could be conducted via contact angle measurement. This will give valuable information regarding its hydrophobicity and hydrophilicity.

This study focuses on the modification of an industrial polyethylene (PE) filter cartridge via gamma irradiation and a simultaneous radiation-induced grafting technique in which glycidyl methacrylate (GMA) was grafted onto the material and then chemically functionalized with various types of amine. Both unmodified and modified filter cartridges have been thoroughly characterized for their degree of surface hydrophilicity using the advanced mode contact angle method via an optical contact angle (OCA). This study provided insight into the wettability evaluation of the adsorbent by contact angle measurement. It demonstrated the success and the impact of the radiation-induced grafting technique and the amine functionalization process.

## EXPERIMENTAL

The industrial source provided was an industrial PE filter cartridge (PENSONIC 0.5 microns). Glycidyl Methacrylate Acid (GMA, ≥90%, Sigma Aldrich), Polysorbate 20 (Tween-20, ≥40%, Sigma Aldrich), Ethylene Diamine (EDA, ≥99%, acros), Dimethyl Amine (DMA, <50%, Sigma Aldrich), Isopropyl Alcohol (IPA, 70%, QRëC) and Methanol (≥99.8%, Friendemann Schmidt) were used in this study in their original grade. Distilled water was used to rinse the grafted material. The chemical structure of EDA and DMA are shown in Figure 1.

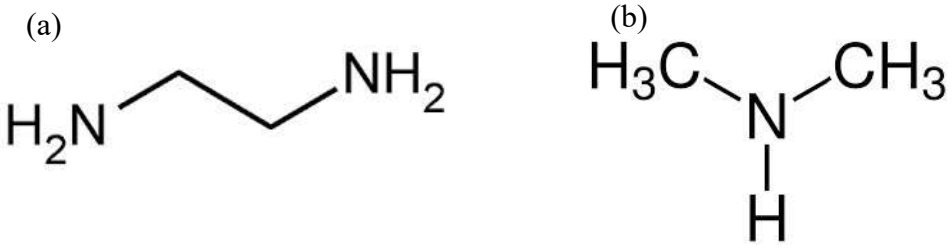


Figure 1. Chemical structure of (a) EDA and (b) DMA

### Simultaneous Radiation Induced Grafting of Industrial PE Filter Cartridge

An emulsion solution composed of GMA at different concentrations (5, 7, and 10% w/w) and Tween-20 (1 wt%) was prepared, followed by de-oxygenation for 15 minutes with $N_2$ bubbling.

The pre-treated PE cartridge was immersed in the grafting solution and the mixture was de-oxygenated again for another 10 minutes and prolonged immersion in the grafting solution at room temperature for 24 hours. The samples were irradiated with $^{60}$Co gamma rays at the SINAGAMA facility. The irradiation was performed at a dose of 25 kGy. An accredited ceric-cerous and ferrous sulfate (Fricke) dosimetry system, which is in compliance with MS ISO/IEC 17025 standards, was used to determine the amount of absorbed dose. Finally, the un-reacted monomer and homopolymers were removed by rinsing with methanol and distilled water.

The samples were dried in a vacuum oven at 60 °C for 24 hours until a constant weight was reached. The grafted filter cartridge was weighed to determine the degree of grafting (DG) using the following Equation (1):

$$DG(\%) = \frac{Wf - Wo}{W_o} \; x \; 100 \qquad (1)$$

Where, $W_f$ and $W_O$ are the weight of grafted and original industrial PE filter cartridges respectively (Othman et al., 2019).

**Chemical Functionalization of Grafted Industrial PE Filter Cartridge**

The grafted industrial PE filter cartridge was chemically functionalized using two types of amine groups EDA and (DMA. Both amine solutions were prepared with 70 wt% and 30 wt% of an IPA.

The grafted sample was immersed in an amine solution and reacted in a water bath at 70°C for 1 hour. The chemically modified PE filter cartridge was washed in methanol and distilled water. Finally, the sample was dried in a drying oven at 60 °C for 24 hours until a constant weight was reached. The functionalized industrial PE filter cartridge was weighed to find out the amine group density (AGD) using the following Equation (2):

$$AGD\ (mmol/g) = \left[\frac{(\frac{Wf - Wo}{W_o})}{MW}\right] \; x \; 1000 \qquad (2)$$

Where $W_f$ and $W_O$ are the weight of functionalized and grafted industrial PE cartridges respectively and MW is molecular weight for amine group (Othman et al., 2019).

**Fourier Transform Infrared Spectroscopy (FTIR)**

The analysis of filter cartridges before and after modification were characterized by Attenuated Total Reflectance Fourier Transform Infrared (ATR-FTIR) using a Bruker Tensor II FTIR spectrometer. The FTIR spectra were recorded by an OPUS software spectrum by transmittance with 16 numbers of scanning at a resolution of 4 $cm^{-1}$ with a wavelength range of 4000 – 500 $cm^{-1}$ at ambient condition.

**Wetting- Surface Characterization of Industrial PE Filter Cartridge**

The raw, grafted, and functionalized industrial PE filter cartridges were measured using an Attention Theta (Biolin Scientific, Finland) interfaced with a PC for control and data acquisition. Two techniques were applied for the assessment, sessile drop goniometry and sessile drop goniometry with surface topography.

**Optical Contact Angle Measurement**

The most common technique used for surface wetting characterization is sessile drop goniometry due to its simplicity. The samples were held vertically to the sample stage during the measurement. The contact angles were obtained by positioning the tip that contains deionized water near the sample surface. The tip squeezes water at a constant drop liquid volume of 7µL. The contact angle measurement was completed within 10s. The measurement of contact angles for raw, grafted, and

functionalized industrial PE filter cartridges was analyzed using the Young equation. This assumes that the material surface is chemically homogeneous and topographically smooth (ideal surface).

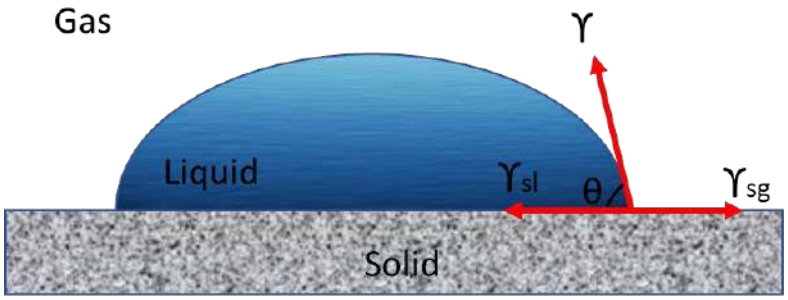


Figure 2. A contact angle on ideal solid surface determined by Young Laplace equation's

Figure 2 shown the droplet on the ideal surface which the Young's equation was applied (Huhtamaki et al., 2018; Young, 1805) and measured the reading of the contact angle as in Equation (3) (Huhtamaki et al., 2018):

$$\cos\theta_{Young} = \frac{\gamma_{sv} - \gamma_{sl}}{\gamma} \qquad (3)$$

Where $\theta_{Young}$ is the Young contact angle, $\gamma$ is the surface tension of the liquid, $\gamma_{sv}$ and $\gamma_{sl}$ are solid-vapor and solid-liquid interfacial tensions respectively.

**Optical Contact Angle with Topography Measurement**

The same measurement was applied to sessile drop goniometry with surface topography. The sample stage contained deionized water and the liquid volume was set up at 7µL depositing the surface material. Before the liquid was dropped on the surface material, the sample was subjected to topography to calculate surface roughness.

The morphology and roughness of the raw grafted with 7% GMA and functionalized industrial PE filter cartridges were measured over a relatively flat surface for practical measurement using optical contact angle with topography. The measurement area for each surface sample was fixed within 1.4 mm x 1.1 mm five times of repeated scanning. The root mean square roughness value was used as the evaluation index to analyze the difference in surface morphology and roughness among raw, grafted, and functionalized materials.

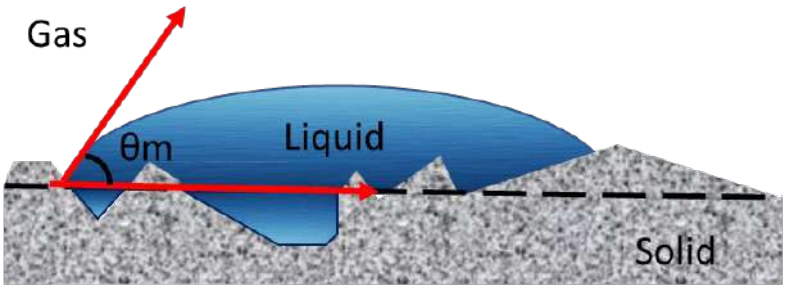


Figure 3. A contact angle on an actual surface material with inherent roughness

The droplet on the actual surface of the material is illustrated as in Figure 3 (Biolin Scientific, 2017). Based on the figure the measurement of contact angle calculated by considered the real surface which the Wenzel statement was applied as in Equation (4) (Wenzel, 1936):

$$\cos\theta_m = r\ \cos\theta_y \qquad (4)$$

Where, $\theta_m$ is the measured contact angle, r is the roughness ratio and $\theta_y$ is the Young contact angle.

Roughness ratio, r is defined as the ratio between the actual and projected surface areas which r is equal to 1 for a smooth surface and greater than 1 for a rough surface. The r for Wenzel equation is determined from the 3D area factor, $S_{dr}$ based on the following Equation (5) (Biolin Scientific, 2017; Peltonen et al, 2004):

$$r = 1 + \frac{Sdr}{100} \qquad (5)$$

## RESULTS AND DISCUSSION

### Modification of the Irradiated Industrial PE Filter Cartridge

The effect of GMA concentrations of 5%, 7%, and 10% on the grafting yield of the industrial filter cartridge was examined. The results obtained are shown in Fig. 4. The simultaneous irradiation technique at a dose of 25 kGy with a reaction time of 24 hours was used for this investigation. The grafting yield increased as the concentration increased to about 10%. However, at monomer concentrations greater than 7%, the formation of homopolymers may also contribute to increased grafting yield. According to Nasef and Sugiarmawan, (2010) grafting yield increased with a GMA concentration of up to 10%. The concentration of GMA above 10% lead to the decreasing in grafting yield thereafter due to the fast-initial reaction rate. This was expected because the monomer was exposed to gamma irradiation. Thus, for practical reasons, GMA concentrations were limited to 5% and 7% w/w.

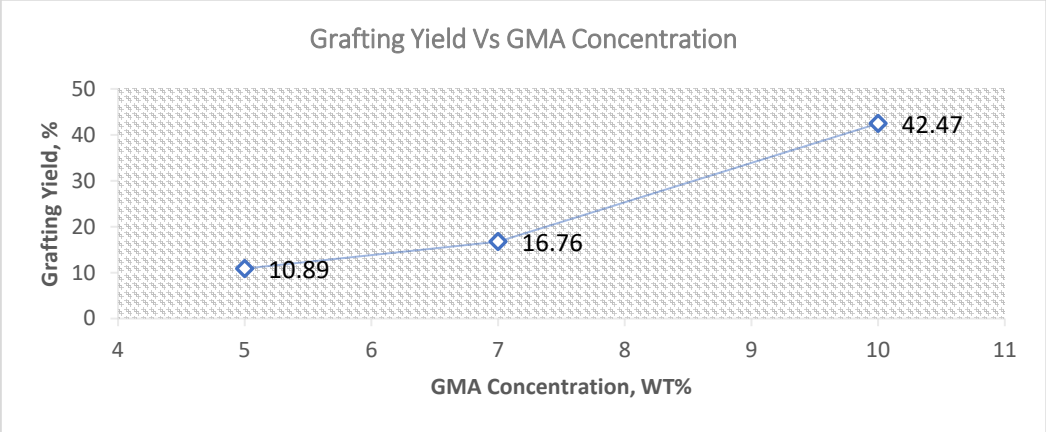


Figure 4. The grafting yield obtained as a function of GMA concentration for irradiated industrial filter cartridge

The amount of functionalized DMA and EDA expressed as AGD was determined gravimetrically. The effect of GMA concentration on AGD is shown in Fig. 5. As expected, the AGD demonstrated an ascending pattern for 5% and 7 % of GMA concentration and insignificantly reduced at 10% of GMA concentration. The EDA density increases from 0.87 mmol/g to 1.29 mmol/g as the GMA concentration increased up to 7%. Similar trends were observed for DMA as well but the AGD was slightly lower than EDA. A higher amine density was observed on the grafted adsorbent when the number of amines was greater (Liu et al., 2010). However, as the concentration of GMA was 10%, the density of EDA was reduced to 0.25 mmol/g. This phenomenon was due to the creation of a homopolymer in which the surface of the adsorbent was fully covered with branched grafted chains of GMA (Desmet et al., 2011) and the possibility of the chain collapsing led to amine attachment failure. Therefore, the highest AGD for an effective adsorbent could be achieved by using the largest number of amine groups, EDA.

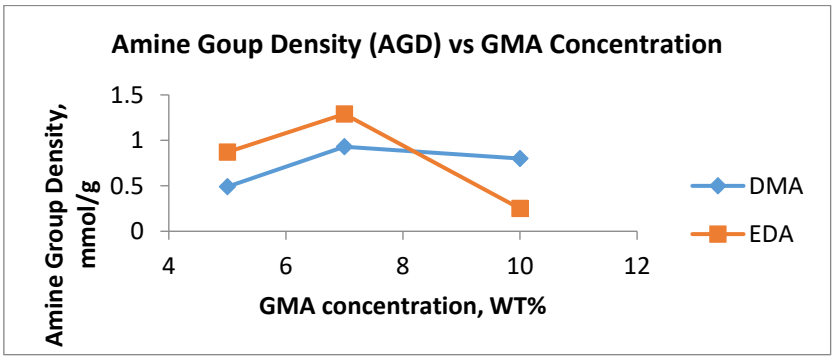


Figure 5. Effect of different GMA concentration on amine group density at 70 $^{0}$C for 1h, 70% Amine: 30% IPA

**FTIR Analysis**

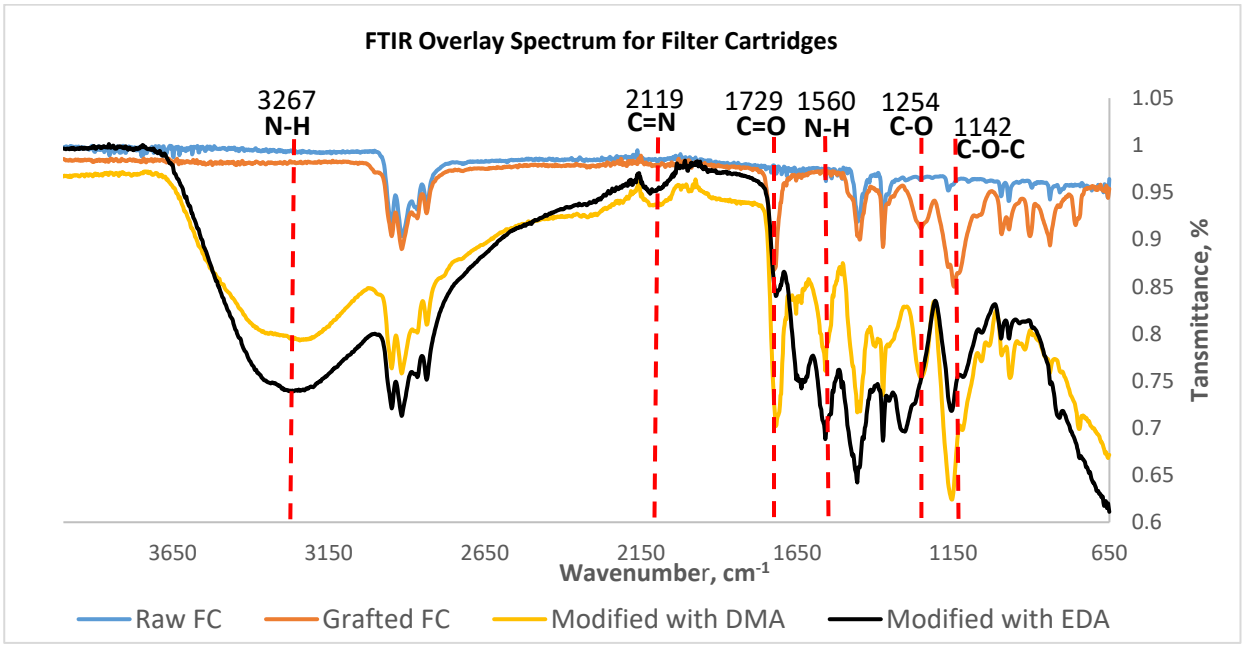


Figure 6. FTIR Spectra of raw, grafted at 7% of GMA concertation and functionalized with DMA and EDA

The FTIR analysis was performed on GMA-grafted material and subsequent chemical functionalization with an amine functional group to enhance its hydrophilicity as an adsorbent. FTIR analysis was used to characterize the surface composition of filter cartridges before and after modification. Figure 6 shows the IR spectra of raw, grafted, and modified filter cartridges. After grafting the filter cartridge with 7% GMA, the spectra exhibited distinct peaks indicating successful grafting interactions. These peaks are carbonyl group (C=O) at 1729 $cm^{-1}$, ester group C–O, and C-O-C vibration which originates from –COO– ester group of GMA at 1254 $cm^{-1}$ and 1242 $cm^{-1}$, respectively (Abudonia et al., 2018). In addition, the characteristics of transmittance peaks arising from aliphatic amine groups are also identified. Specifically, the peaks at 3267 $cm^{-1}$ correspond to N-H stretching, whereas the peaks at 2119 $cm^{-1}$ and 1560 $cm^{-1}$ represent the C=N group and N-H bending respectively (Rania, 2023). In addition, these peaks further verify the success of the radiation-induced grafting technique used to modify the sample.

**Water Contact Angle Analysis**

The water contact angle on the surface of raw, grafted, and functionalized industrial PE filter cartridges based on GMA concentration was measured. The results are exhibited in Fig.7(a)-(c). The raw industrial filter cartridge displayed a higher contact angle since PE is hydrophobic in nature. However, based on Fig.7(b), modified industrial PE filter cartridges showed a significant reduction in contact angle at 7% of GMA concentration. The contact angle reduced from 139º to 133.57º after grafting, and then to 122.53º and 114.11º after functionalization, respectively. This is due to the existence of polar functional groups such as carbonyl (C=O) in GMA and amine ($NH_2$) in DMA and EDA (Hebbar et al., 2017). As a polar group, carbonyls have a partially charged ion. The negative charge of the oxygen atom may interact with water molecules to form hydrogen bonds and become more hydrophilic. Similarly, the amine group is also negatively charged and capable of H-bonding, which supports polar hydrophilic groups.

Furthermore, EDA contact angle values are much lower than DMA due to the presence of two $NH_2$ molecules attached to the hydrocarbon chain. Hence, the changes in wetting properties of the raw filter cartridge can be correlated with functional groups attached to the surface. This is due to the simultaneous irradiation grafting technique. The contact angle measurement is also influenced by the material surface roughness.

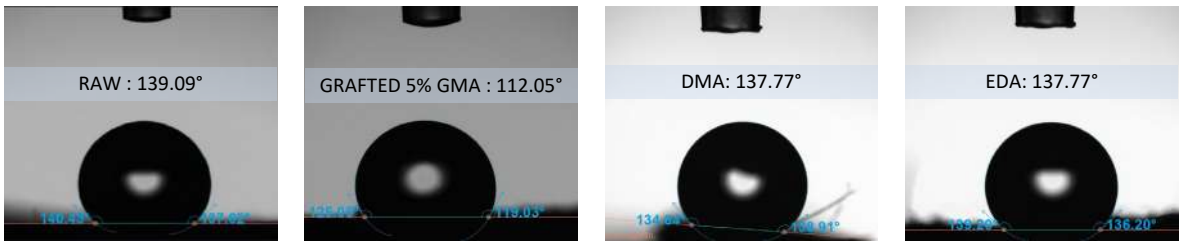


Figure 7(a). Contact angle for raw, grafted and modified industrial PE filter cartridge with 5 wt% of GMA

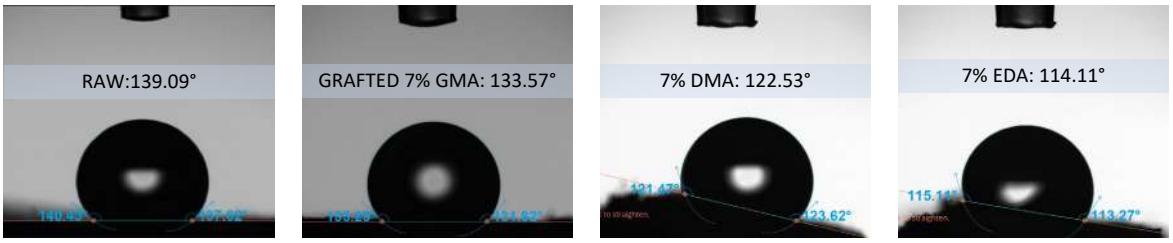


Figure 7(b). Contact angle for raw, grafted and modified industrial PE filter cartridge with 7 wt% of GMA

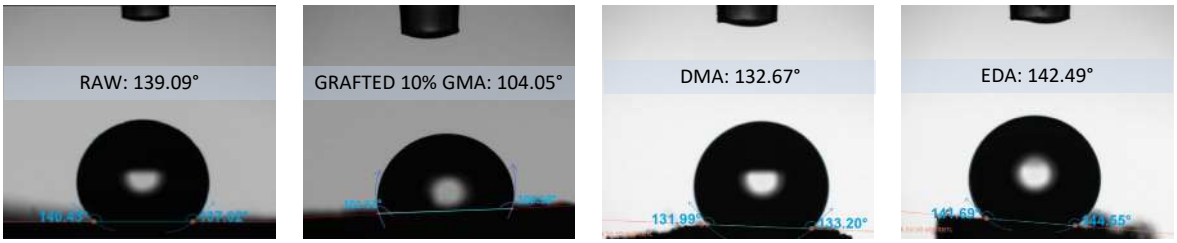


Figure 7(c). Contact angle for raw, grafted and modified industrial PE filter cartridge with 10 wt% of GMA

**Surface Roughness on Water Contact Angle of Modified Industrial PE Filter Cartridge**

Figure 8 and Fig.9 present optical images and 3D topography of the fractured surface for each sample, respectively.

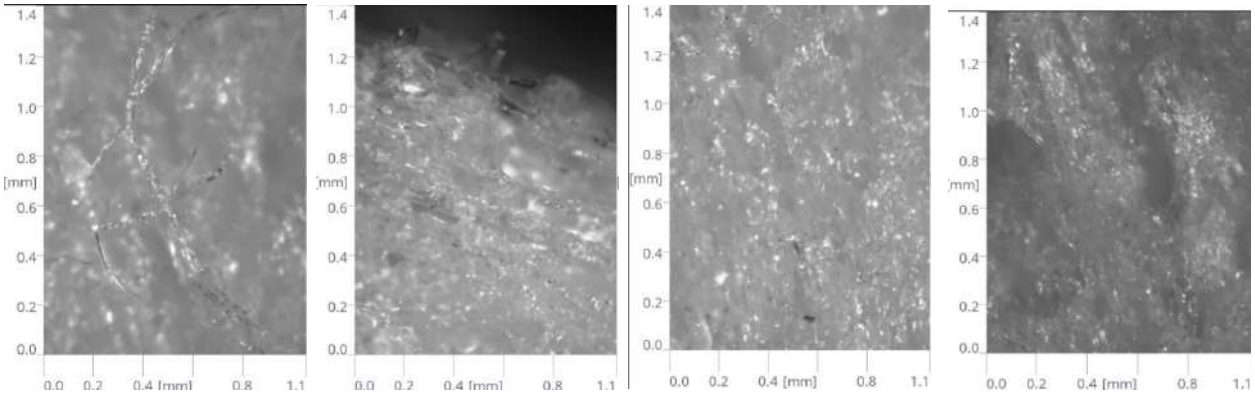


(a) (b) (c) (d)

Figure 8. Optical images of the industrial PE filter cartridge samples: (a) raw, (b) g-7% GMA, (c) functionalized with DMA, g-7% GMA-DMA and (d) functionalized with EDA, g-7% GMA-EDA

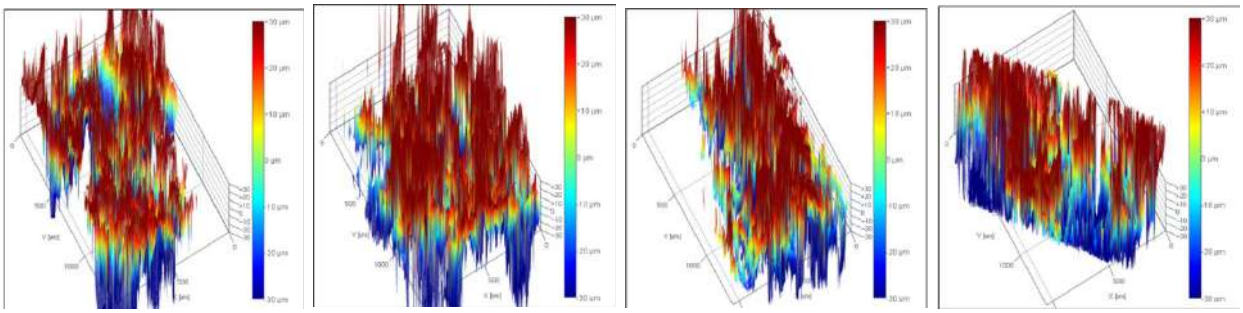

(a) (b) (c) (d)

Figure 9. 3D reconstructed topography images of the industrial PE filter cartridge samples: (a) raw, (b) g-7% GMA, (c) functionalized with DMA, g-7% GMA-DMA and (d) functionalized with EDA, g-7% GMA-EDA

The root mean square roughness of surface topography (Sq) between the samples is 41.27 micron (μm) for raw, 41.48 μm for grafted with 7% GMA, 40.60 μm for functionalized g-7% GMA-DMA, and 44.05 m for functionalized g-7% GMA-EDA. Different types of materials have varying roughness levels based on their origin (Li et al, 2021; Stout et al., 2006). Therefore, raw, grafted, and functionalized industrial PE filter cartridges have naturally fractured surfaces with different roughnesses.

Table 1. Representative advanced contact angles with topography (Corrected Contact Angle, CAc) of 7% GMA concentration

| Material (Industrial PE Filter cartridge) | Grafting Yield (%) | Contact Angle, CA (°) | Corrected Contact Angle, CAc (°) |
|---|---|---|---|
| Raw | - | 139.09 | 93.75 |
| g- 7% GMA | 16.76 | 133.57 | 92.76 |
| g-7% GMA- DMA | 16.76 | 122.53 | 92.51 |
| g-7% GMA- EDA | 16.76 | 114.11 | 91.96 |

The contact angle (CA) and corrected contact angle (CAc) obtained for modified PE filter cartridges are shown in Table 1. Both CA and CAc showed a descending trend after grafting at 7% GMA and functionalization with DMA and EDA, respectively. The presence of carbonyl and amine groups during the modification process only reduces the contact angle. Ideally, the angle measured below 90° is perceived to be hydrophilic, and an angle above 90° is classified as hydrophobic (Li et al., 2021; Good, 1992). However, the CA values indicate that the sample surface is hydrophobic, even though it is decreasing. This is because the CA values are calculated based on Young's theory, which assumes the sample surface is ideal (absolute smoothness).

The CAc analysis is designed to measure the contact angle in consideration of the original surface roughness. Surface roughness topography values lead to CAc becoming more hydrophilic. As defined by Wenzel in 1936, the actual contact angle is determined based on the relationship between surface roughness and wettability. The increase in surface roughness will enhance wettability due to hydrophilic substances' surface composition (Erbil et al., 2014; Huang et al., 2010; Stout et al., 2006; Wenzel, 1936). Thus, the actual contact angle values of raw and modified industrial PE filter cartridges are measured by considering the roughness ratio.

## CONCLUSION

The results indicate that the modification of an industrial PE filter cartridge as an adsorbent by simultaneous radiation-induced grafting using gamma radiation was successfully prepared and led to a decrease in hydrophobicity. Herein, a significant correlation between contact angle measurement and the attachment of functional groups (C=O and $NH_2$) to the surface material is established. This study indicates an increase in the wettability properties of the industrial PE filter cartridge as an adsorbent experimentally. Additionally, this study revealed the actual contact angle measurement of the material affected by surface roughness based on real surfaces using an advanced mode contact angle method. As a result of this discovery, the adsorbent's performance and functionality may be improved if it is combined with the desired wetting nature gained through simultaneous radiation-induced grafting.

## ACKNOWLEDGEMENTS

The authors would like to thank the Radiation Processing Technology Division (BTS), Malaysian Nuclear Agency for the support in providing facilities for the experiments.

## REFERENCES

Abinder, P., Macchi, C., Amalvy, J., and Somoza, A., (2016), Chitosan-graft-poly(n-butyl acrylate) polymer: synthesis and characterization of a natural/synthetic hybrid material, J. *Carbohydrate polymers*, 145: 86-94.

Abudonia, K. S., Saad, G. r., Naguib, H. F., Eweis, M., Zahran, D., and Elsabee, M. Z., (2018) Surface modification of polypropylene film by grafting with vinyl monomers for the attachement of chitosan, J. *Polym Res,* 25:125

Artico, M., Roux, C., Peruch, F., Mingotaud, A.F., and Montanier, C. Y., (2023). Grafting of protein onto polymeric surfaces: A synthesis and characterization challenge, J. *Biotechnogy Advances,* 64: 108106

Barsbay, M., and Güven, O., (2013), RAFT mediated grafting of Poly(Acrylic Acid) (PAA) from Polyethylene/Polypropylene (PE/PP) nonwoven fabric via preirradiation, J. *Polymer*, 54(18): 4838–4848.

Barsbay, M., Güven, O., and Kodama, Y., (2016), Amine functionalization of cellulose surface grafted with glycidyl methacrylate by gamma-initiated RAFT polymerization, J. *Radiation Physic & chemistry*, 124: 140-144.

Biolin Scientific., (2017), The Attension Theta optical tensiometer with 3D topography: For roughness corrected contact angles, *Attension 3D Topography Module Method,* Nordic Instrumentation, Finland: Susanna, L.

Chalykh, A. E., Khasbiullin, R. R., Aliev, A. D., Matveev, V. V., Gerasimov, V. K., Slesarenko, N. A., Avilove, I. A., Volkov, V. i., and Tverskoy, V. A., (2023), The effect of Divinylbenzene on the structure and properties of polyethylene films with related radiation chemical grafted polystyrene and sulfocationite membranes, J. *membranes,* 13(6):287.

Desmet, G., Takács, E., Wojnárovits, L., and Borsa, J., (2011), Cellulose functionalizationvia high energy irradiation initiated grafting of glycidyl methacrylate and cyclodextrin immobilization, J. *Rad Phys & Chem*, 80(12): 1358-1362.

Erbil, H.Y., (2014), The debate on the dependence of apparent contact angles on drop contact area or three phase contact line: A review, *Surface Science Reports,* 69 (4): 325-36.

Good, R.J., (1992), Contact angle, wetting and adhesion: A critical review, J. A*dhesion Sci.Tech,* 6: 1269-1302.

Hebbar, R. S., Isloor, A. M., and Ismail, A.F., (2017), Contact angle measurements, *In*: *Membrane Characterization,* Elsevier Inc, 219-255, ISBN: 97804446377765.

Huang, F. L., Wang, Q. Q., Wei, Q. F., Gao, W. D., Shou, H. Y., and Jiang, S. D., (2010), Dynamic wettability and contact angles of poly (vinylidene fluoride) nanofiber membranes grafted with acrylic acid, *eXPRESS Polymer Letters,* 4(9): 551-558.

Huhtamaki, T., Tian, X., Korhonen, J., and Ras, R.H.A., (2018), Surface-wetting characterization using contact angle measurements, *Nature Protocols*, 13(7): 1521 – 1538.

Junchou, W., Yankun, W., Yijun, C., Guosheng, L., and Yinfei, L., (2020), Influence of surface roughness on contact angl ehysterisis and spreading work, J. *Coll. & Poly Sci,* 298: 1107-1112.

Kavakli, C., Barsbay, M., Tilki, S., Güven, O., and Kavakli, P.A., (2016), Activation of polyethelyne/polypropylene nonwoven fabric by radiation-induced grafting for the removal of Cr (VI) from aqueous solutions, J. *Water, Air & Soil Pollution*, 227(12):473.

Kumar, R., Sharma, R.K., and Singh, A. P., (2019), Grafting of cellulose with N-isopropylacrylamide and glydidyl methacrylate for efficient removal of Ni (II), Cu (II) and Pd (II) ions from aqueous solution, J. *Separation & Purification Technology*, 219: 29-259.

Kolya, H. and Kang, C. H., (2023), Next-generation water treatment: Exploring the Potential of Biopolymer-based Nanocomposites in Adsorption and Membrane filtration, J. *Polymers,* 15(16):3421

Li, C., Zhang, J., Han, J., and Yao, B., (2021), A numerical solution to the effects of surface roughness on water-coal contact angle, *Sci Rep,* 11 (1).

Liu, C., Bai, R., Hong, l., and Liu, T., (2010), Functionalization of adsorbent with different aliphatic polyamines for heavy metal ion removal: Characteristic and performance, J. *Colloid & Interface Sci*, 345 (2): 454-460.

Lombardo, A. W., & Brigano, F. A. (2014). Designing Filtration Systems to Remove Heavy Metals from Water. International Journal of High Speed Electronics and Systems, 23(01n02), 1420008.

Madrid, J.F., Nuesca, G. M., and Abad, L.V., (2013), Gamma radiation-induced grafting of glycidyl methacrylate (GMA)onto water hyacinth fibers, J. *Radiation Physics and Chemistry*, 85: 182–18.

Mozetič, M., (2019), Surface modification to improve properties of materials, J. *Materials*, 12(3):441.

Nasef, M.M., and Sugiarmawan, I. A., (2010), Radiation induced emulsion grafting of Glycidyl Methacrylate onto High Density Polyethylene: A kinetic study, J.*Fund.Sciences,* 6 (2): 93-97.

Nor Fadzil, N. F. E., Abouzari-lotf, E., Sha'rani, S. S. M., Ting, T. M., Che Jusoh, N. W., and Ahmad, A., (2020), Preparation of porous membrane with graphene oxide for vanadium redox flow battery. In: *IOP Conf. Series: Materials Sciences and Engineering 8th Conference on Emerging Energy & Process Technology 2019 (CONCEPT 2019).* 27 – 28 November 2019, Kuala Lumpur, Malaysia. 808: 012012.

Othman, N. A. F., Selambakkannu, S., Tuan Abdullah, T. A., Hoshina, H., Sattayaporn, S., and Seko, N., (2019), Selectivity of copper by amine-based ion recognition polymer adsorbent with different aliphatic amines, J. *Polymers*, 11(12):1994.

Peltonen, J., Jãrn, M., Areva, S., Linden, M., and Rosenholm, J. B., (2004), Topographical parameters for specifying a three-Dimensional surface, *Langmuir,* 20: 9428-9431.

Rania, F. K., (2023) Radiation-grafting on polypropylene copolymer membranes for using in Cadmium adsorption, J. *polymers,* 15(3):686

Rehman, K., Fatima, F., Waheed, I., & Akash, M. S. H. (2018). Prevalence of exposure of heavy metals and their impact on health consequences. *Journal of cellular biochemistry*, *119*(1), 157-184.

Shin, I. H., Hong, S., Lim, S. J., Son, Y. S., and Kim, T. H., (2017), Surface modification of PVDF membrane by radiation-induced graft polymerization for novel membrane bioreactor, J. *Ind. Eng. Chem.,* 46: 103 - 110.

Stout, K. J., Blunt, L., Sullivan, P. J., Dong, W. P., Mainsah, E., Luo, N., Mathia, T., and Zahouani, H., (2006), The development of methods for the characterization of roughness in 3 dimensions (1st Ed), Butterworth-Heinemann, ISBN: 9781857180237.

Thakur, V. K., Singha, A. S., & Thakur, M. K., (2012), Graft copolymerization of methyl acrylate onto cellulosic biofibers: synthesis, characterization and applications, J. *Polymers and the Environment,* 20(1): 164–174.

Wenzel, R.N., (1936), Resistance of solid surfaces to wetting by water, *Ind.Eng.Chem.,* 28: 988.

Young, T. (1805), An essay on the cohesion of fluids, *philos.Trans. R. Soc. Lond.*, 95: 65-87.

e-Jurnal Sains Nuklear Malaysia, 2023, Vol. 35 (No.2): 38 – 48
*eISSN: 2232-0946*

# SULPHUR-FREE PREVULCANIZATION OF MALAYSIAN NATURAL RUBBER LATEX USING A HYBRID ULTRAVIOLET-PEROXIDE VULCANIZATION METHOD

***I. Sofian*, C. K. Chai, B. Muhammad Hannan, S. Hasan, M. L. Mohd Noorwadi, A. R. Anwar, A. K. Ahmad Bazlie and M. A. Noor Hasni***

Malaysian Nuclear Agency, 43000 Kajang, Selangor, Malaysia
*Corresponding author: sofian_ibrahim@nm.gov.my

## ABSTRACT

*A preliminary study on vulcanized natural rubber latex via hybrid ultraviolet C (UVC) and peroxide vulcanizations was conducted using 2-hydroxy-2-methyl-1-phenylpropanone (Irgacure 1173) as the photoinitiator, 1,6-hexanediol diacrylate (HDDA) and tert-butyl hydroperoxide (t-BHPO) as the sensitizers/coagents. The effects of various amounts of t-BHPO on crosslink density, mechanical and physical properties of UV-peroxide prevulcanized natural rubber latex were investigated and recorded. The tensile strength, modulus at 500% and modulus at 700% elongation of rubber film obtained from one-hour UVC irradiation (temperature within 70-75 ºC) were 22.0, 3.0 and 9.0 mPa respectively, which is more than 83 % of increment compared to the control sample. The crosslink density of the rubber films showed an increment of 28.5 %.*

**Keywords**: UVC, vulcanization, irradiation, latex

## INTRODUCTION

Natural rubber latex or its scientific name *cis*- 1, 4- polyisoprene naturally exists in the form of a white, sticky and non-elastic liquid. In the middle of the 19th century, Charles Goodyear managed to find a method to overcome all the weaknesses found in natural rubber. This method is known as sulphur vulcanization. The sulphur vulcanization requires four different materials that need to be mixed in the natural rubber latex; i.e. sulphur as the cross-linking agent, carbamate compounds as accelerator, zinc oxide (ZnO) as activator and potassium hydroxide (KOH) as stabilizer. The mixture is then heated to a temperature of 40-65 ºC for a maximum duration of 10 hours. This process can impart some major properties such as chemical resistance, aging resistance, improved film properties and mechanical strength which are not present in the unvulcanized natural rubber latex.

However, the chemicals used in this process tend to cause health problems such as skin allergies to users of the latex products. In 2016, it was reported that average prevalence of latex allergy worldwide remains at 9.7%, 7.2%, and 4.3% among healthcare workers, susceptible patients, and the general population, respectively [Wu *et al.,* 2016]. Researchers have found out that the carbamate compounds that are used as accelerators to speed up the vulcanization process and reduce the reaction temperature have high risk on tissue irritations and cytotoxicity. This issue has led researchers to look for vulcanization technique that is free from sulphur and its related compounds.

Currently, there are two alternative crosslinking processes that are free from sulphur, i.e. peroxide (chemical vulcanization) and ionizing radiation (electron and gamma rays). Both of this processes do not use chemicals related to sulphur vulcanization such as accelerator and activator which may cause skin allergic, emission of sulphur dioxide, high residual chemical in the end product and pollution to environment. However, further consideration has to be made since both crosslinking techniques had

their own issues such as high capital investment in infrastructure, production and maintenance cost, low physical properties of final products and longer vulcanization time than sulphur vulcanization [Lazim *et al.,* 2021].

Since the last decade, the study on vulcanization of natural rubber latex through the use of non-ionizing UV radiation has begun to receive attention from researchers. Schlögl [2010] has successfully produced prevulcanized natural rubber latex with the help of a photoinitiator and a poly-functional thiol. Through this vulcanization technique, sulphur-free prevulcanized natural rubber latex with good biocompatibility and low amount of leachable chemical compound has been successfully produced. Wiroonpochit [2017] thru her research has combined the use of photoinitiator with coagents such as 1,4-butanediol diacrylate (BTDA), 1,6-hexanediol diacrylate (HDDA) and 1,9-nonanediol diacrylate (NDDA). The results of the study showed that prevulcanized natural rubber latex with relatively good mechanical strength has the potential to be produced.

The present work attempts to combine UV and peroxide vulcanizations with the presence of acrylate coagent. Effects of the following factors on the mechanical properties (tensile strength) of the resulting prevulcanized natural rubber latex were assessed in order to determine optimal conditions for prevulcanization, i.e. amount of peroxide and the duration of the UV irradiation. This research output may trigger the diversification encourage the use of sulphur free prevulcanized natural rubber latex in local latex product industries and abroad.

## MATERIALS AND METHODS

### Materials

The natural rubber latex (NRL) utilised in this work was a high ammonia type (HA latex) supplied by Getahindus (M) Sdn. Bhd., Malaysia. The sensitizer used was hexanediol diacrylate (HDDA) supplied by Allnex, China and tert-butyl hydroperoxide (*t*-BHPO) supplied by Fluka. The photoinitiator, 2 hydroxy-2-methyl-1-phenylpropanone (Irgacure 1173) was purchased from Sigma Aldrich (M) Sdn. Bhd., Malaysia. The stabilizer used was Potassium laurate supplied by Tiarco Chemical (M) Sdn. Bhd., Malaysia. The activator used was Hydroxyacetone (HAC) supplied by Sigma Aldrich (M) Sdn. Bhd., Malaysia. All the stated materials were used as received.

### Preparation of the latex formulation

Latex formulations prepared in this study were planned and decided based on present study objectives and findings of previous studies [Lazim, M. N. M., *et al.,* 2021; Cahya, W. & Herry, P. 2018; Hansupalak *et al.,* 2016 & Wiroonpochit *et al.,* 2017]. The steps for preparing the latex formulations are described below.

### Preparation of UV prevulcanized natural rubber latex in the presence of diacrylates (control sample without peroxide)

A latex formulation of 52% total solid content was prepared from materials listed in Table 1. The NRL was transferred to a beaker and followed by addition of stabilizer, sensitizer, photoinitiator and water while stirring within 5 minutes interval. The beaker was covered with aluminum foil to avoid light exposure [Lazim, M. N. M., *et al.,* 2021 & Sofian *et al.,* 2018]. The latex mixing was done at room temperature in the dark. Once the addition of the materials was completed, the latex mixture

was left stirring for one hour. The formulated latex was then transferred into 250 x 350 mm polyethylene (PE) bags and sealed, of which the thickness of the plastic bag containing latex sample is less than 10 mm. The latex sample in PE bags were subjected to UVC irradiation for one hour as described the UVC irradiation section. After irradiation, the latex was made into film using a coagulant dipping method and the mechanical properties of latex films were performed [Pairu *et al.,* 2016].

Table 1. Compounding formulation of UV prevulcanized natural rubber latex (Control)

| **Materials** | **Part per hundred rubber (pphr)** |
|---|---|
| NRL (62% *TSC) | 100.0 |
| Stabilizer | 0.1 |
| HDDA | 2.0 |
| Irgacure 1173 | 2.0 |
| Water | Add to 52% TSC |

*TSC- Total solid content

**Preparation of hybrid UV-peroxide prevulcanized natural rubber latex at different amount of *t*-BHPO**

Latex formulations as shown in Table 2 were prepared by adding the stabilizer, sensitizer, peroxide (various amount), activator, photoinitiator and water into NRL within 5 minutes interval while stirring in the dark and at room temperature. The latex mixture was stirred for one hour, followed by transferring to 250 x 350 mm PE bag and sealed. The thickness of the plastic bag containing latex sample is less than 10 mm. The latex samples were subjected to UVC irradiation for one hour as described in the UVC irradiation section. After irradiation, coagulant dipped rubber films were prepared from the latex samples and the mechanical properties of latex films were performed.

Table 2. Compounding formulation of Hybrid UV-peroxide prevulcanized natural rubber latex at different amounts of *t*-BHPO

| **Materials (pphr)** | **Part perhundred rubb** |
|---|---|
| NR Latex (62% TSC) | 100.0 |
| Stabilizer | 0.1 |
| HDDA | 2.0 |
| *t-BHPO<br>0.5/1.0/1.5 | |
| Irgacure 1173 | 2.0 |
| HAC | 0.5 |
| Water<br>TSC | Add to 52% |

**UVC irradiation**

The latex formulations packed in plastic bags were irradiated with four UVC lamps (Philips TUV PL-L 55W/4P HF 1CT); of which two UVC lamps were placed at the top and another two UVC lamps placed at the bottom as shown in Figure 1. The intensity of the incident radiation at the surface of the plastic bag was 3707.9 μW/cm$^2$ (measured by Non Ionized Radiation Group, Malaysian Nuclear

Agency). The distance between the lamps and the surface of the latex sample were 100 mm and all experiments were conducted in a dark room.

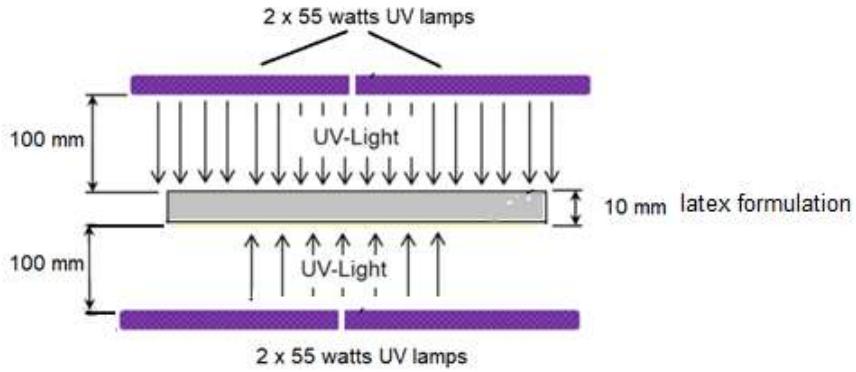


Figure 1. The experimental setup for UVC irradiation of latex formulation samples

**Measurement of tensile properties**

The latex films made by the coagulant dipping method were cut into dumbbell shape test pieces according to MS 1523:2001 (Figure 2). For each latex film sample, five dumbbell test pieces were used for the tensile test (using Universal Testing Machine SHIMADZU, M703911, 50N) and a median value was taken as the final result in accordance with ASTM D412.

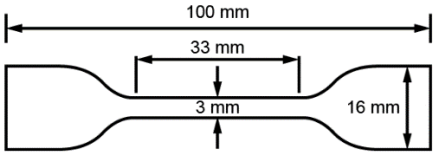


Figure 2. Dimension of dumbbell cutest piece

**Determination of gel content**

The gel content or percentage of latex film crosslinked density was determined by the extraction of latex film in toluene for 8 hours using Soxhlet apparatus as required by [ASTM D3616-95, 2014; Jayasuriya *et al*. 2001]. Then the extracted samples were dried in an oven at 70°C till constant weight was achieved. The gel fraction was calculated as Equation (1):

$$\text{Gel content, } \% = \frac{w_1}{w_o} \times 100 \quad (1)$$

where $W_0$ and $W_1$ are the weights of the dried samples before and after extraction, respectively.

**Determination of total solid content (TSC)**

The total solids content (TSC) is the percentage by weight of latex which is non-volatile at a definite temperature. The standard method is as described in ISO 124:2014. In this method, 2.0 g ± 0.5 g of latex was poured into the petri dish and weighted to the nearest 0.1 mg. Then the dish was placed into

an oven and heated at 70ºC ± 2 ºC for 16 h or at 105 ºC ± 5 ºC for 2 hours or until the test portion has lost its whiteness. After that, the dish was cooled down in a desiccator and weighted, and the mass of dry latex was recorded. The TSC was calculated as Equation (2):

$$\text{Total solid content, } \% = \frac{m_1}{m_o} \text{ x } 100 \quad (2)$$

Where $m_0$ and $m_1$ is the weight (gram) of the latex and dried latex, respectively.

**Determination of alkalinity**

ISO 125 standard was referred for determination of alkalinity. 5 g of latex sample was poured into a 500 $cm^3$ beaker and followed by 200 $cm^3$ of water. The solution was stirred thoroughly. While stirring, the pH meter electrode was inserted into the solution. Hydrochloric acid solution was added slowly into the solution via titration until the pH is reduced to a value of 6.00 ± 0.05.

The alkalinity of the latex was calculated as Equation (3):

$$\text{Alkalinity} = \frac{1.7cV}{m} \quad (3)$$

Where *c* is the actual concentration of HCl per cubic decimetre of acid used, *V* is the volume, in cubic centimetre, of acid used; and *m* is the mass, in grams, of the latex sample.

**Determination of mechanical stability (MST)**

The latex samples were subjected to MST testing using Klaxon MK3 machine in accordance with ISO 35:2004 requirement, where 80.0 g ± 0.5 g of the latex was first added into MST machine container. Then the container was positioned in the Klaxon MK3 MST machine and stirred at 14000 rev/min ± 200 rev/min throughout the test until the end-point is reached. The arrival of the end-point is preceded by a marked decrease in the depth of the vortex around the stirring shaft, loss of turbulence and change in the sound of stirring action. The end-point which is the first appearance of flocculum was determined by removing a drop of the sample with a clean glass rod at intervals of 15 seconds and gently spreading the sample on a suitable surface; for example, the palm of the hand.

**Measuring of viscosity**

Latex sample with temperature range at 25 – 29 ºC was measured its viscosity in accordance with MS 281 standard requirement. The viscometer used in this study was Brookfield model DV-II +. 200 g of latex was weighed into a 250 ml capacity beaker. Then the spindle was inserted into the latex and the machine was set at 60 rotation speed per minute (RPM) frequency. The equilibrium viscosity reading is attained after 20 to 30 seconds.

## RESULTS AND DISCUSSION

### Effect of *t*-BHPO on mechanical properties of hybrid UV- peroxide prevulcanized natural rubber latex

In UV vulcanization, the UVC light will be absorbed by photoinitiator present in latex formulation to form free radicals. These free radicals will help to form crosslinks in polyisoprene. For this study, the UV dose delivered to form free radicals were calculated as below;

UV dose = UV light intensity ($\mu Wsec/cm^2$) x time (s)
= 3707.9 x 3600 = 13348440 $\mu Wsec/cm^2$; which $1 \mu Wsec/cm^2 = 0.001$ mJ/sec*$cm^2$
= 13348.44 $mJ/cm^2$

Besides, the vulcanization method using UV radiation will also generates heat from the UV lamps. Since the hybrid UV-peroxide vulcanization method uses peroxide as the co-sensitizer, the heat produced from the UV lamps (irradiation for one hour has caused the temperature of the samples to increase within 70-75 ºC) will be manipulated to decompose the peroxide compounds for the formation of radicals that will help in improving the mechanical properties and cross-link density of hybrid UV-peroxide prevulcanized natural rubber latex. The heat was produced alongside UV irradiation and caused the increment of latex temperature up to 70 – 75 ºC. In peroxide vulcanization, heat is required to decompose peroxide compounds to form free radicals and produce crosslinks to improve the mechanical properties of the vulcanized latex. Hence, it is anticipated that the produced heat from UV irradiation can be a compliment to UV and photoinitiator in decomposing peroxide to achieve vulcanization of natural rubber latex.

### Tensile strength properties

Tensile strength is considered one of the most important parameters by latex product industries when qualifying a latex product for intended use during the development and quality control stages. A latex product must possess the required minimum tensile strength to confirm its quality and usefulness. For example, a nitrile examination glove requires a minimum tensile strength of 14 mPa, whereas a latex surgical glove may need a minimum tensile strength of 24 mPa [ASTM D3577].

Modulus is another mechanical property of latex film. However, it cannot be used as an indicator of the quality of natural rubber latex films. Although modulus value is frequently used to indicate the degree of crosslinking in a film, it does not reveal the film's physical strength. In industry, modulus value is used to quantify the stiffness of a film that is subjected to stress. Tensile strength values are the greatest stress that a film can bear while being stretched before breaking, and they are a significant factor in defining the elasticity of the film. Therefore, for this study, the modulus and tensile strength of the films were measured.

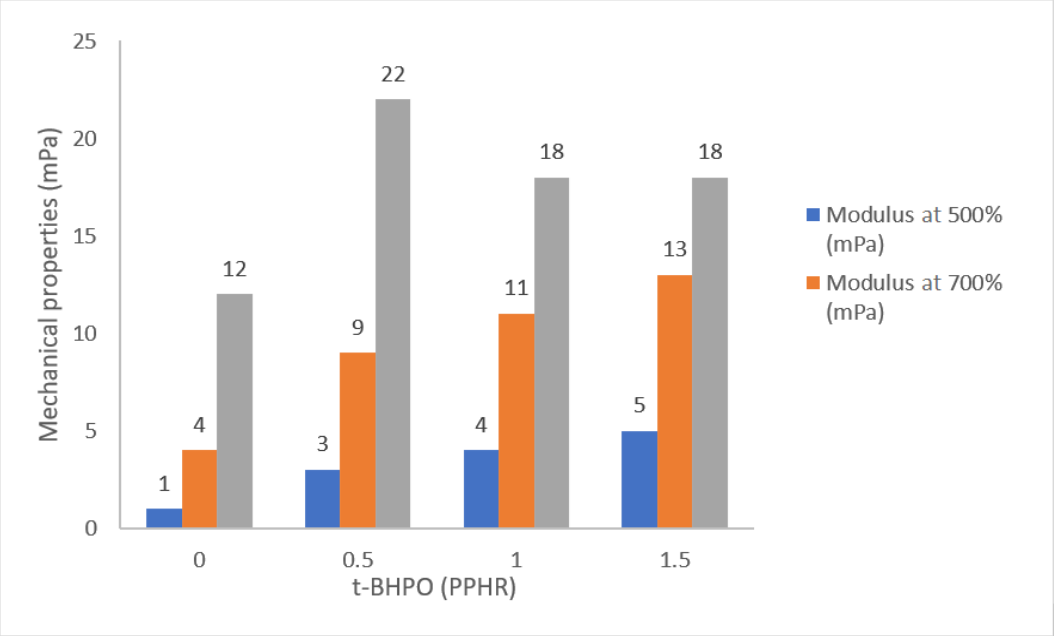


Figure 3. Mechanical properties of hybrid UV-peroxide prevulcanized natural rubber latex (taken as the median values from tensile test results) prepared with different amount of *t*-BHPO

Figure 3 gives the mechanical properties of control and hybrid UV-peroxide prevulcanized natural rubber latex samples that have been prepared by UV irradiation at various amount of *t*-BHPO and tested as required by ASTM D412 standard. In comparison to the control sample, it is obvious that hybrid UVNRL-peroxide samples with *t*-BHPO showed improved mechanical properties upon UV irradiation. The tensile strength and modulus of hybrid UVNRL-peroxide sample with 0.1 pphr *t*-BHPO showed around 100% increment compared to the control sample. The increment in tensile strength, modulus at 500% and modulus at 700% are due to the enhancement of intra-particle crosslink density (chemical crosslinking) induced by UV radiation and monogeneity of the vulcanization from the UV radiation and peroxide [Siri Upathum 1996]. However, it was observed that the addition of 0.2 and 0.3 pphr of *t*-BHPO into the formulation will produce latex films with higher modulus at 500% and modulus at 700% but lower tensile strength values. This indicates that the formation of cross-links occurs at a high rate as well, causing the C-C bond to become too stiff and easy to break, hence, latex films with lower tensile strength.

**Effect of irradiation doses on gel content of hybrid UV-peroxide prevulcanized natural rubber latex**

Gel content is a measurement of crosslinking that exists in latex polymer film. Gel content is also one of the important parameters in latex product manufacturing as it correlates with the mechanical properties such as tensile strength. Gel content provides stronger evidence to support the tensile strength and modulus value obtained from the previous section.

Based on the modulus value shown in Figure 3, it was observed that the value increases as the concentration of *t*-BHPO increases, as well as the decrement of tensile strength with *t*-BHPO beyond 0.1 pphr. It was assumed that there is a higher amount of crosslinking produced that made the latex film become stiff. From the data obtained that was illustrated in Figure 4, the average gel content of the latex film increases as the concentration of *t*-BHPO increases. It can conclude that the concentration of *t*-BHPO is directly proportional to modulus value, but it was inversely proportional with tensile strength beyond 0.1 pphr of *t*-BHPO, due to an increase of gel content or crosslink.

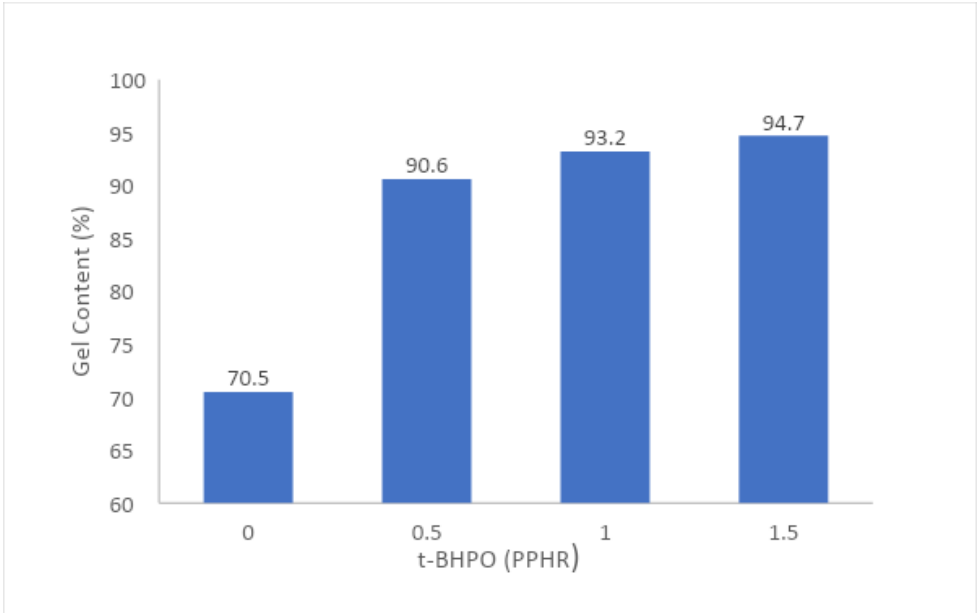


Figure 4. Gel content of hybrid UV-peroxide prevulcanized natural rubber latex prepared at different concentration of *t*-BHPO

**Effect of *t*-BHPO on physical properties of hybrid UV-peroxide prevulcanized natural rubber latex**

Table 3. Comparisons of physical properties of the raw latex, control (UVNRL) and hybrid UVNRL-peroxide

| **Sample**<br><br>**Physical Properties** | **Raw latex** | **Control (UVNRL)** | **Hybrid UVNRL-peroxide** | **Specification** | **Test Method** |
|---|---|---|---|---|---|
| TSC, % | 62.13 | 52.25 | 52.11 | Min 52 | ISO 124 |
| Alkalinity, % | 0.65 | 0.57 | 0.50 | 0.3-0.7 | ISO 125 |
| MST, sec | 950 | 1000 | 1150 | 650 | ISO 35 |
| Viscosity, cps | 31.71 | 33.75 | 35.55 | 30-40 | MS 281 |

TSC is the measurement of the percentage of rubber (hydrocarbon) and non-rubber contained in latex. TSC is an important indicator to show a latex formulation is correctly prepared in accordance to plan. Additionally, through this method the presence of non-volatile but soluble additives are also measurable [Akademi Hevea Malaysia 2012].

During the preparation of the hybrid UVNRL-peroxide prevulcanized natural rubber latex, the final latex concentration along with a mixture of acrylate, peroxide, activator, stabilizer, photoinitiator and water will be ensured at a minimum of 52% TSC. The selection of 52% of TSC was made for two reasons. The first reason is to prevent an increase in latex viscosity after the UV radiation procedure is complete and the second is to improve the crosslink density in prevulcanized natural rubber latex by the presence of OH radicals produced from water radiolysis [Makuuchi 2003]. However, one needs to be careful as latex with a low percentage of TSC will be difficult to produce thick rubber latex products due to a lack of rubber molecules in the latex.

Apart from TSC, measuring the alkalinity of the prevulcanized latex is also crucial. Alkalinity refers to the latex's free alkaline content, which is typically expressed as the latex's ammonia concentration in percentage. Ideally, prevulcanized latex's alkalinity should fall between 0.3% and 0.7%. Under an alkaline environment, fatty acids and proteins will be ionized to produce negative charges on the rubber particles surface. The colloid stability of the latex will be maintained by the presence of this charge particles since two particles with similar negative charges that are nearby will repel one another due to electrostatic attraction.

When the latex alkalinity is lower than 0.3 %, it will create a suitable environment for the bacteria to break down natural proteins in latex and spoiling it [Abu Bakar & Rosley 1994]. Meanwhile, ammonia over 0.7 % will disrupt the production process of dip-products through difficulty to form thin latex gelatine lining in the industrial production line. According to the results of this study, adding *t*-BHPO, HDDA, HAC and Irgacure 1173 had no significant effect on the alkalinity of the hybrid UVNRL-peroxide samples as compared to control.

The MST test is used to examine the stability and resistance of latex to mechanical agitation. In addition, it can be described as the amount of time, measured in seconds, needed for rubber particles to coalesce when latex is stirred at a high speed under precise circumstances [Akademi Hevea Malaysia 2012]. In the production of latex dip-products, the minimum requirement for the MST of the prevulcanized latex is 650 seconds. In dipping tanks at factory production lines, latex with a low MST value can clump quite quickly. This will cause a defect in the manufactured products. From Table 3, it was found that the addition of *t*-BHPO, HDDA, HAC and Irgacure 1173 into the hybrid UVNRL-peroxide compounding formulation can help to improve the stability of the latex towards mechanical agitation.

According to the research of Blackley (1997) and Roshanie (2010), oxygen (from the air) can create hydroperoxide groups on rubber molecules, and those groups may be ionised to unstable ions. Subsequently, this ion encourages the breakdown of proteins and phospholipids to produce polypeptides and amino acids, the latter of which can be converted into a variety of compounds, including glycerol, fatty acid anions, and phosphate anions. These materials are then absorbed at the particle interface, increasing the latex's stability. Coincidentally, oxygen and water are the by-products of peroxide decomposition in peroxide vulcanization. Thus, it was proposed that oxygen produced by the breakdown of *t*-BHPO might aid in increasing the latex's stability.

The final physical properties measured are latex viscosity. The viscosity of the prevulcanized latex must be kept under control at a specific range so that the finished goods fall within the desired thickness range, which makes this parameter crucial to the manufacturer of latex dip-products. Typically, the manufacturer specifies a viscosity range of 30 to 40 centipoise (cps). According to Table 3, despite the fact that the viscosity of the hybrid UVNRL-peroxide sample increased marginally, it still falls within the acceptable range. It is suggested that the addition of *t*-BHPO, HDDA, HAC and Irgacure 1173 or other chemicals will disturb the stability of the rubber particles in the hybrid UVNRL-peroxide and cause a minor increment of latex viscosity. This can be tackled by increasing the amount of stabilizers used in the compounding formulation of hybrid UVNRL-peroxide.

## CONCLUSION

Prevulcanized NRL with good mechanical properties can be prepared by hybrid UV and peroxide vulcanization. UV irradiation of latex formulations based on 2.0 pphr of Irgacure 1173 as photoinitiator, 2.0 pphr of HDDA and 0.1 pphr of *t*-BHPO as co-sensitizers at one-hour exposure time (temperature within 70-75 $^{o}$C) can produced rubber film with tensile strength of 22 mPa and crosslink percentage of 90.6%. In addition, this vulcanization method does not cause significant adverse changes to the physical properties of the prevulcanized natural rubber latex. Hence, it can be concluded that hybrid UV-peroxide vulcanization is a potential sulphur-free vulcanization method for natural rubber latex.

## ACKNOWLEDGEMENTS

The authors would like to express their deepest appreciation to the Malaysian Ministry of Science, Technology and Innovation (MOSTI) for financial support under Technology Development Fund 1 (TDF07211421(A)) and the Malaysian Nuclear Agency for providing research facilities for this work.

## REFERENCES

Abu Bakar, A. & Rosley, A. 1994. *Teknologi Perladangan dan Pemprosesan Getah*. Kuala Lumpur: Institut Penyelidikan Getah Malaysia.

Akademi Hevea Malaysia. 2012. Kursus ujian lateks. *Lecture Note of Short Course on Latex Testing*. Lembaga Getah Malaysia, 25-28 Jun.

ASTM D3577-01a. 2001. *Standard Specification for Rubber Surgical Gloves*. ASTM International. West Conshohocken, PA.

ASTM D3578 – 05. 2015. *Standard Specification for Rubber Examination Gloves*. ASTM International. West Conshohocken, PA.

ASTM D3616-95. 2014. *Standard Test Method for Rubber—Determination of Gel, Swelling Index, and Dilute Solution Viscosity*. ASTM International. West Conshohocken, PA.

ASTM D412-16. 2016. *Standard Test Methods for Vulcanized Rubber and Thermoplastic Elastomers-Tension*. ASTM International, West Conshohocken, PA.

Blackley, D. C. 1997. *Polymer Latices: Science and Technology*. Vol. 2. New York: Springer.

ISO 124:2014 Latex, rubber — Determination of total solids content. . International Organization for Standardization. Geneva, Switzerland.

Cahya, W. & Herry, P. 2018. Design of A Prototype Photoreactor UV-Leds For Radiation Vulcanization of Natural Rubber Latex. International Journal of Technology (2018) 1: 130-141.

Hansupalak, N., Srisuk, S., Wiroonpochit, P. & Chisti, Y. Sulfur-Free Prevulcanization of Natural Rubber Latex by Ultraviolet Irradiation. *Ind. Eng. Chem. Res.* **55**, 3974–3981 (2016).

ISO 125. 2011. *Natural rubber latex concentrate - Determination of alkalinity*. International Organization for Standardization. Geneva, Switzerland.

ISO 125: 2020 - Natural rubber latex concentrate — Determination of alkalinity. International Organization for Standardization. Geneva, Switzerland.

ISO 35. 2004. *Natural rubber latex concentrate - Determination of mechanical stability*. International Organization for Standardization. Geneva, Switzerland.

ISO 35:2004- Determination of the mechanical stability of natural rubber latex concentrate. International Organization for Standardization. Geneva, Switzerland.

Jayasuriya M M, Makuuchi K and Yoshi F 2001 *European Polymer Journal* 37 93-98.

Lazim, M. N. M., Mohd, A. F., Chai, C. K., and Ibrahim, N. (2021). The Effects of HDDA and n-BA & TMPTMA on Physical, and Thermal Properties of UV Irradiation Vulcanization Natural Rubber Latex. *International Transaction Journal of Engineering, Management, & Applied Sciences & Technologies*, 12(9), 12A9F, 1-11.

Makuuchi K. 2003. *An Introduction to Radiation Vulcanization of Natural Rubber Latex*. Bangkok. T.R.I. Global Co., Ltd.

MS 1523:2001, *Rubber - Temperature, Humidities and Times for Conditioning and Testing.* Malaysian Standard, Malaysia.

Pairu, I.; Rusli, D.; Wan Manshol, W. Z., *Radiation Effects and Defects in Solids*, 2016,171, 1006-1015.

Roshanie, L. K. S. 2010. A Study on the effect of aeration on mechanical stability of concentrated natural rubber latex upon maturation. Master Thesis, University of Moratuwa Sri Lanka.

Schlögl, S.; Temel, A.; Schaller, R., *Rubber Chemistry and Technology*: 2010, Vol. 83, No. 2, pp. 133-148.

Siri Upathum, C.; Sonsuk, M. Development of An Efficient Process for Radiation Vulcanization of Natural Rubber Latex Using Hydroperoxide With Sensitizer. *Proceedings of the Second International Symposium On RVNRL*, Kuala Lumpur, Malaysia, July 15-17, 1996.

Sofian I, Khairiah B, Chantara T R and Noor Hasni M A 2018 *Radiation Effects and Defects in Solids* 173, 427-434.

Wiroonpochit, P., Uttra, K., Jantawatchai, K., Hansupalak, N. and Chisti, Y. (2017). Sulfur-Free Prevulcanization of Natural Rubber Latex by Ultraviolet Irradiation in the Presence of Diacrylates. *Industrial & Engineering Chemistry Research* 2017 *56* (25), 7217-7223

Wu, M., McIntosh, J. Liu, J., (2016), Current Prevalence Rate of Latex Allergy: Why it Remains a Problem?. *Journal Occupational Health*, Volume 58, pp. 138-144

e-Jurnal Sains Nuklear Malaysia, 2023, Vol. 35 (No.2): 49 – 57
*eISSN: 2232-0946*

# STABLE ISOTOPES OF CARBON, NITROGEN, AND SULPHUR AS POLLUTION SOURCE INDICATORS IN KUALA SELANGOR NATURE PARK

***[1]Mohd Noor Hidayat Adenan*, [2]Jalal Sharib, [1]Ahmad Nazrul Abd Wahid, [1]Rafiah Mohamed Roshidi, [2]Mohamad Izwan Abdul Adziz, [2]Mohd Tarmizi bin Ishak, [2]Lakam Anak Mejius, [2]Nurrul Assyikeen Md. Jaffary, [2]Nooradilah Abdullah, [1]Shyful Azizi Abdul Rahman, [2]Jeremy Andy Anak Dominic Daung, [2]Dainee Nor Fardzila Ahmad Tugi, [2]Siti Aminah Omar, [2]Shakirah Abd. Shukor, [3]Azharuddin Abd. Aziz and [3]Munirah Abdul Zali***

[1]Agrotechnology and Biosciences Division,
Malaysian Nuclear Agency, Bangi, 43000 Kajang, Malaysia
[2]Waste Technology and Environmental Division,
Malaysian Nuclear Agency, Bangi, 43000 Kajang, Malaysia
[3]Department of Chemistry Malaysia, Jalan Sultan,
46661 Petaling Jaya, Malaysia
*Correspondence author: hidayat@nm.gov.my

## *ABSTRACT*

*Anthropogenic activities such as changes of land use for coastal development are the major factors affecting the sustainability of mangrove area. Mangrove forests in Kuala Selangor Nature Park (KSNP) is one of the areas that should be monitored for any potential source of pollution, and this can be performed by using stable isotopes as the important indicators. Vegetation samples from several palm and mangrove species were analysed for $\delta^{13}C$, $\delta^{15}N$ and $\delta^{34}S$ stable isotopes. The samples were collected from nine different locations comprising of KSNP area, water canal, residential area, sluice gate, aquaculture area, landslide area, agriculture area, jetty and river confluence area. The $\delta^{13}C$, $\delta^{15}N$ and $\delta^{34}S$ value in the samples are found to be ranged from -33.05‰ to -13.33‰, +1.69‰ to +9.27‰, and +7.83‰ to +8.50‰, respectively. IsoSource modelling software was used and found that 50% is the highest source proportion identified in aquaculture location demonstrating that the area is the main pollution source in this study. The findings from this study could be used for further control measures by local authority in order to preserve the flora and fauna in KSNP.*

**Keywords:** Carbon, nitrogen, sulphur, stable isotope, indicators, pollution source, Kuala Selangor Nature Park

## INTRODUCTION

Stable isotope analysis (SIA) is a powerful technique for environmental assessment and monitoring that provides information about anthropogenic activities over time. Stable isotope compositions of $^{13}C/^{12}C$, $^{15}N/^{14}N$ and $^{34}S/^{32}S$ change in predictable ways due to mixing and fractionation, giving insights into sources and cycling of these elements in biosphere (Fry, 2006). SIA has been widely used in mangrove ecosystem studies to better understand food web interactions (Abrantes et al., 2015), mangrove nutrient uptake (McKee et al., 2002), mangrove water use (Hayes et al., 2019), cycling of carbon (C) (Sasmito et al., 2020), nitrogen (N) (Fry and Cormier, 2011) and sulphur (S) (Raven et al., 2019).

The presence of pollutants in the food web depends on more than one factor and contamination of the surface water, sediment, or particulate matter, can affect the ecosystem structure and its trophic relationships (Bayen, 2012). Anthropogenic pollution of atmosphere causes diverse variations of carbon stable isotope ($\delta^{13}C$) values of plants. Plant vegetative parts during pollution frequently record a positive shift of $\delta^{13}C$, which is usually explained by photosynthesis at closed stomata (Savard, 2010). However, there are data suggested that the content of $^{13}C$ might be lower during pollution (Cada et al., 2016). Besides, man-made pollutants provide both enrichment (Pearson et al., 2000) and depletion (Kwak et al., 2009) of plants in $^{15}N$. Therefore, nitrogen stable isotope ($\delta^{15}N$) values can be used as they can provide reliable information about the source (anthropogenic vs. natural) of nutrients within the coastal areas (Fry, 2006). The stable isotopes of sulphur ($\delta^{34}S$) are also important in the study of the effects of pollutant sulphur on the environment particularly to differentiate between organic and inorganic matter (Trust and Fry, 2002).

Human activities continue to affect coastal ecosystems throughout the world and the situation is very worrying. Excessive nutrient inputs (eutrophication) from intensive agricultural activity and growing populations within coastal regions usually result in rapid degradation of water quality and modifications of ecological features. Mangrove forests could play an important role in mitigating eutrophication in coastal settings as they have been described as nutrient limited ecosystems with a generally positive physiological response to nutrient addition (Reef et al., 2010). Mangrove plants, which can grow extensively and form stable stands within most protected coastal regions of the tropics and subtropics could be of particular importance for remediation.

Disturbances in mangrove areas not only affect recruitment, but can also change the cycling of C, N and S. Loss of mangrove trees and root structures can change organic matter inputs, sediment oxygenation and degradation of sediment organic matter. These changes alter overall sediment conditions, with consequences for benthic assemblages (Harada et al., 2019), sediment C and N stocks (Adame et al., 2018), and associated nutrient processes. Kuala Selangor Nature Park (KSNP) which is located in Northwestern Selangor, Malaysia also affected by anthropogenic pollution. It is the mangrove forest with many flora and fauna species. In this study, the aim is to determine C, N and sS stable isotope values in order to investigate the source of pollution from biota samples that have been collected from the study site.

## MATERIALS AND METHODS

### Area of study and sample collection

Kuala Selangor Nature Park (KSNP) (0320.0266,N,10114.4201,E) (Fig. 1), one of the attractive places in Northwestern Selangor, Peninsular of Malaysia is the habitat for 156 species of birds and frequently used as research for interested scientists and tourists (Rohaizah et al., 2020). In the present study, vegetation samples from several palm and mangrove species were collected from nine different locations comprising of KSNP area, water canal, residential area, sluice gate, aquaculture area, landslide area, agriculture area, jetty and river confluence area. These sampling sites are connected by Selangor river.


Figure 1. Location map of the KNSP sampling sites by Google Earth

Samples were collected during the dry season in February 2022. These plants were collected by hand, and carefully shaken to remove animal-related debris or soil particles. The plant samples also were clean using deionized water before kept in storage. They were then stored in clean containers and labelled accordingly to the sampling locations.

**Sample Processing**

All of the plant vegetation samples (leaves) were dried at 60 °C for 72 hours in oven (Memmert, Germany) and then ground to obtain homogeneity below 100 µm particles size. The samples were ground using ultra centrifugal mill ZM 200 (Retsch, Germany). Approximately 2 mg of samples were weighted and then inserted into tin capsules for bulk C, N and S isotopes analysis using Elemental Analyzer Isotope Ratio Mass Spectrometer (EA- IRMS) (Finlay, 2001).

**Chemical Analysis**

All the samples were analysed for $^{13}C/^{12}C$, $^{15}N/^{14}N$ and $^{34}S/^{32}S$ isotope ratios using EA-IRMS analyser. The analysis process is comprising of three stages namely combustion, reduction, and stable isotope ratio.

**Combustion**

Combustion which is the first process in the EA-IRMS will produce $CO_2$, $H_2O$, $N_2$, $NO_x$, $SO_2$ and $SO_3$ and volatile halogenated compounds. Therefore, the combustion tube is filled with tungsten trioxide ($WO_3$), which delivers additional oxygen to the reaction, prevents the formation of non-volatile sulphates and binds alkali and alkali earth elements.

**Reduction**

The carrier helium gas, with the combustion products, flows from the combustion tube to a reduction tube via a heated bridge. It is important that this bridge is heated to prevent $H_2O$ condensing and reacting with the $SO_3$ and the $SO_2$. The reduction tube is filled with copper and facilitates the reduction of $NO_x$ to $N_2$ and $SO_3$ to $SO_2$. Silver wool is also present in the reduction tube to react with any volatile halogen compounds that may have formed. From the reduction tube, the gas flows into an absorption tube which is filled with phosphorous pentoxide (Sicapent®) to remove water. After these reactions, the combusted sample has been quantitatively converted into the target gas species $N_2$, $CO_2$ and $SO_2$ used for detection of elemental concentrations and stable isotope ratios.

**Stable Isotope Ratio**

The gas stream ($N_2$, $CO_2$ and $SO_2$) passes into a gas chromatograph where components of interest are separated and then bled into a mass spectrometer where the isotope species are ionised then separated in a magnetic field. These isotopic species are detected separately and from their ratios, after then the level of $^{15}N$, $^{13}C$, $^{34}S$ are calculated.

**Stable Isotope Analysis**

Carbon, nitrogen and sulphur isotopes data are reported in a δ notation in per mil against the international reference material USGS 40, USGS 41a and IA-R025, respectively.

$$\delta \frac{13C}{12C} = \left( \frac{13C\ (sample)}{12C\ (standard)} - 1 \right) * 1000$$

The data quality of carbon, nitrogen and sulphur isotope analysis were rigorously monitored using a number of in-house standards, international reference materials and duplicated samples. In this case, we have developed sulphanilamide as our in-house standard.

**IsoSource Mixing Model**

IsoSource software was used to identify the contribution of different sources to the mixture. Users are required to insert the isotopic values of the sources and mixture, the source increment, and mass balance tolerance. Once completed, IsoSources generated output files that consist of all feasible source combinations and descriptive statistics of each source distribution for the analysis (Fig. 2). In this study, the isotopic values of water canal, residential area, sluice gate, aquaculture area, river, landslide area, agriculture area, jetty and river confluence area were categorised as potential sources that contributed to the pollution and KSNP was categorised as mixture. The source increment and the mass balance tolerance were set at 5% and 0.6% respectively in the IsoSource software. By default, the settings are 1% (increment) and 0.1 (mass balance tolerance) to determine the source contribution in pollution investigation study. However, users are able to modify the value for optimum data interpretation.

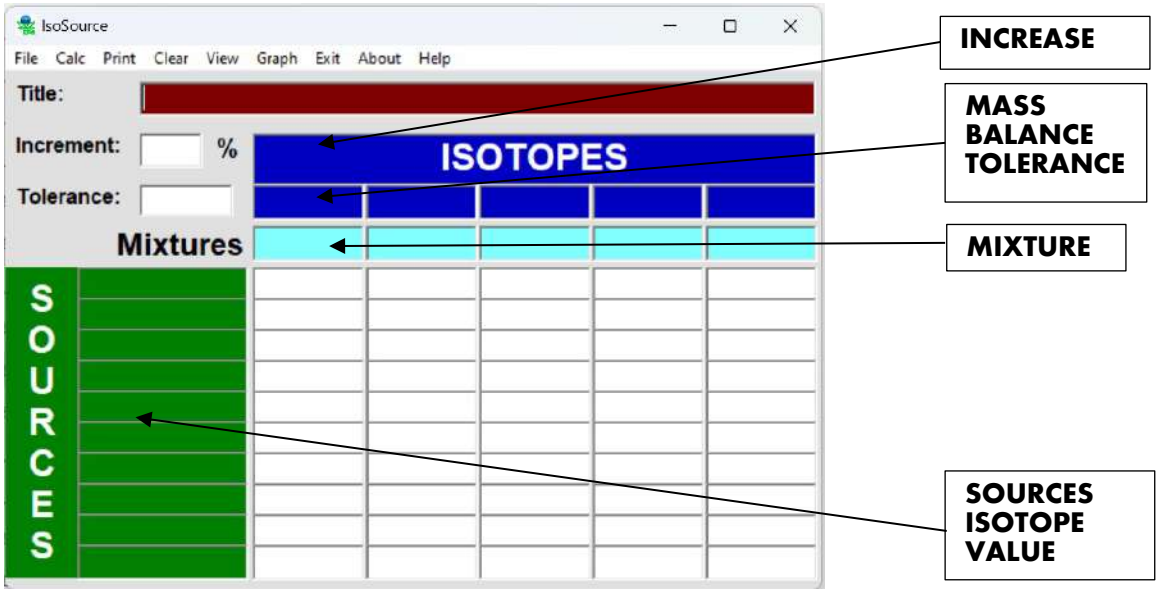


Figure 2. The IsoSource mixing model

## RESULTS AND DISCUSSION

### Carbon, Nitrogen and Sulphur Isotopic Values

The $\delta^{13}C$, $\delta^{15}N$ and $\delta^{34}S$ value in the samples are ranged from -33.05‰ to -13.33‰, +1.69‰ to +9.27‰, and +7.83‰ to +8.50‰, respectively (Table 1).

Table 1. The carbon ($\delta^{13}C/^{12}C$), nitrogen ($\delta^{15}N/^{14}N$) and sulphur ($\delta^{34}S/^{32}S$) isotopic values of sources and mixture in the study

| Sampling Locations | Stable Isotope Value (‰) | | |
|---|---|---|---|
| | $\delta^{13}C/^{12}C$ | $\delta^{15}N/^{14}N$ | $\delta^{34}S/^{32}S$ |
| Water canal | -13.33 | 8.79 | 8.27 |
| Residential area | -25.63 | 6.60 | 7.83 |
| Sluice gate | -30.94 | 7.40 | 8.45 |
| Aquaculture area | -30.14 | 9.27 | 8.45 |
| Landslide area | -29.42 | 7.63 | 8.22 |
| Agriculture area | -33.05 | 2.23 | 8.18 |
| Jetty | -28.33 | 8.98 | 8.46 |
| River confluence area | -30.01 | 1.69 | 8.50 |
| KSNP | -30.33 | 8.48 | 8.32 |

From the results, the samples collected from the residential area, sluice gate, aquaculture area, landslide area, agriculture area, jetty, river confluence area and KSNP are categorised as C3 plants since the $\delta^{13}C/^{12}C$ isotopic ratio are within –22 to −38 ‰ (Venkatesalu et al., 2008). The plant samples from water canal is categorised as C4 plants because the $\delta^{13}C/^{12}C$ isotopic ratio is within the range of –8 to −15 ‰ which is -13.33‰. Pollutants also are possible to cause the enrichment of $^{13}C$ isotope value. In certain cases, the $^{13}C$ signature of plant sample can be enriched by 2 ‰ in highly polluted area (Rikj and Ekblad, 2019).

Nitrogen stable isotope is very useful to be used as indicator to study nutrients derived from anthropogenic sources and it provide reliable information about the source of nutrients within coastal areas. From the results, aquaculture area shows the highest $\delta^{15}N/^{14}N$ value with 9.27 ‰. High $\delta^{15}N$ values arise due to the presence of excess nutrients in the environment allowing increased isotope fractionation via increased volatilisation of ammonia and increased microbial processing. Gritcan et al. (2016) reported that $\delta^{15}N$ values of around 10 ‰ are attributable to human and animal sewage, which is generally correlated with the presence of excess nutrients by eutrophication.

Sedimentary sulphate and sulphide minerals are the major sources of sulphur which available to plants. The results show that the $\delta^{34}S/^{32}S$ value of the samples are from +7.83‰ to +8.50‰. This result is in the range of – 50 to +10‰ indicates that the sulphur values are influenced by sedimentary sulphide. The sulphide in sediments is mainly derived from the products of sulphate-reducing bacteria, which are currently responsible for oxidising over half the organic matter flux reaching sediments. Pollution can cause strong depletion in $\delta^{34}S$ value in sulphide minerals that leads to the depletion of $\delta^{34}S$ value in plant (Tcherkez and Tea, 2013).

**Source Contribution Rate Using IsoSource Software**

The IsoSource software produced source proportion percentage of each location in the study that visualised possible pollution sources that contributed to KSNP area (Fig. 3).

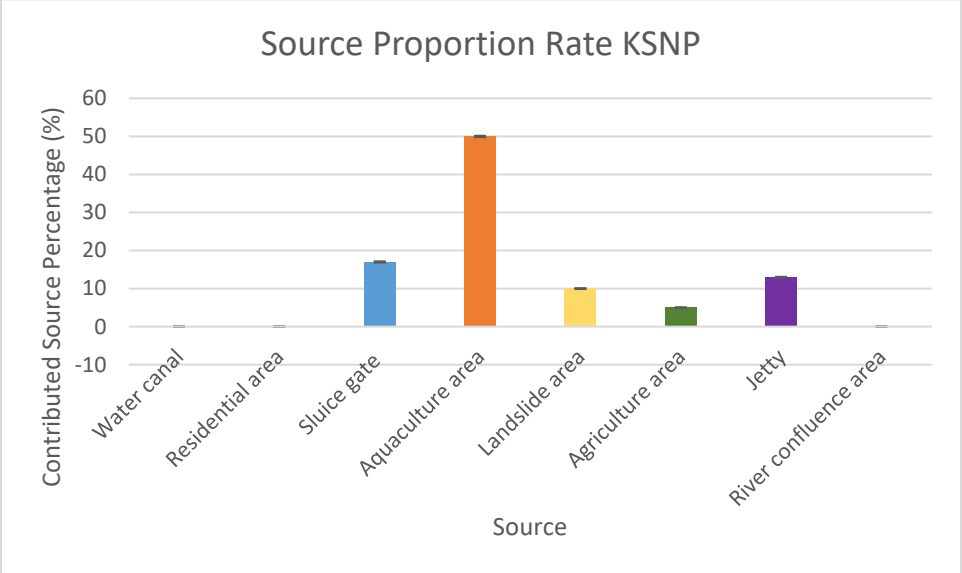


Figure 3. The contribution rate of the sources from different sampling locations in KSNP area

From the results, the highest proportion rate is from aquaculture area in the study with the value of 50%. The percent of frequency is shown in Fig. 4. The source is present between 0% and 65% and not present below 0% or more than 65%. The aquaculture area may be the main contributor to the pollution in KSNP is also supported by the high value of $\delta^{15}N$ at 9.27 ‰ which is due to the presence of excess nutrients that leads to increased volatilisation of ammonia and increased microbial processing. According to Singh et al. (2013), aquaculture and other anthropogenic activities such as illegal logging, land reclamation industrial and domestic use and pollutant runoff are threats to the mangroves.

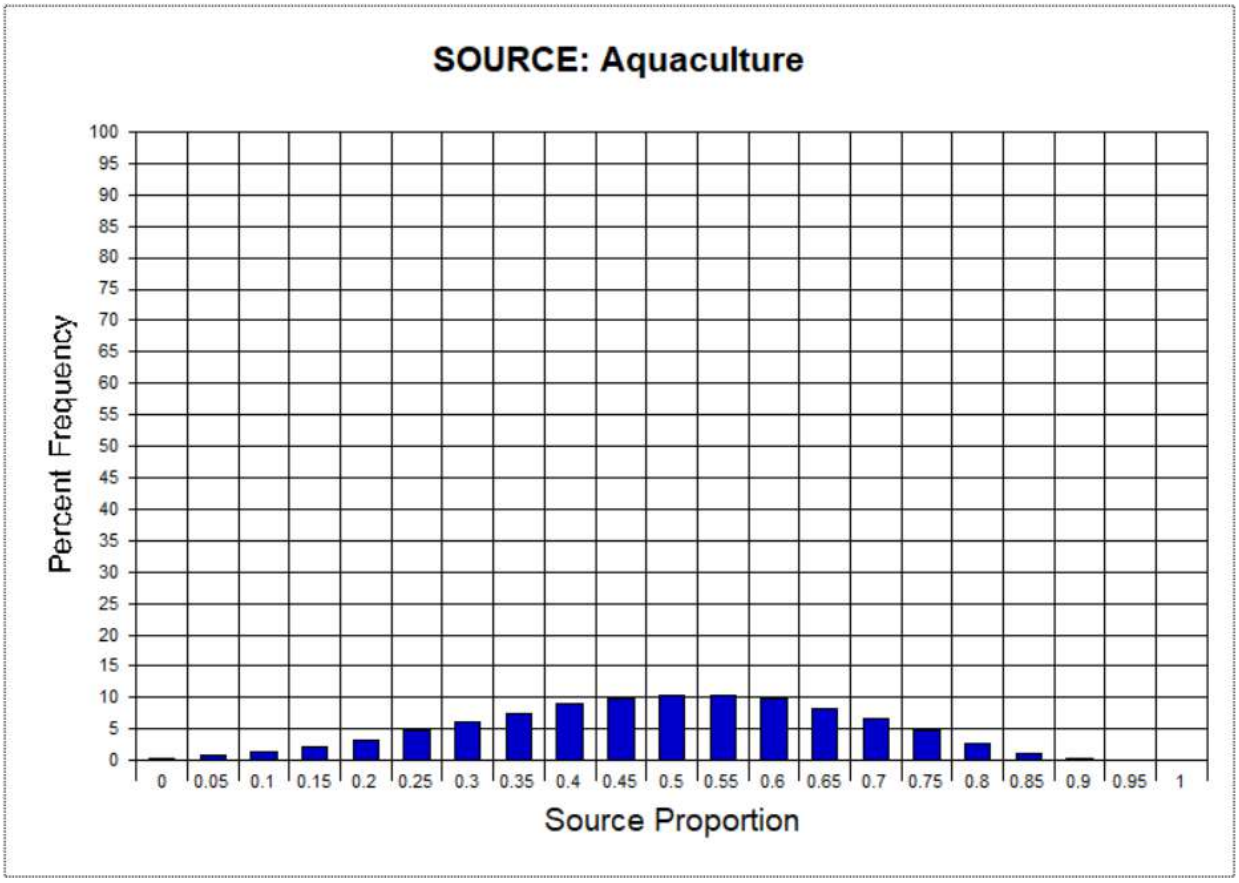


Figure 4. The most frequent proportion for aquaculture area is 50%

## CONCLUSION

Mangroves can absorb N, C and S in coastal waters and its environment which are reflected in their tissue stable isotope values. Anthropogenically derived elements discharge into coastal waters, such as aquaculture runoff is possible to cause the major pollution problems in KSNP. The SIA is proven to be valuable method to determine source of pollution in an area. The pollution issues can potentially harm the flora and fauna species in the area and leads to the ecosystem imbalance. All the man-made activities should be controlled to ensure the sustainability of the ecosystem.

## ACKNOWLEDGEMENTS

The authors wish to express their sincere thanks to International Atomic Energy Agency (IAEA) and Malaysian Nuclear Agency in the collaboration project of RAS 7037. The authors are very fortunate to have committed team members and laboratory staff in the project to ensure the success of the planned activities.

## REFERENCES

Abrantes, K. G., Johnston, R., Connolly, R. M., and Sheaves, M. (2015). Importance of Mangrove Carbon for Aquatic Food Webs in Wet–Dry Tropical Estuaries, Estuaries and Coasts, 38, 383-399.

Adame, M., Zakaria, R., Fry, B., Chong, V., Then, Y., Brown, C., and Lee, S. Y. (2018). Loss and recovery of carbon and nitrogen after mangrove clearing, Ocean & Coastal Management, 161, 117-126, 2018.

Bayen, S. (2012). Occurrence, bioavailability and toxic effects of trace metals and organic contaminants in mangrove ecosystems: A review. Environmental International, 48, 84–101.

Cada, H. Santruckova, J. Santrucek, L. Kubistova, M. Seedre, and Svoboda, M. (2016). Complex physiological response of Norway spruce to atmospheric pollution—decreased carbon isotope discrimination and unchanged tree biomass increment, Front. Plant Sci. 7, 805.

Finlay, J. C. (2001). Stable-Carbon-Isotope Ratios of River Biota: Implications for Energy Flow in Lotic Food Webs. Ecology, 82(4), 1052–1064.

Fry, B. (2006). Stable Isotope Ecology. New York, NY: Springer Science Business Media, LLC, 40–75.

Fry, B., and Cormier, N. (2011). Chemical Ecology of Red Mangroves, Rhizophora mangle, in the Hawaiian Islands1, Pacific Science, 65, 219-235.

Gritcan, A., Duxbury, M., Leuzinger, S. and Alfaro, A. C. (2016). Leaf stable isotope and nutrient status of temperate mangroves as ecological indicators to assess anthropogenic activity and recovery from eutrophication, Frontiers in Plant Sciences, 7, 1922.

Harada, Y., Fry, B., Lee, S. Y., Maher, D. T., Sippo, J. Z., and Connolly, R. M. (2019). Stable isotopes indicate ecosystem restructuring following climate-driven mangrove dieback, Limnology and Oceanography, 2019.

Hayes, M. A., Jesse, A., Welti, N., Tabet, B., Lockington, D., and Lovelock, C. E. (2019). Groundwater enhances above-ground growth in mangroves, Journal of Ecology, 107, 1120-1128.

Kwak, J. H., Choi, W. J., Lim, S. S. and Arshad, M. A. (2009). Delta C-13, delta N-15, N concentration, and Ca- to-Al ratios of forest samples from *Pinus densiflora* stands in rural and industrial areas, Chem. Geol. 264 (1–4), 385–393.

McKee, K. L., Feller, I. C., Popp, M., and Wanek, W. (2002). Mangrove isotopic ($\delta^{15}N$ and $\delta^{13}C$) fractionation across a nitrogen vs. phosphorus limitation gradient, Ecology, 83, 1065-1075.

Pearson, J. D., Wells, M., Seller, K. J., Bennett, A., Soares, A., Woodall, J. and Ingrouille, M. J. (2000). Traffic exposure increases natural N-15 and heavy metal concentrations in mosses, New Phytol. 147 (2), 317–326.

Raven, M. R., Fike, D. A., Gomes, M. L., and Webb, S. M. (2019). Chemical and isotopic evidence for organic matter sulfurization in redox gradients around mangrove roots, Frontiers in Earth Science, 7, 98.

Reef, R., Feller, I. C. and Lovelock, C. E. (2010). Nutrition of mangroves, Tree Physiology, 30(9), 1148–1160.

Rijk, I. J. C. and Ekblad, A. (2020). Carbon and nitrogen cycling in a lead polluted grassland evaluated using stable isotopes ($\delta^{13}C$ and $\delta^{15}N$) and microbial, plant and soil parameters, Plant Soil, 449, 249-266.

Rohaizah, A. L., Herindran, R. S., Munira, S. and Chiew B. T. (2020). Assessing ecotourism product at Kuala Selangor Nature Park, Selangor, International Journal of Management, 11(12), 2020, 382-394.

Sasmito, S. D., Kuzyakov, Y., Lubis, A. A., Murdiyarso, D., Hutley, L. B., Bachri, S., Friess, D. A., Martius, C., Borchard, N. (2020). Organic carbon burial and sources in soils of coastal mudflat and mangrove ecosystems, CATENA, 187, 104414.

Savard, M. M. (2010). Tree-ring stable isotopes and historical perspectives on pollution - An overview, Environmental Pollution. 158 (6SI).

Singh, H. R., Yahya, M. A. and Ismail, M. F. (2013). An assessment of coastal fish community adjacent to prawn farms at Kuala Selangor, Selangor, Advancements in Marine and Freshwater Sciences, 426-432.

Tcherkez, G. and Tea, I. (2013). $^{32}S/^{34}S$ isotope fractionation in plant sulphur metabolism, New Phytologist, 1-10.

Trust, B. A. and Fry, B. (1992). Stable sulphur isotopes in plants: A review, Plant, Cell and Environment. 15, 1105-1110.

Venkatesalu, V., Senthilkumar, A., Chandrasekaran, M. and Kannathasan, K. (2008). Screening of certain mangroves for photosynthetic carbon metabolic pathway, Photosynthetica, 46(4), 622-626.

e-Jurnal Sains Nuklear Malaysia, 2023, Vol. 35 (No.2): 58 – 68
*eISSN: 2232-0946*

# A STUDY OF SOIL EROSION AND SEDIMENTATION BETWEEN TWO DIFFERENT SEASONS IN SEMBRONG CATCHMENT USING CESIUM-137

***Jalal Sharib@Sarip*, Dainee Fardzila Ahmad Tugi, Mohd Tarmizi Ishak, Chriscius Anthonius, Mohd Izwan Abdul Adziz and Nurrul Assyikeen Md Jaffary***

Radiochemistry and the Environment Group
Waste and Environment Technology Division
Malaysian Nuclear Agency (Nuclear Malaysia)
Bangi, 43000 Kajang, Selangor, MALAYSIA
*Corresponding author email: jalal@nm.gov.my

## ABSTRACT

*Incidents of soil erosion and sedimentation occur frequently in catchments area around the world as a result of human activities and the impacts of global climate change. This research paper aims to determine the rate of soil erosion and sedimentation by using Cesium-137 ($^{137}Cs$) as a medium-term tracer in the Sembrong catchment over two different study seasons. The Sembrong catchment area is located in Kluang, Johor and is one of the most important ecosystems in Peninsular of Malaysia. Soil and sediment samples were collected using a standard metal corer and integrated suspended sediment trap samplers. A total of 50 samples were collected at 20 sampling stations consisting of various land uses in the vicinity of the site for both the dry and wet seasons. The dry season of soil erosion rate ranged between 5.09 t/ha/y to 65.2 t/ha/y. Meanwhile, soil erosion and sedimentation rates during wet season ranged between 8.02 t/ha/y to 39.78 t/ha/y and -4.81 t/ha/y to -50.81 t/ha/y, respectively. Rubber and oil palm plantations referring to station 17, stations 4 and 6 located near Sembrong Lake and Sembrong River had the highest rates of soil erosion and sedimentation at 51.03 t/ha/y and -50.81 t/ha/y, respectively. This situation may be due to the fact that rubber and oil palm plantations in these two areas are still new planting areas and allows the rainfall received in both seasons to continue to penetrate into the soil. In conclusion, $^{137}Cs$ as a medium-term tracer was successfully used to determine rates of soil erosion and sedimentation in two different seasons for the Sembrong catchment area. The data on soil erosion and sedimentation rates will be very useful for present and future land and water management in the Sembrong catchment area, and may be compared with other similar catchments in Malaysia.*

**Keywords:** Soil erosion; sedimentation; Cesium-137; gamma spectrometry; catchment management

## INTRODUCTION

Soil erosion is a process that involves the removal of the soil surface as a result of the effects of receiving large amounts of rain and the resulting flooding. It follows the transport of particles or grains of soil and rock from the surface of the earth through the action of natural processes such as wind or water flow and then transported with the flow of rainwater to lower areas. Excessive soil erosion will cause huge problems such as desertification, reduction of agricultural productivity due to land degradation, sedimentation of waterways, destruction and collapse of ecosystems due to the

loss of nutrients in the upper layer of the soil surface. Soil erosion is one of the latest conditions that are so significant to the global environmental problems faced now as the diversity of human activities has increased the rate again from 10-40 times (Blanco et al., 2010; Toy et al., 2002). Among them is one of the activities that are so widespread at the moment such as deforestation and land clearing aimed at clearing land for agricultural activities and settlement development with the opening of new residential. However, this activity has caused the strength of the soil to decrease and when there is heavy rain filled with such a large amount of volume, there will be a process or state of landslides due to the rapid activity of surface runoff.

Erosion events become even worse when the land surface lacks any vegetation that can prevent landslides continues. A high rate of rainfall is one of the main contributing factors to soil erosion and this kind of situation occurs as a result of the water content in the soil becoming saturated. The soil cannot receive or accommodate an excessive amount of water, especially during the rainy or monsoon season. The situation becomes even worse if the amount of rain received exceeds the level received before. Incidents like this are further reinforced by the existence of various development activities carried out in the highlands and slopes for economic, tourism and settlement purposes. This is further reinforced by the slope terraces that are not carried out in an orderly and neat manner in addition to a very weak slope management system such as cutting the slope vertically. There is no drainage system that is not very good for the purpose of water flow and is not accompanied by earth cover plants to prevent surface erosion also increases the occurrence of soil erosion especially in hilly and mountainous areas.

Meanwhile, the term "Environmental Isotope" or Fallout Radionuclide (FRNs) is usually used to refer to isotopes that are common and widely distributed in the environment or landscape and, although occurring at relatively low levels, can be easily measured. In most cases, it is of natural origin but in some cases, it is man-made. One of the most frequently used FRNs in soil erosion and deposition studies in catchment systems is $^{137}$Cs. $^{137}$Cs is an artificial or anthropogenic environmental radionuclide that can also be classified as a fall radionuclide. Over the last few decades, there have been many publications related to the various uses of FRNs especially $^{137}$Cs in soil erosion studies (Ritchie & McHenry, 1990; Walling and Quine, 1990; Walling and Quine, 1993; Zapata, 2002: Ritchie et al., 1974). Thus, this $^{137}$Cs tracer has also been found to be very effective as a diagnostic property in fingerprinting sediment sources (Wallbrink et al., 1998; Motha et al., 2003) and it has been widely used as a medium-term sediment tracer (Ritchie & McHenry, 1990; Zapata, 2002). Apart from that, some local and international studies have also reported to determine the rate of erosion and deposition by using the FRNs approach as a tracer especially short and medium term, Beryllium-7 ($^{7}$Be) and $^{137}$Cs between two different seasons (Blake et al., 1999, 2000, 2002; Jalal et al., 2019, 2020, 2021) in Timah Tasoh study site, Perlis. In addition, the use of these FRNs can also be seen in the use of $^{7}$Be to determine the penetration rate into the interior of the soil based on the two different seasons, namely the wet season and the dry season at the study site in Bangi, Selangor (Jalal et al., 2020, 2021).

The findings from these three studies have proven that the use and importance of FRNs as a tracer has been successful and can identify erosion and sedimentation rates for the short and medium term. A study using the Compound Specific Stable Isotope (CSSI) approach was also carried out in the Timah Tasoh catchment area, Perlis to identify the source or cause of sediment contribution to the catchment area (Jalal et al., 2020). Moreover, this can be seen clearly, that there is a relationship between sediment sources, sediment mobilization, transport, deposition, storage and sediment yield at the basin outlet can be very complex, especially in situations where sediment storage equals or exceeds sediment export (Trimble, 1983; Phillips, 1992; Walling et al., 2000). Sediment budgets,

which provide information on sediment sources, sediment sinks and sediment yields (Golosov et al., 1992; Reid and Dunne, 1996; Walling, 2000, Walling et al., 2001). Therefore, it is increasingly seen as a key sediment management tool (Walling and Collins, 2008). It is considered to be the single most important information about the fluvial system (Dietrich et al., 1982; Meade, 1982; Trimble, 1983; Reid and Dunne, 1996; Walling, 1998) and its importance in carrying sediments along with heavy metal concentrations and geochemical to the interior of the catchment area.

The study of soil erosion and sedimentation must be seen from various angles of interest, especially from the factors of ecological balance and natural ecosystems as well as their importance to humans. Therefore, humans need to take various initiatives in slope management that are more systematic and detailed so that the destruction of nature is more controlled and not destroyed for the benefit of future generations. This matter also determines that universal security can be preserved and that it will be able to avoid the loss of life, property and public facilities every time there is a major flood and then soil erosion, especially landslides. This research study aims to determine the soil erosion and sedimentation rate by using $^{137}Cs$ as a medium-term tracer in the Sembrong catchment, Kluang, Johor, Malaysia.

## MATERIALS AND METHOD

### Study area

The Sembrong Reservoir is one of the important ecosystems in Peninsular Malaysia since the 1960s and it has evolved from a natural ecosystem to a human-dominated one. The Sembrong catchment is located in Kluang, Johor between latitudes 3°26′42″ to 3°26′42″ N and longitudes 102°54′18″ to 102°55′54″E (Fig. 1). The morphology provides significant information about the physical characteristics of the reservoir (Table 1). The freshwater reservoir area is 7.7547 km$^2$ with an estimated storage capacity of 24.84 million m$^3$, while the catchment area is about 130 km$^2$. Thus, prior to conduct of this study, land use had changed considerably, with an increase in agricultural activity covering 8% (1984) to 82% (2010) in the area around the study site.

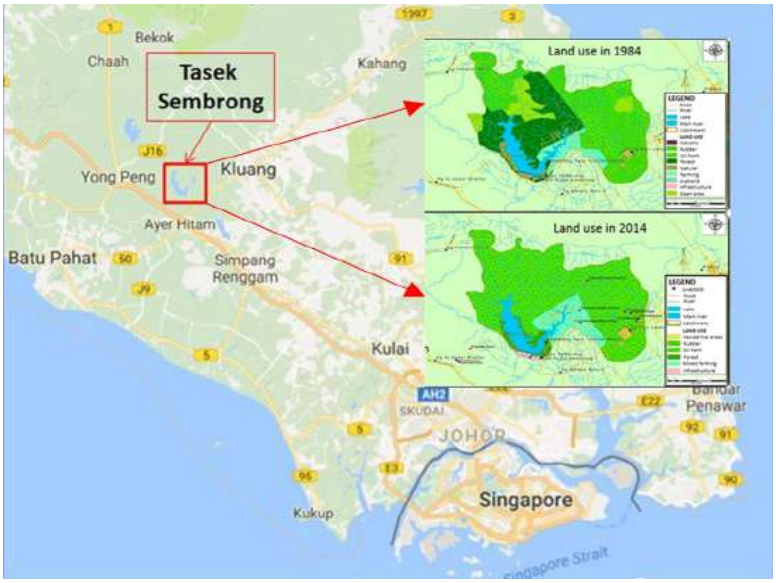


Figure 1. Study site in Sembrong catchment and land use

Table 1. The physical characteristics of Sembrong catchment

| No. | Parameter | Result |
|---|---|---|
| 1. | Lake area ($km^2$) | 7.7547 |
| 2. | Volume ($km^3$) | 36 |
| 3. | Maximum depth (m) | 7 |
| 4. | Mean depth (m) | 3.2 |
| 5. | Mean slope (%) | 4 |
| 6. | Height (m) | 9 |
| 7. | Catchment's area ($km^2$) | 130 |
| 8. | Storage capacity (million $m^3$) | 24.84 |
| 9. | Spillway | Concrete Fixed Ungated Ogee Crest |

**Soil sampling and preparation of samples**

All soil and sediment samples were collected using metal corers and integrated suspended trap samplers of the type described by Philips et al. (1993) and Russell et al. (2001) at 20 sampling stations (Figure 2). The samples were then taken to the Radiochemical and Environmental Laboratory (RAS), Nuclear Malaysia for further treatment. Hence, all samples were dried in an oven at 45 - 60 ºC for several days until they reached a consistent or stable weight. The completely dried sample was pounded using a mortar and pestle until fine and sieved with a 2 mm siever before being transferred into a 250 ml Marinelli beaker for the $^{137}Cs$ counting and analysis.

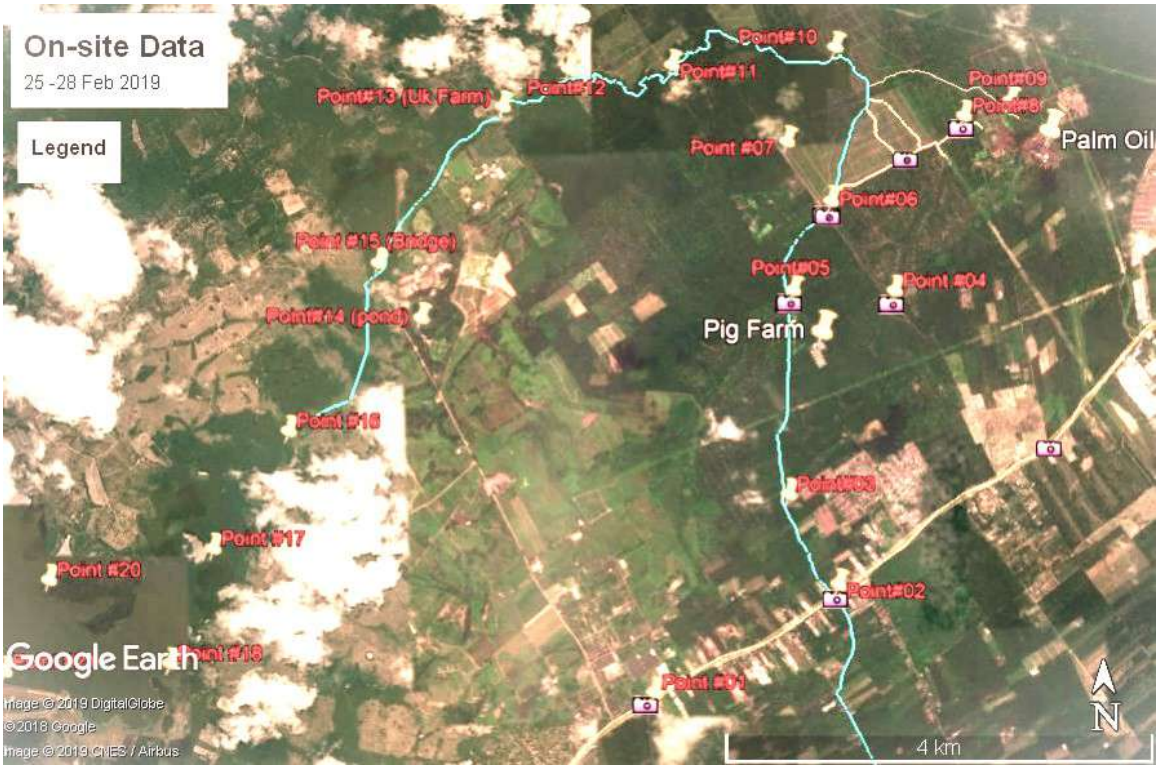


Figure 2. Sampling activities at 20 sampling stations

**Measurements of $^{137}$Cs radioactivity in soil and sediment sample**

Measurement of $^{137}$Cs by gamma spectrometry using a high purity Germanium (HPGe) detector with a relative efficiency of 28%. The detector was calibrated for selected measurement geometries and different soil densities by standard calibration samples and specialized computer software was used for gamma spectrum analysis. Walling and Quine (1993) have suggested that the sample counting time be extended to identify relatively low fallout activity such as $^{137}$Cs, usually taking in a very efficient time period ranging from 29000 to 55000s to achieve better measurement accuracy (>10%) at the 95% confidence level. Meanwhile, the detection limit of $^{137}$Cs for this measurement was estimated to be about 0.3 Bq/kg for the Marinelli geometry.

Thus, the charge magnitude in the crystal detector of gamma spectrometry was directly related to the energy emitted from the gamma rays from the sample. The γ-rays emitted from the detector sample are absorbed and subsequently lost during processing between the detector and the sample, where the γ-ray emission loses all energy by producing an electron pulse (Blake et al., 2000). Electron pulses generated from radioactivity emitted from the sample were amplified by a pre-amplifier as voltage pulses into a multi-channel analyser. The multi-channel analyser works by compiling the output pulses from multiple channels into a counting system, while transferring the emitted γ-ray pulses into a total count that were processed and displayed in the gamma spectrometry screen (Blake et al., 2000). Furthermore, the $^{137}$Cs activity from the samples was calculated using Equation (1) as below:

$$A = \frac{N}{\varepsilon . p_{\gamma} . m . t} \qquad (1)$$

where N was the net count under the peak of 662 keV gamma line energy that characterized $^{137}$Cs (in counts), ε was the efficiency of the detection system for the 662 keV gamma line energy (in counts.Bq$^{-1}$.s$^{-1}$) obtained from Equation (1), $p_{\gamma}$ was the absolute probability transition for 662 keV keV gamma line for $^{137}$Cs . Meanwhile, m and t are mass and time based on the number of minutes or seconds for $^{137}$C measurement from soil and sediment samples and it is measured based on concentration (Bq/kg). Moreover, the conversion of concentration into FRNs inventory, A are as follows:

$A = CMS$ (Bq/m$^2$)

Where;

*C* = FRNs activity concentration of the sample (Bq/kg),

*M* = total dry mass of the collected soil core (kg),
S = cross-section of the sampling corer (in m$^2$), which two types of inventories will be used for comparing;

- Reference inventory
- Sample inventory

The soil erosion rate was estimated by comparing the sample and reference inventory using a conversion model, that expressed in ton/hectare/year (t/ha/y). The conversion model used in this study was the Proportional Model ( Walling *et al.,* 2002). This model is based on the total fallout input of $^{137}$Cs being completely mixed in the plowed or cultivated layer. Thus, soil loss is directly proportional to the reduction in $^{137}$Cs inventory due to soil loss from the soil profile, since the beginning of $^{137}$Cs accumulation or the beginning of cultivation . Therefore, if half of the $^{137}$Cs input was removed, the

total soil loss over the period assumed to be 50% of the plough depth. The model represented as follows:

$$Y = 10\frac{BdX}{100TP}$$

Where:

$Y$ = mean annual soil loss (t/ha/yr);

$d$ = depth of the plough or cultivation layer (m);

$B$ = bulk density of soil (kg/m$^3$);

$X$ = percentage reduction in total $^{137}$Cs inventory (defined as ($A$ref-$A$)/$A$ref×100);

$T$ = time elapsed since the initiation of $^{137}$Cs accumulation or the commencement of cultivation, whichever is later (w/yr);

$A$ ref = local $^{137}$Cs reference inventory (Bq/m$^2$);

$A$ = measured total $^{137}$Cs inventory at the sampling point (Bq/m$^2$);

$P$ = particle size correction factor for erosion (P=1).

## RESULTS

Table 2 shows the overall results of the analysis of soil erosion and sedimentation rates from 20 stations throughout the study period. Indications of the results of this comprehensive analysis show various rates of soil erosion and sedimentation from the diversity of land use. The dry season indicated the result of soil erosion rate only at each station when compared to the wet season which is more mixed with the rate of sedimentation and soil erosion itself. The soil erosion rates showed values between 5.09 t/ha/y to 65.2 t/ha/y throughout both seasons. Stations 10 and 11 from mixed crop recorded the highest erosion rate values compared to station 14 from modern agriculture which were only able to record the lowest rate. However, the soil erosion rate values for all study seasons did not show any significant differences (p value is > 0.05). The difference in values between the highest and lowest values is clearly visible, and this is most likely due to the diversity of the soil which plays an important role especially in the process of soil erosion. However, these two values are also not significantly different compared to the highest value recorded (p value is > 0.05).

The dry season has provided the results of overall erosion values, while no sedimentation values were recorded for all study stations. However, the wet season recorded both erosion and sedimentation values. The sedimentation rate ranged from -4.81 t/ha/y to -50.81 t/ha/y. Meanwhile, the soil erosion rate in the wet season signified a slightly lower value compared to the dry season. This situation is likely due to the factor of receiving a volume of rain that is much more than the normal level at a certain time. This situation has also allowed such rainwater to penetrate the soil surface and further cause it to become softer resulting in a higher incidence of soil erosion than usual. Stations 4 and 6 recorded the highest values and while stations 1-3 were the lowest and likely due to different land use factors in addition to other factors. Stations 4 and 6 were areas that overgrown with new oil palm plantations. This may affect more sedimentation events in this area due to the lack of palm oil leaves to cover or prevent the amount of rain from falling directly to the ground surface. Furthermore, the

boundaries between these palm trees that are not covered by grass accelerate the rate of erosion further bringing mud to the surrounding area as sediment piles.

Table 2. Soil erosion and sedimentation rate during two seasons at different land use estimated using $^{137}$Cs

| **Sampling location** | **Land use** | **Erosion/sedimentation rate (t/ha/yr)** | |
|---|---|---|---|
| | | **Dry season** | **Wet season** |
| Station 1-3 | Settlement | 41.4 | -4.81 |
| Station 4 and 6 | Oil Palm Plantation | 28.39 | -50.81 |
| Station 5 | Animal farm | 6.33 | -8.16 |
| Station 7 | Modern agriculture | 35.6 | 23.8 |
| Station 8<br>Station 9 | Oil palm plantation | 11.06 | -7.88 |
| Station 10<br>Station 11 | Mixed crop | 65.2 | 29.78 |
| Station 12 | Banana plantation | 15.39 | 28.11 |
| Station 13 | UK's Farm | 28.66 | 8.0 |
| Station 14 | Modern agriculture | 5.09 | 8.02 |
| Station 15 | Mixed crop | 21.63 | 28.42 |
| Station 16 | Oil palm plantation | 11.08 | 19.44 |
| Station 17 | Rubber tree plantation | 51.03 | 39.78 |
| Station 18 | Fruit orchard | 36.26 | 9.38 |
| Station 19<br>Station 20 | Forest | 18.11 | 23.92 |

Note: (-) values indicate sedimentation

Station 14 is an area that carries out modern agricultural activities and this gives a soil erosion rate value that is not significantly different from the other study stations (p value is > 0.05). The use of a systematic farming system has been able to reduce the occurrence of soil erosion despite receiving a large volume of rain. A very similar situation can also be seen at Stations 19 and 20, where the soil erosion rate values for both are not very different. This situation is likely due to the position of the trees found in the forest quite close to each other along with the concept of "canopy" by the plants in the forest of this station. However, Stations 13 and 18 showed a difference in the rate of soil erosion for each other. The dry season recorded a high soil erosion rate compared to the wet season. This kind of situation occurs due to the rain factor received together with the number of livestock were released

in both seasons to graze grass in the UK's Farm area. Various factors also be considered such as soil types, the total volume of rainfall received for both seasons, as well as differences in land use at the study stations.

Several studies have been reported by Zullyadini et al., (2013) and (Jalal et al., 2019, 2020, 2021) in the Timah Tasoh study area in determining the rate of soil erosion and sedimentation. Zullyadini et al., (2013) reported that the total amount of annual erosion of the cliffs at Sungai Tasoh was the highest at 348.76 tonnes (1.38%) followed by Sungai Pelarit Hilir at 25.64 tonnes (0.68%), Sungai Jarum at 55.45 tonnes (0.55%), Sungai Chuchuh at 12.58 tonnes (1.18%) and Sungai Pelarit Hulu at 17.41 tonnes (0.27%), each respectively. Jalal et al. (2019, 2020, 2021) observed in the same area erosion and sedimentation rate estimates that are not significantly different when utilising the medium term FRNs approach as $^{137}$Cs for this study area are similar to those in the Timah Tasoh, Perlis study site. The rates are still considered very low when compared under cultivation in large agricultural areas in the United States and from silt or soil brought into production in the last century in Northeastern China, 6 Mg ha −1 yr−1 and 15 Mg ha−1 yr−1, each respectively (Mark A.N. et al., 2017).

## CONCLUSION

The rate of soil erosion and sedimentation analysis gave different values in all 20 study stations. Overall, the dry season has yielded soil erosion rate results only at each station when compared to the rainy season which is more mixed with both soil erosion and sedimentation rates. It has given the rate and soil erosion of values ranging from 5.09 t/ha/y to 65.2 t/ha/y throughout for both seasons, at two stations 10 and 11 from mixed crop and station 14 from modern agriculture, which are contributed the highest and lowest soil erosion rate values for both seasons. This can be clearly seen that the difference in the soil erosion rates between the highest and lowest values is not notable and is likely due to the diversity of land use and the amount of rainfall received together with other factors that play a very important role, especially the occurrence of soil erosion in the study site. Nevertheless, the rainy/wet season has provided soil erosion values and sedimentation rates only in some land use areas with reported values ranging from 8.02 t/ha/y to 39.78 t/ha/y and - 4.81 t/ha/y to - 50.81 t/ha/y, respectively. However, the value of the soil erosion rate in the rainy season gives a lower value when compared to the dry season in some study stations. The values of soil erosion and sedimentation rates from this study are not much different from studies that have been reported by previous studies for both seasons, the Timah Tasoh catchment area. Precisely, the values from this study for both soil erosion and sedimentation are still classified as small amounts when compared to the values of both in cultivated areas in large agricultural areas of the United States and from silt or soil brought into production on century ago in Northeast China due to several factors that need to be considered. In conclusion, $^{137}$Cs as a medium-term tracer has been successfully used to determine the rate of soil erosion and sedimentation in two different seasons for the Sembrong catchment area throughout the study period based on several factors that have been considered.

## ACKNOWLEDGEMENT

The author would like to thank the cooperation and assistance provided by the members of the IAEA/RCA RAS 5084: Assessing and Improving Soil and Water Quality to Minimize Land Degradation and Enhance Crop Productivity Using Nuclear Techniques project who were directly

involved in the sampling activities, sample preparation and analysis to ensure this research project runs smoothly and ends successfully. Finally, gratitude is extended to the International Atomic Energy Agency (IAEA) for providing the chance to participate in this very interesting research project to further enhance cooperation and knowledge together with great and dedicated international experts.

## CONFLICTS OF INTEREST

The authors declare no conflict of interest.

## REFERENCES

Blake, W.H. 2000. The use of $^{7}$Be as a tracer in sediment budget investigations. Geography Department, University of Exeter

Blake, W.H., Walling, D.E. and He, Q. (2002) Using cosmogenic beryllium-7 as a tracer in sediment budget investigations. Geografiska Annaler, 84A, 89-102.

Blake, W.H., D.E. Walling, and Q. He. 1999. Fallout beryllium-7 as a tracer in soil erosion investigations. Appl. Radiat. Isot. 51:599–605.

Blanco, Humberto & Lal, Rattan. 2010. "Soil and water conservation". Principles of Soil Conservation and Management. Springer. m/s. 2. ISBN 978-90-481-8529-0.

Dietrich, W.E., Dunne, T., Humphrey, N.F. & Reid, L.M. (1982) Construction of sediment budgets for drainage basins. In: Workshop on Sediment Budgets and Routing. Eds. Swanson, F., Janda, R.J., Dunne, T., Swanston, D. Pp

Golosov, V.N., Ivanova, N.N., Litvin, L.F. and Sidorchuk, A.Yu. 1992, Sediment budget in river basins and small river aggradation. *Geomorphologiya,* Vol.4, pp. 62-71 (in Russian)

Jalal , S., Dainee , N.F.A.T., Noor Fadzilah,Y., Mohd,T.I .,Mohd ,I.A.A., (2020). The Depth Distribution of Beryllium 7 In The Soil Study, International Journal of Agriculture, Forestry and Plantation, Vol. 9 (Feb) ISSN 2462-1757:11-18

Jalal , S., Zainudin, O., Dainee , N.F.A.T (2019). Determination of Medium-Term Soil Erosion and Sedimentation Rates in Two Seasons, International Journal of Agriculture, Forestry and Plantation, Vol. 8 (June) ISSN 2462-1757:120-127

Jalal , S., Zainudin, O., Dainee , N.F.A.T., (2021). Quantifying the Relative Amounts of Soil Erosion and Sedimentation in Different Land Use, ASM Sc.J.,16, Special Issue 1, 2021 for SCIEMATHIC 2019, 172- 179

Jalal , S., Zainudin, O., Dainee , N.F.A.T., Noor Fadzilah,Y., Mohd,T.I .,Mohd ,I.A.A., (2020). The Compound Specific Stable Isotope (CSSI) values in Timah Tasoh Soil Erosion Study , International Journal of Agriculture, Forestry and Plantation, Vol. 9 (Feb) ISSN 2462-1757:1-10

Jalal , S., Zainudin, O., Dainee , N.F.A.T., Noor Fadzilah,Y., Mohd,T.I .,Mohd ,I.A.A., (2020). The Short-Term Erosion Rates In Different Land Use Study, International Journal of Agriculture, Forestry and Plantation, Vol. 9 (Feb) ISSN 2462-1757:19-27

Jalal , S., Zainudin, O., Dainee , N.F.A.T., Nurrul , A.M.J., Nooradilah, A., Mohd, T.I., (2021). The Beryllium-7, $^{7}$Be Depth Penetration in Two Seasons Study at Timah Tasoh , Perlis, ASM Sc.J.,16, Special Issue 1, 2021 for SCIEMATHIC 2019, 180- 186

JC Ritchie, JR McHenry . 1990. Application of Radioactive Fallout Cesium-137 for Measuring Soil Erosion and Sediment Accumulation Rates and Patterns: A Review. Journal of environmental quality. Wiley Online Library

Mark A.Net al., (2017) Natural and anthropogenic rates of soil erosion , International Soil and Water Conservation Research Volume 5, Issue 2, Pages 77-84

Meade, 1982. Sources, Sinks, and Storage of River Sediment in the Atlantic Drainage of the United States. The Journal of Geology volume 90 number 3 (1982). The University og Chicago press Journals

Motha, J.A., P.J. Wallbrink, P.B. Hairsine, and R.B. Grayson. 2002. Tracer properties of eroded sediment and source material. Hydrological Processes 16:1983-2000

Phillips JD. 1992. The source of alluvium in large rivers of the lower Coastal Plain of North Carolina. Catena 19: 59–75.

Reid, L. R., Dunne, T, 1996. *Rapid Evaluation of Sediment Budgets*. Catena special publication (Geo-ecology Report). Catena Verl. GMBH Germany

Ritchie J.C. and McHenry J.R., 1974. Fallout $^{137}$Cs: A tool in conservation research. *Journal of water and Soil Cultivation*. 30, 283-286

Toy, T.J., Foster, G.R., Renard, K.G. 2002. Soil erosion: processes, prediction, measurement, and control. NewYork, New York. Wiley. ISBN 978-0-471-38369-7.

Trimble, S. W., 1983. A sediment budget for Coon Creek basin in the Driftless area, Wisconsin, 1883–1977. Am. J. Sci. 283: 454– 474.

Wallbrink, P.J., Murray, A.S. and Olley, J.M., 1998. Determining sources and transient times of suspended sediment in the Murrumbidgee River, New South Wales, Australia, using fallout $^{137}$Cs and $^{210}$Pb. Water Resour. Res., 34(4):879-887.

Walling D.E. and Quine T.A., 1990: Calibration of caesium-137 measurements to provide quantitative erosion rate data. *Land Degradation and Rehabilitation* 2: 161-175.

Walling DE, Collins AL (2008) The catchment sediment budget as a management tool. Environ Sci Policy 11: 136–143

Walling et al., 1998 D.E. Walling, P.N. Owens, G.J.L. Leeks The role of channel and floodplain storage in the suspended sediment budget of the River Ouse, Yorkshire, UK Geomorphology, 22 (1998), pp. 225-242

Walling, D.E. and Quine, T.A., (1993). Use of Caesium-137 as a Tracer of Erosion and Sedimentation: Hand Book for the Application of the Cesium Technique. Overseas Development Administration Research Scheme R4579. Department of Geography, University of Exeter, UK.

Walling, D.E., A.L. Collins, H.M. Sichingabula and G.J.L. Leeks. 2001. Integrated assessment of catchment suspended sediment budgets: a Zambian example. Land degradation & development, 12, pp.387-415

Walling, D.E., A.L. Collins. 2000. Integrated assessment of catchment sediment budgets: a technical manual. University of Exeter, UK, 168 p.

Zapata, F. (ed.) (2002) Handbook for the Assessment of Soil Erosion and Sedimentation Using Environmental Radionuclides. Kluwer, Dordrecht.

Zullyadini A. R, Mohd. F.M, Mohamad.A. O & Wan. R.I (2013) The Contribution of Riverbank Erosion to the Suspended Sediment Transport in Timah Tasoh Reservoir, Perlis, Geografi Vol 1, No 2, 17 – 29, Penerbit Universiti Pendidikan Sultan Idris

e-Jurnal Sains Nuklear Malaysia, 2023, Vol. 35 (No.2): 69 – 78
*eISSN: 2232-0946*

# A REVIEW OF A CASE STUDY ON RARE EARTH ELEMENTS RECOVERY FROM SECONDARY RESOURCES IN EUROPEAN HYDROWEEE PROJECT

***Khaironie Mohamed Takip*** and Roshasnorlyza Hazan***

Industrial Technology Group, Malaysian Nuclear Agency,
43000 Kajang, Selangor, MALAYSIA.
*Correspondence author: khaironie@nm.gov.my

***ABSTRACT***

*Rare earth elements (REE) are high-value raw materials and of strategic importance in various applications, including emerging technologies globally. The fast-evolving and rapid technological changes have caused the demand for REE continuously increase. In the future, conventional deposits may no longer satisfy industrial demand. Therefore, a holistic study on REE recovery from potential secondary sources must be carried out. This paper presents the recent findings on the recovery of REE from waste electrical and electronic equipment (WEEE) or e-waste as an alternative to extraction from mines. The HydroWEEE project in Italy, funded by the European Union (EU) from 2009 until 2016, is used as the case study. The future perspectives regarding the circular economy, benefits, and challenges in implementing the recovery of REE from WEEE are also discussed.*

**Keywords**: Rare earth elements, recovery, waste electrical and electronic equipment, carbon reduction

## INTRODUCTION

Rare earth elements (REE) are a set of 17 chemical elements which consist of yttrium (Y) and scandium (Sc), as well as the 15 lanthanide elements: lanthanum (La), cerium (Ce), praseodymium (Pr), neodymium (Nd), promethium (Pm), samarium (Sm), europium (Eu), gadolinium (Gd), terbium (Tb), dysprosium (Dy), holmium (Ho), erbium (Er), thulium (Tm), ytterbium (Yb), and lutetium (Lu). They are of growing interest, and their applications cover many fields such as high-tech components, green technologies and material industries of high-temperature superconductors, secondary batteries, and electric or hybrid cars.

REE are grouped depending on the atomic number, into light rare earth elements (LREE) – La, Ce, Pr, and Nd, and into 'middle and heavy' HREE – Sm, Eu, Gd, Tb, Dy, Ho, Er, Tm, Yb and Lu. Minerals containing REE are differentiated into various groups depending on the content of REE: monazite, xenotime, and bastnaesite are the three most frequently extracted rare earth (RE) minerals. In addition, the interest in ion adsorption clay deposit (IAC) has gained of late as it is becoming a significant source of HREE (Chen et al. 2019).

Modern society faces the problem of a continuous increase in demand for raw materials, including mineral resources, due to the rapid population and economic growth (Nasrollahi et al., 2020). REE are included in the list of 'critical' raw materials in the United States of America (USA), the European Union (EU), and Japan. REE are considered critical because they are at risk of diminishing supply and their impact on the economy is higher than most other raw materials.

Over 90% of the world's economically recoverable REE are present in primary mineral deposits, i.e., in bastnaesite ores, which are in China (Bayan Obo) (Habib & Wenzel, 2014) and the USA (Mountain Pass in California). The monazite deposits are the second largest REE-bearing mineral and are primarily located in Australia, South Africa (Jun et al., 2010), Brazil, Malaysia (Kołodyńska &

Hubicki, 2012), India (Maitra et al., 2009) and Russia (Kalinnikov et al., 2010). China has almost half of the world's known reserves and dominates 94% of REE global production (Schlinkert & Van Den Boogaart, 2015).

The stages of REE production consist of mining, separating, refining, alloying, and manufacturing RE into end-use items and components (Borowik et al., 2012). Because of the growing demand and the desire to have no supply constraints, many countries, including Malaysia, are evaluating the potential to exploit their resources. Due to the low concentrations in the earth's crust, REE recovery from secondary resources could become a new source of supply and has been rapidly growing globally. One of the possible ways is to recover REE from Waste Electrical and Electronic Equipment (WEEE).

WEEE, also known as e-waste, is defined as any broken, non-working, old or obsolete electric or electronic appliance such as a TV, computer, air conditioner, washing machine or refrigerator. It is generally grouped into two main types, either e-waste generated from the industrial sector or household. WEEE is becoming a global issue, where the more electrical and electronic equipment is produced, the more e-waste needs to be disposed of or managed properly. In addition to containing toxic and hazardous materials such as lead, cadmium, and arsenic, WEEE also contains economically significant levels of precious and critical metals, for example, gold, copper, silver and REE. Therefore, WEEE represents a potential secondary source of valuable material, whose recovery is a growing business activity worldwide (Europian Commission, 2019).

This paper aims to review a successful case study of urban mining dealing with two research projects funded within the European FP7 framework. The HydroWEEE Project developed an innovative hydrometallurgical process to recover REE from WEEE. Furthermore, the economically convenient from a circular economy perspective and the benefits and challenges in implementing the concept of recycling and recovery REE are discussed. The assessment will enable knowledge expansion in current research to better understand the challenges in REE recovery from secondary resources for the upcoming research strategy.

## CASE STUDY

In Europe, REE are categorized under the critical raw material (CRM). These raw materials are economically and strategically important for the European economy but have a high-risk associated with their supply. The REE gained international attention in 2011 when prices rose after the Chinese export quota restriction. Aside from mining, one of the alternative options for extracting REE is to recover them from waste. Therefore, further advancement in alternative processing techniques was required for the circular economy and sustainability of the REE industry. It is generally aimed to achieve economic development while respecting resource limitations.

In particular, the European Union (EU) was aimed at WEEE recycling to reduce the disposal of waste and “to contribute to the efficient use of resources and the retrieval of valuable secondary raw materials”. WEEE is the fastest-growing waste stream in Europe. These wastes represent an important secondary source of REE in Europe. Examples of electronic waste that has an important percentage of REE are spent fluorescent lamps and cathode ray tubes (CRTs). However, these devices are classified as hazardous materials for the high concentration of heavy and toxic metals and must be appropriately disposed of.

Therefore, the EU had established the directives for their disposal and recycling, given their high concentration of REE. The ideas and insights on minimizing waste and conserving essential resources

inspired Relight Ltd to participate in a groundbreaking initiative funded by the European Framework Programme (FP7), called HydroWEEE (2009-2012). This project was followed by HydroWEEE-Demo (2012-2016). The outcomes of both projects were documented in the HydroWEEE Project Consortium and the HydroWEEE-Demo Project Consortium reports for the Framework Programme.

Relight Ltd was established in 1999 by a project with Philips to create a network to collect and recover fluorescent lamps in Italy. Relight has been a pioneer in collecting, treating, and recovering WEEE since 2005. It is a leading Italian company that recycles WEEE in general. The core of its business is the treatment of WEEE belonging to televisions and monitors, which accounts for 80% of the input waste, and the treatment of fluorescent lamps, which accounts for 4% of the input waste of about 824 tonnes/year. In 2014, Relight treated 600 tonnes of lamps, accounting for 54% of the annual quantity collected in Italy, and produced 15 tonnes of fluorescent powder from lamps. In addition, it has been involved in a lot of research and development regarding waste management, one of which was the HydroWEEE projects, for recovering REE, namely, Eu, Tb and Y from spent lamps and CRTs by hydrometallurgical processes and the development of HydroWEEE demo plants.

## HydroWEEE Projects

The first phase of the HydroWEEE Project (2009-2012) dealt with recovering rare and precious metals from WEEE, including lamps, and spent batteries, by the hydrometallurgical process. The idea was to develop a mobile demo plant using hydrometallurgical processes to extract metals like Y, indium, lithium, cobalt, zinc, copper, gold, silver, nickel, lead, and tin in high purity (above 95%). For the content of REE, the lamps have different phosphors: the red phosphors ($Y_2O_3$:$Eu^{3+}$), the green phosphors ($LaPO_4$:$Ce^{3+}$, $Tb^{3+}$) and the blue phosphors ($BaMgAl_{10}O_{17}$:$Eu^{2+}$) (Jastel et al., 2008; Yu & Chen, 1995; Ronda, 1995). Figure 1 demonstrates the flow of hydrometallurgical processes developed for recycling and recovering REE from fluorescent lamps and CRTs (Innocenzi et al., 2016).

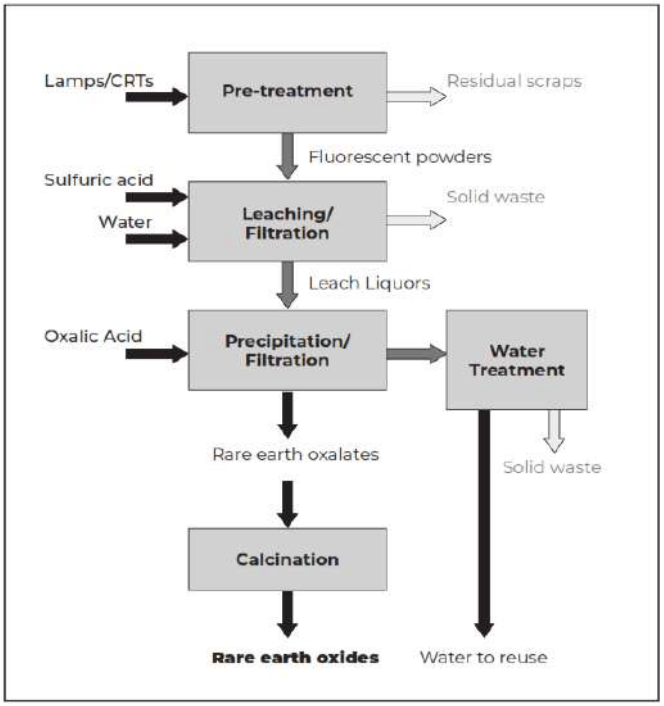


Figure 1. Hydrometallurgical process for Y and Eu recovery from lamps and CRTs

After collecting the spent lamps and CRTs, the recycling processes start with a mechanical pre-treatment of the waste, including crushing, diamond cutting technology (for CRTs) and sieving. The analysis showed that the fluorescent powders consists of Y, Eu and Tb with the concentration of 15%, 0.6% and 0.5%, respectively. For CRTs, the analysis showed that Y and Eu were, on average, 14% and 0.9%, respectively.

A mobile demo plant as shown in (Fig. 2) was developed when the hydrometallurgical processes were attained (Kopáček, 2013). The innovative process was designed as the universal process; thus, several fractions such as lamps, CRTs, LCDs, printed circuit boards and Li-batteries can be treated in the same mobile plants in batches. The development of the mobile demo plant has benefited small and medium enterprises (SMEs) as several companies can use it at different times. Therefore, the necessary quantities of waste, as well as investments, can be limited.

Figure 2. View from (right) back, (left) front side of HydroWEEE mobile demo plant

A stationary demo plant as shown in Figure 3 was set up during the second phase of the HydroWEEE Project (2012-2016) (Kopáček, 2013). The demo plant can recover REE from various electronic wastes such as batteries, LCD screens and circuit boards. However, it is most suited for the recovery of Y, Eu, Tb and other REE from fluorescent powders resulting from the exhausted lamps and CRTs recovery. The plant operated two batches per day with the capacity of producing 184.8 tonnes per year of fluorescent powder from spent lamps. The annual mass balance of the hydrometallurgical process (precipitation of REEs) is 59.7 tonnes of REOs mixture per year, consisting of 91.3% yttrium oxide ($Y_2O_3$), 4.07% europium oxide ($Eu_2O_3$), 1.08% gadolinium oxide ($Gd_2O_3$), 0.28% terbium oxide ($Tb_2O_3$), 0.11% cerium oxide ($Ce_2O_3$) and 0.01% lanthanum oxide ($La_2O_3$) (Favot & Massarutto, 2019). Innocenzi et al. (2016) reported that 93% of Y and Eu from lamps and 74% of Y from CRTs could be recovered from the process.


Figure 3. HydroWEEE Stationary Demo

## CIRCULAR ECONOMY

The conventional REE processing approach to producing lamp phosphors from primary sources using conventional hydrometallurgical approaches is in the linear economy of "extract, make, consume and dispose of", as demonstrated in Figure 4 (European Commission, 2019). However, the entire process is often associated with environmental impacts and elevated human health risks due to the existence of radioactive material, thorium, and uranium, in the host material.

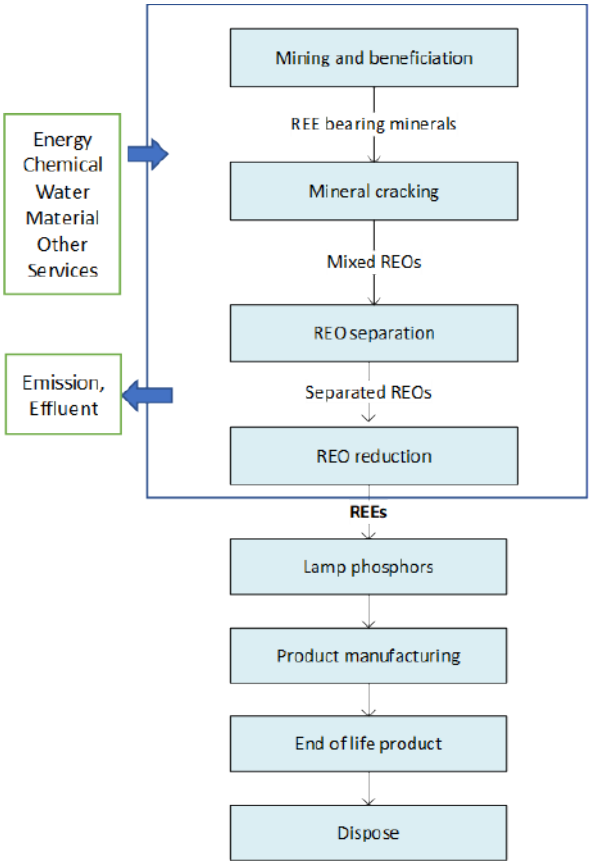


Figure 4. Linear economy in REE industry

With a revolution such as the hydrometallurgical recovery process from the HydroWEEE project, a linear economy in REE industry has transformed into a circular economy framework. This transformation has expanded the benefits of improving resource efficiency and the contribution of the circular economy to the sustainability of REE consumption. The process flow for the life cycle of REE towards the circular economy in fluorescent lamp production is shown in Figure 5 (Binnemans et al., 2013).

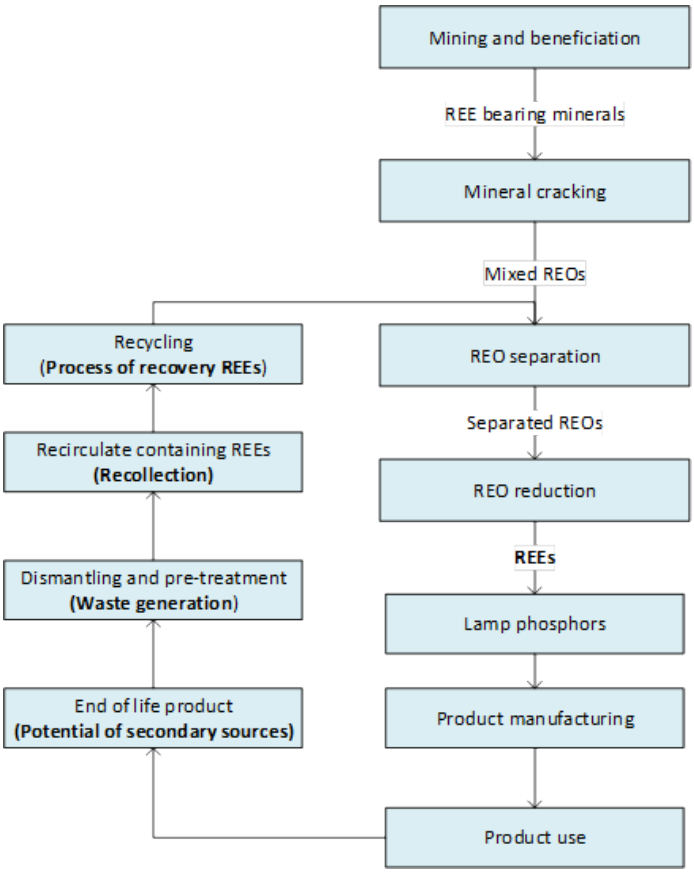


Figure 5. Recycling prospect for REEs and opportunities for sustainable development

## BENEFITS OF REE RECYCLING AND RECOVERY

Recovery of the REE is the most drastic recycling method, but it delivers the purest end products in the form of high-purity rare earth oxide (REO). In this approach, the lamp phosphor fraction is considered a high-value rare-earth ore, with a high concentration of REE such as europium, terbium, and yttrium considered precious material. Therefore, they can be used for making new lamp phosphors or for making new REE-containing compounds for other applications; for example, europium can be used in security markers, terbium in magnets and yttrium in phosphors as well as in high-tech ceramics. Therefore, properly managing the REE recovery and recycling process from WEEE will benefit the environment, economy, and society.

Primarily, it may abate environmental and health problems associated with hazardous substances. Owing to the increased demand for REE, adverse environmental impacts associated with the production of REE have become a global concern. In general, REE recycling has significant advantages over the mining of rare earth, including savings in energy, water, and chemicals

consumption, along with a significant reduction of carbon emissions, effluents and solid waste generation resulting from the extraction and processing of rare earth ores. REE recyclate does not contain radioactive thorium and uranium, unlike the primary mined rare-earth ores. Therefore, radioactive tailing stockpiles and mining health problems can be, at least partially, avoided. There are also possible benefits from avoiding land allocation for the mine and radioactive waste streams and transportation. Energy use (which is associated by $CO_2$ emissions and other greenhouse gas (GHG) emissions) and water use are typically much lower for secondary than primary material. The recycling process may reduce the environmental burdens associated with the consumption of primary new materials (Cucchiella et al., 2015).

Furthermore, the process may deliver scarce and valuable materials for the economy as the current demand for REE has significantly increased, which has caused an increase in their prices. The balance between the demand by the market and the natural abundance of the rare earth in ores is a significant problem for manufacturers of these elements. Therefore, recycling helps address the so-called "balance problem", namely that certain REEs with high demand levels, for instance, europium, are present in small quantities in REE ores along with other REEs with low demand, such as lanthanum and cerium. In order to meet the demand for the former, the latter is produced in excess and is stockpiled. The ideal situation is a perfect match between the demand and production of rare earth so that there are no surpluses of any REE. This situation would result in the lowest market price for rare earth because all the elements share the production costs. Therefore, recycling these REEs from end-of-life fluorescent lamps can help keep the rare-earth markets balanced.

Finally, recycling may provide ancillary social benefits such as social inclusion opportunities in different ways: employment for disabled people or the long-term unemployed, helping to bridge the digital divide, and other related benefits (Kissling et al., 2012). There is likely to be less social resistance as efforts toward a circular economy for REE develop alongside their green economic uses in products.

## CHALLENGES

Firstly, the ability to achieve higher recycling rates of REE from the WEEE will be disturbed due to non-systematic e-waste collection, lengthy product life span and high cost in producing the purest end-product. The WEEE represents the fastest-growing waste stream in the EU, generating about 12 million tonnes in 2019 (Forti et al., 2020). In many cases, and sometimes despite legislation, the WEEE is not collected separately for recycling but is disposed of with mixed Municipal Solid Waste (MSW). One of the limiting factors that affect the volume and availability of material for recycling is the waste leakage into the 'grey market' of informal or illegal low-technology recyclers. This problem typically leads to losing the products' small quantities of hard-to- extract metals.

Secondly, although recycling is a promising option for mitigating REEs supply issues and reducing overall environmental burdens associated with the production and consumption of these metals, it is not a short-term solutionbecause many emerging technologies that rely on REE, such as wind turbines, electric vehicles, have a long-life span and are not yet ready to be recycled. This matter will still cause a shortage of material supply as well.

Finally, the non-eco-friendly treatment and recovery processes with higher operating costs required to purify the mixtures obtained from consumer devices. For example, according to Wang et al. (2011), the REE content in the phosphors of lamps can reach 27.9%, but only 10% is currently recovered. The low percentage of REE recovery is due to the high acid resistance of some types of phosphors during the conventional recovery process that uses acid for leaching. While Favot and Massarutto

(2019) studied the economics of yttrium recycling from spent lamps, they reported that recycling is a valid option in economic terms if the market price is above 14 €/kg. Considering the external costs of mining REE, which have been computed at 4.46 €/kg, the recycling option is convenient when the price of yttrium oxide is above 9.54 €/kg. They determined that in 2012 and 2013, it was convenient to recover yttrium because its price was higher than the costs of separated waste collection plus the cost of treatment and recovery. However, between 2014 and 2016, the market price of yttrium did not cover such costs, thus making the treatment and recovery of yttrium less convenient than disposal. Therefore, the low-priced green technologies for separations systems are expected to effectively contribute to recycling REE from end-of-life rare-earth-containing products.

## CONCLUSION

The detailed process analysis in the laboratory and the practical experience gained from the HydroWEEE projects will give useful indications about this new approach to the WEEE recycling business in Malaysia. In the medium to long term, the supply of REE is expected to exceed demand, except for a few essential REE such as Y, Dy, Nd, Eu, and Tb which are used in the production of high-tech consumer products, such as cellular telephones, computer hard drives, electric and hybrid vehicles. The increase in the price of REE since 2009 has increased interest in the substitution and recycling of REE. To this point, the recovery of REE from spent fluorescent lamps is the most mature in the industrial-scale application. The economics of the REE recycling determined by the costs of the process and the need to achieve economies of scale and the REE market pricing as well as the absence of a supply chain structure geared towards the pre-processing of WEEE with an emphasis on REE. Therefore, an effective supply chain for recovery and recycling is necessary to ensure the availability of suitable recyclates with high REE concentrations, thus contributing to the sustainable development of REE and the circular economy.

## ACKNOWLEDGEMENTS

The author would like to thank all colleagues at the Malaysia Nuclear Agency for their encouragement and support throughout the review process.

## REFERENCES

Binnemans, K., Jones, P.T., Blanpain, B., Van Gerven, T., Yang, Y., Walton, A. & Buchert, M. (2013). Recycling of rare earths: A critical review, *J. Clean. Prod*. 51: 1–22.

Borowik, M., Malinowski, P., Biskupski, A., Dawidowicz, M., Schab, S., Rusek, P., Igras, J. & Kęsik, K. (2012). Production technology of nitrogen-sulphur-calcium fertilizers on the base of urea and phosphogypsum, *Chemik*. 66(5): 525-534.

Chen, Y., Li, J., Zhang, X., & Wang, Y. (2019). Ion adsorption clay deposits: A promising alternative for heavy rare earth element resources. *Journal of Rare Earths*. 37(4): 439-451.

Cucchiella, F., D'Adamo, I., Koh, S.L. & Rosa, P. (2015). Recycling of WEEEs: An economic assessment of present and future e-waste streams, *Renewable and Sustainable Energy Reviews*. 51: 263-272.

European Commission. (2019). Waste Electrical and Electronic Equipment (WEEE). Retrieved from https://ec.europa.eu/environment/waste/weee_en.htm

Favot, M. & Massarutto, A. (2019) Rare-earth elements in the circular economy: The case of yttrium. *J Environ Manage*. 240: 504-510.

Forti, V., Baldé, C.P., Kuehr, R. & Bel, G. (2020). Quantities, flows and the circular economy potential, The Global E-Waste Monitor 2020.

Habib, K. & Wenzel, H. (2014). Exploring rare earths supply constraints for the emerging clean energy technologies and the role of recycling, *Journal of Cleaner Production*. 84: 348- 359.

HydroWEEE Project Consortium. (2009-2012). HydroWEEE: Developing a new recycling technology for WEEE containing liquids. European Commission, 7th Framework Programme.

HydroWEEE-Demo Project Consortium. (2012-2016). HydroWEEE-Demo: Demonstration of the HydroWEEE technology for the treatment of WEEE containing liquids. European Commission, 7th Framework Programme.

Innocenzi, V., Michelis, I. D., Sgarioto, S., Gotta, D., Kopacek, B. & Vegliò, F. (2016). Recovery of critical metals from lamps and CRTs, *Electronics Goes Green (EGG):* 1-5

Jastel, T., Nikol, H., & Ronda, C. (2008). New developments in the field of luminescent materials for lighting and displays, *Angewandte Chemie International Edition*. 47(37): 7188-7206.

Jun, T., Jingqun, Y., Ruan, C., Guohua, R., Mintao, J. & Kexian, O. (2010). Kinetics on leaching rare earth from the weathered crust elution-deposited rare earth ores with ammonium sulfate solution, *Hydrometallurgy*. 101(3): 166-170.

Kalinnikov, V. T., Kasikov, A. G., Orlov, V. M., Grishin, N. N. & Freidin, B. M. (2010). Studies and developments of the Institute of Chemistry and Technology of Rare Elements and Mineral Resources of the Kola Research Center, Russian Academy of Sciences, in the field of materials science for the solution of special technical problems, *Theoretical Foundations of Chemical Engineering*, 44(4): 557-562.

Kissling, R., Fitzpatrick, C., Boeni, H., Luepschen, C., Andrew, S. & Dickenson, J. (2012). Definition of generic re-use operating models for electrical and electronic equipment, Resources, *Conservation and Recycling*. 65: 85-99.

Kołodyńska, D., & Hubicki, Z. (2012). Investigation of Sorption and Separation of Lanthanides on the Ion Exchangers of Various Types. In: D. Jemcová & M. Kubáček (ed.). Chapter 6, INTECH, 189-211.

Kopáček, B. (2013). Mobile hydrometallurgy to recover rare and precious metals from WEEE. In: M. Kubáček & D. Jemcová (ed.). CRC Press/INTECH, 385-404.

Maitra, M., Chattopadhyay, B., Sengupta, S. K. & Nandy, S. (2009). Presence of niobian rutile and its exsolution phases in rare element pegmatite of Belamu area, Purulia district, West Bengal, *Journal of the Geological Society of India*. 74(3): 296-298.

Nasrollahi, Z., Hashemi, M., Bameri, S., & Taghvaee, V. M. (2020). Environmental pollution, economic growth, population, industrialization, and technology in weak and strong sustainability: Using STIRPAT model, *Environment, Development and Sustainability.* 22(7): 1105-1122.

Ronda, C. R. (1995). Phosphors for lamps and displays – an application view, *Journal of Alloys and Compounds*. 225: 534–538

Schlinkert, D & Van Den Boogaart, K.G. (2015). The development of the market for rare earth elements: Insights from economic theory, *Resources Policy*. 46: 272-280.

Yu, Z. S., & Chen, M. B. (1995). Rare Earth Elements and Their Applications. Metallurgical Industry Press, Beijing (P.R. China).

Wang, X., Li, W. & Li, D. (2011). Extraction and stripping of rare earths using mixtures of acidic phosphorus-based reagents, *Journal of Rare Earths*. 29: 413–415.